Section B. Creep, damage processes and transformations

Results of EC-projects: BOS-129-NL and MA1B-0058-NL (1986-1991)
Consist (outer TU-Delft reports and section B-reports) of 4 separated parts:
B.1. Deformation and damage processes in wood,
B.2. Transformations of wood and wood-like polymers
B.3. Theoretical derivation of the WLF- and annealing equations
B.4. A new theory of nucleation,
as discussion of the Section B-reports, which are published in 2 parts: B.1. and together: B.2 to B.4. Here follows B.3. and B.4. after section B.2.

B.2. Transformations of wood and wood-like polymers

A new theory of:

Solidification, Nucleation, Glass transition,
Annealing, Diffusion, Rouse/Zimm spectra,
Power law, Reaction order, etc.

T.A.C.M. van der Put,
TU-Delft, Civil Engineering and Geosciences, Timber Structures and Wood Technology,
Wielengahof 16 NL 2625 LJ Delft, Netherlands Tel: +31 152851980, E-mail: vanderp@xs4all.nl

Discussion of B(2005), and B(2010), B(2011):

Delft Wood Science Foundation Publication Series 2015 nr. 2-2 - ISSN 1871-675x

Contents **page**

1. Introduction and justification

Strength, deformation and other important properties of wood materials are time dependent and dependent on physical properties as temperature and moisture content what only can be explained and described by the acting physical and chemical processes, thus by statistical mechanics and reaction kinetics [1], and as shown, the in [2] (Section B.1) developed limit analysis equilibrium theory of deformation kinetics is fundamental and explains all aspects as creep, damage, aging, annealing [3], nucleation B(2011), transformations as glass transition, rubber behavior, diffusion, etc. by the same constitutive equation. The consequence is that the contradictory phenomenological models, as the free volume model for glass-transition, the instability model of nucleation, the tunneling model of activation and the extrapolated flexible chain model, with non-existent linear visco-elastic relaxation spectra for rubber behavior and creep of materials, etc., have no meaning and are rejected by this exact approach.
It is shown that wood does not follow real transformation up to the very high temperatures where decomposition starts and is in the glass-state, even at these high temperatures.
It is evident for wood, as a glassy and crystalline polymer, that time dependent behavior can not be explained and described by flexible chain models of dilute solutions (rubber theory) or by other Newtonian visco-elastic models (as is still generally practice). Linear visco-elasticity does not exist and also for real rubbers, the "rubber theory" does not apply because this phenomenological model is questionable as shown in [4] and in Appendix I.
Regarding the models, proposed for wood, the following can be stated:

- The, in literature (C. Huet, [16], COST 508, and EC-MA1B report), proposed phenomenological multi-transitions model, based on a spectrum of transformations, cannot exist because the response below a transformation cannot interact or contribute to the response above that transformation, and thus a spectral interaction cannot exist. But, also the spectral, parabolic, form of the loss tangent can not exist. In fact, a constant value of the loss tangent is measured for all structural materials like wood (see fig. 3.8, explained by theory [2]). The chosen Cole-Cole-circle (or parabola) for the loss tangent, represents not real, but idealized (non-existent) material behavior. As known from literature, this plot only can partly and roughly represent phenomenological, the response in the zone of glass-rubber transition to disappearing stiffness of rubbers and solutions, and thus may roughly represent the low frequency end of the glass-transition zone of a lightly cross-linked rubber or gel, showing the best such a broad curved loss compliance. Thus, the Cole-Cole plot is not able to represent the glass-state and the leather-state (which may be approximated for wet, saturated, wood at very high loading and temperature). The not existent multi Cole-Cole-parabolic logarithmic decrements are introduced to indicate the supposed separate glass-transitions of e.g. cellulose, hemicelluloses and lignin in wood, as stated in [16] and related publications. However, wood behaves like a copolymer and can only show one glass transition (see e.g. fig. 5.1) and not the transitions of the separated wood components and the multi-glass-transitions model or multi-Cole-Cole plot thus has no theoretical and physical background and is not able to predict behavior and thus should be forgotten.
- The same applies for the "Tammann-Hesse law" [16], being identical to the empirical nucleation and step-growth equation of the liquid-solid phase transformation, and thus can not be proposed to be the generalization to all kinds of transformations, as is done. Other transformations don't show the property changes like the liquid-solid transformation and no transformation needs infinite energy, (according to the empirical Tammann-Hesse law), to reach equilibrium. This choice of liquid-like behavior can not be right for structural polymers like wood, but also the Tammann-Hesse equation itself, thus the chosen empirical nucleation model, appears to be theoretically not right, as is

shown here in 2.5 and 2.6. This transformation model further is based on a first order transformation equation (the nucleation of the liquid-solid phase), although it is proposed in all publications (mentioned e.g. in [16]) to apply for glass-transitions, what are second order transformations (depending on other physical parameters than the first order transformations). Therefore this "Tammann-Hesse law" also can not replace the WLF-equation of glass transition, as is proposed, also because the WLF-equation is not a replaceable empirical equation any more, but is a theoretical expression, based on the exact explanation of certain flow behavior near glass-transition as is derived by the equilibrium theory of reaction kinetics, see [2] and [3] or Section B.1 and Section B.3.

- Similar remarks apply for the, e.g. in [16] proposed, phenomenological Zimm model and other models of dilute solutions, (Rilem), that have nothing to do with transformations and nothing to do with the physical behavior of wood that is not a solution.
- This also applies for the, also for wood (E.C.- MA1B, Rilem, reports), introduced solutions model of paper science, what is identical to the well-known theoretical "regular solutions" model, where the transition between two different phases is based on the change of the lattice coordination number, what is the change of the way of packing of the atoms, and thus on the change of the enthalpy and thus is based on a first order transformation. This wrongly is used to estimate the glass transition temperature because a glass transition is a second order transition (showing no enthalpy jump).
- Because the models above are not able to fit data, the power law fit is always used instead. The power law is shown here to give the first two terms of an expansion around some measured value by any formula (see 2.5.3). The power law thus may represent any model, when it is applied in a limited range of the variable around the measurement, or in this case, in a relatively small time range around a mean time value. Thus, the power law cannot be applied for extrapolation of behavior to longer times as wrongly is done for creep, etc. Because of the lack of a theoretical meaning and because of the impossibility to predict behavior, even not of a single test-procedure, the power law fitting procedure, is theoretical useless. The "power law" is the oldest fitting formula of time dependent behavior, used before 1800, and is as old as the first publication of this subject and appears to be not rejectable although this law predicts the physical impossible infinite rate at the start, while there always is a delay time with a negligible rate at the start of transport phenomena, and predicts a (physically impossible) unlimited increase with time, thus is, in principle, not able to fit total to any test-result (see Appendix I for real, possible, precise data fits (with correlation ~ 1) by deformation kinetics theory).

In the following chapter, the untenable phenomenological models of transformations will be discussed and replaced by the exact theory of reaction kinetics, to make a real explanation and prediction of time dependent behavior possible. This leads to a new theory of solidification, nucleation, glass transition, annealing, diffusion, Rouse and Zimm and other spectra, power law, reaction order, etc., and leads to the demanded calculable reliability.

2. General aspects of transformations

2.1. Introduction

As discussed above, the description of the mechanical behavior of glasses like wood, still is based in literature, on extrapolations of not valid transformation models of soft and liquid-like materials. It thus is necessary to discuss general possible behavior of materials in relation to wood using the exact theory. This exact theory is shown to explain all phenomena and fits the data of tests, done on the same specimen, thus on the same structure, with a

correlation close to one (as is necessary for a molecular theory).
For the discussion of the applied transformation models, a general discussion is necessary of phase transformations what are changes of the characteristics and physical properties of materials on alteration of the external constraints such as pressure and temperature due to changes of the microstructure. Such a transformation involves a considerable atomic rearrangement so that the required structural and compositional changes can occur. Homogeneous transformations show compositional changes and no structural changes. Wood-like polymers, on the contrary, can not show compositional changes at a transformation, but only structural changes in the side-bond structure (as will be discussed in 2.2). Thus, models based on typical homogeneous transformations behavior cannot be applied to wood.

2.2. Heterogeneous transformations

Heterogeneous transformations occur at interfaces and are initiated at microscopically small volumes of the product phase. This is known as nucleation. Nucleation may occur at quenched-in crystal defects or at foreign particles. The process of growth, following after nucleation, involves growth of the nuclei by thermal activated long-range or short-range diffusion and transfer processes at the interface, or may involve a martensitic transformation, showing no compositional change, but a small change of the configuration, caused by a high internal driving force. Typical heterogeneous transformations are:

- liquid-solid transformations like crystallization and melting;
- solid-solid transformations that may follow the common behavior of thermal activation, or may occur by activation due to a very high internal stress as martensitic transformation.

The martensitic transformation will not be discussed because it does not occur in wood and wood-products. There even is no indication of such a transformation at the lowest temperatures (where the side bonds are strong and don't flow). Even when a martensitic configuration may exist in wood, the elementary crystalline fibrils in wood of 3 nm are too small to make martensitic nucleation possible because this is below the critical dimension to make it possible to build up high enough internal stresses for this transformation.
The common thermal activated transformations, at lower stresses, are distinguished into processes showing a short-range transport, like the polymorphic transformation, the massive transformation, order-disorder reaction, and recrystallization, and into processes showing a long or medium range transport like the eutectoid reaction, cellular reaction, precipitation and coarsening.
The transformations with a short-range transport of atoms do not show major compositional changes. The polymorphic transformations, (from one equilibrium structure to the other), in metals and ceramics, only show the nucleation and growth of a new lattice into the product phase. Also, the massive transformation only shows a change of the crystal structure and no change of composition. The same applies for the order-disorder reaction, showing the nucleation and growth of the ordered phase in the disordered phase, and for recrystallization involving the creation of a strain free lattice at the expense of its, e.g. by cold work, strained lattice (or for wood, involving the re-extension of crystallites).
Because the (infinite) long wood-polymers only may show structural changes by secondary side bond breaking, transformations by long-range transport of atoms are not possible. Transformations of wood thus only may show a comparable behavior in some aspects with the transformations showing a short-range transport, like the massive transformation or recrystallization, with the exclusion again of the short-range transformations needing a free transport of atoms like e.g. the order-disorder reaction.
Because all transformations are diffusive, diffusion, as general common behavior, should be discussed first.

2.3. Derivation of the right diffusion equations for the different cases

Polymers like wood may show diffusion of whole sections of chains and not of molecules because there is no covalent bond breaking and bond formation that provides chain breaking and chain extension. Diffusion in solids the best can be discussed by the simple example of diffusion of interstitial atoms in metals where no doubt is possible about the mechanism. The interstitial atoms jump from one interstitial position to a neighbouring one. Consider a set of parallel atomic planes of interplanar distance λ, having a concentration gradient of diffusing particles along the x-axis perpendicular to the atomic planes. The probability of an interstitial atom to jump in any direction per second is denoted here by p. Because the concentration of interstitials is small, p can be considered independent of the concentration. The probability for a jump in forward direction will be denoted by fp and the number of diffusing particles per unit area, on the plane located at x, by n(x). By expansion at time t:

$n(x + \lambda) = n(x) + (\partial n/\partial x)\lambda + 0.5(\partial^2 n/\partial x^2)\lambda^2 + \ldots\ldots$

$n(x - \lambda) = n(x) - (\partial n/\partial x)\lambda + 0.5(\partial^2 n/\partial x^2)\lambda^2 - \ldots\ldots.$ (2.3.1)

At instant $t + \delta t$, where $\delta t << 1/p$, the increase δn of the number of particles on the plane at x is, for a one-dimensional flow, equal to the number of particles jumping from $(x + \lambda)$ into x, minus the number of particles jumping away from plane x. Thus, using eq.(2.3.1):

$\delta n(x) = \delta(n(x + \lambda) - n(x)) = fp\delta t(n(x + \lambda) - n(x)) \approx fp\delta t(\partial n/\partial x)\lambda$, or:

$\partial n/\partial t = D\partial n/\partial x$ (2.3.2)

This is Fick's first law, representing a forward reaction only. The equation only is able to describe a part of the process that is far out of equilibrium. More general is the reaction in forward and backward direction that also may contain the equilibrium state. Then δn is given by the number of particles jumping from $(x - \lambda)$ into x, plus the number of particles jumping from $(x + \lambda)$ into x, minus the number of particles jumping away from plane x. Thus according to eq.(2.3.1):

$\delta n(x) = \delta(n(x + \lambda) + n(x - \lambda) - 2n(x)) = fp\cdot\delta t\cdot(\partial^2 n/\partial x^2)\cdot\lambda^2$, or:

$\partial n/\partial t = fp\lambda^2\cdot(\partial^2 n/\partial x^2) = D(\partial^2 n/\partial x^2)$ (2.3.3)

what is Fick's second law. In eq.(2.3.3), f is determined by the geometry of the lattice. For instance, in the b.c.c. lattice of iron it is possible from 2/3 of the interstitial positions to jump in forward or in backward direction and from the positions in which this is possible, one of the four possible directions is a forward or a backward jump. Thus:

$f = (2/3)\cdot(1/4) = 1/6$ and in that case: $D = (\lambda^2/6)\cdot p$.

The jump probability p is determined by the probability of a particle to have a sufficient high thermal energy to overcome the resistance from the other atoms when moving from one interstitial position to the other, thus when moving from one minimum potential energy position to the other against an intermediate energy barrier. Thus the probability p of having the energy G' at T degree Kelvin is:

$p = \nu\cdot\exp(-G'/kT)$,

in which ν is the frequency of vibration or the number of attempts to cross the barrier per second and G' is the activation energy or the height of the potential energy barrier and kT is the mean vibrational energy of the particles. Thus:

$D = (\lambda^2/6)\cdot\nu\cdot\exp(-G'/kT) = (\lambda^2/6)\cdot\nu\cdot\exp(-H'/kT + S'/k)$ (2.3.4)

where S' in $G' = H' - TS'$ is the entropy difference between the interstitial position and the activated state halfway between two interstitial positions at the top of the barrier and H' is the activation enthalpy for these atomic jumps.

Eq.(2.3.3) is used to describe diffusion e.g. of water in wood, ([2], pg. 102). The equation is based on a small (only one term of the expansion) chemical potential gradient and a negligible driving force (random walk of the jumping elements). For the general case, the dif-

ferences in forward and backward reactions due to any possible driving force should be regarded. Then eq.(2.3.3) becomes:

$\delta n(x) = \delta(n(x+\lambda) + n(x-\lambda) - 2n(x)) = f\cdot\delta t\cdot[(p_f - p_b)\cdot\lambda\cdot\partial n/\partial x + (p_f + p_b)\cdot\lambda^2\cdot(\partial^2 n/\partial x^2)/2]$

or: $\partial n/\partial t = f\cdot\nu\cdot\exp(-H'/kT + S'/k)\cdot[(\exp(\Delta E'/kT) - \exp(-\Delta E'/kT))\cdot\lambda\cdot\partial n/\partial x +$

$+ (\exp(\Delta E'/kT) + \exp(-\Delta E'/kT))\cdot\lambda^2\cdot\partial^2 n/\partial x^2/2]$

or: $\partial n/\partial t = f\cdot\nu\cdot\exp(-H'/kT + S'/k)\cdot[2\cdot\sinh(\Delta E'/kT)\cdot\lambda\cdot\partial n/\partial x +$

$+ \cosh(\Delta E'/kT)\cdot\lambda^2\cdot\partial^2 n/\partial x^2]$ (2.3.5)

For high driving forces this is:

$\partial n/\partial t = f\cdot\nu\cdot\exp(-H'/kT + S'/k)\cdot[\exp(\Delta E'/kT)\cdot\lambda\cdot\partial n/\partial x + \exp(\Delta E'/kT)\cdot\lambda^2\cdot\partial^2 n/\partial x^2/2]$

or: $\partial n/\partial t \approx f\cdot\nu\cdot\exp(-H'/kT + S'/k)\cdot\exp(\Delta E'/kT)\cdot\lambda\cdot\partial n/\partial x$ (2.3.6)

And for low driving forces, e.g. in Newtonian like liquids, eq.(2.3.5) becomes:

$\partial n/\partial t = f\cdot\nu\cdot\exp(-H'/kT + S'/k)\cdot[2\cdot(\Delta E'/kT)\cdot\lambda\cdot\partial n/\partial x + \lambda^2\cdot\partial^2 n/\partial x^2] \approx$ (2.3.7)

$\approx f\cdot\nu\cdot\exp(-H'/kT + S'/k)\cdot[2\cdot(\Delta E'/kT)\cdot n\cdot\lambda/L + n\cdot\lambda^2/L^2] \approx$

$\approx n\cdot(2f\lambda/hL)\cdot\exp(-H'/kT + S'/k)\cdot\Delta E'$ (2.3.8)

when the gradient: $\lambda/L << 2\Delta E'/kT$ as can be the case at transformations, showing a jump of the activation energy of $2\Delta E'$ outside the transition temperature.

When $\Delta E' \rightarrow 0$, near equilibrium, eq.(2.3.7) becomes:

$\partial n/\partial t = f\cdot\nu\cdot\exp(-H'/kT + S'/k)\cdot(\lambda^2\cdot\partial^2 n/\partial x^2)$,

showing the right value of D of eq.(2.3.3) of: $D = f\cdot n\cdot\lambda^2\cdot\exp(-H'/kT + S'/k)$.

It is seen that eq.(2.3.3) only applies when processes are possible at near zero driving forces, when there is a concentration gradient and no transformation.

The reaction, in a heterogeneous system, can be interface controlled, what means that the process is governed by molecular diffusion at the interface. When, at the other hand, in a heterogeneous system, the reaction at an interface is very fast, diffusion through the material towards that interface is slower and is determining. Then the activation energy for the process at the interface shows a value equal to the activation energy for the determining diffusion through the material.

At the interface the gradient $\partial n/\partial x$ of e.g. eq.(2.3.2) is due to the reduction of n to zero within a thin layer L, adjacent to the interface giving $\partial n/\partial x = n/L$ and eq.(2.3.2) gets the form of the mono-molecular forwards reaction:

$\partial n/\partial t = C\cdot n$ (2.3.9)

with $C = D/L$. The same follows from eq.(2.3.3) with $C = D/L^2$, if a curved gradient is assumed to exist, that can be approximated by a parabola, as is possible in any thin layer:

$n_x = n\,x^2/2L^2$ or $\partial^2 n_x/\partial x^2 = n/L^2$.

However the diffusion equation applies for small gradients and the lower order term $\lambda^2\cdot\partial^2 n_x/\partial x^2$ disappears in a thin layer ($\lambda << 1$) and eq.(2.3.5) will become:

$\partial n/\partial t = f\cdot\nu\cdot\exp(-H'/kT + S'/k)\cdot 2\cdot\sinh(\Delta E'/kT)\cdot\lambda\cdot\partial n/\partial x =$

$= \nu\cdot(2\cdot f\cdot\lambda/L)\cdot n\cdot\exp(-H'/kT + S'/k)\cdot\sinh(\Delta E'/kT) =$

$= \nu\cdot n\cdot\exp(-H'/kT + S''/k)\cdot\sinh(\Delta E'/kT) =$

Thus: $\partial n/\partial t = C'\cdot n\cdot\sinh(\Delta E'/kT)$, (2.3.10)

identical to the general reaction equation of equilibrium theory. The overall behavior always can be given in the form of eq.(2.3.10) of a first order reaction depending on the local concentration near the interfaces. This concentration follows from measuring the reaction rate. Processes in wood and structural materials thus follow the elementary reaction equation what is further discussed below in 2.4.

2.4. Transformation kinetics

2.4.1. General aspects of reaction kinetics and reaction order

Mostly a reaction equation is given in the beginning and end states of the reacting materials thus as a sum of the amounts of reactants turning to the sum of amounts of products. In such a reaction equation the reaction order is not known but regarding this equation as if it is a true equation in molecules, an empirical reaction order is obtained. For instance the rate of the turnout of the product P by the reaction of the reactants A and B is:

$dP/dt = kA^nB^m$ (2.4.1.1)

where n and m are empirical values. When this equation does not give the molecular reality of n molecules A and m molecules B, it should not be used because it will not apply in all circumstances. The reaction equation thus should be given at the molecular level where n and m are numbers of reacting molecules. At the molecular level, there always are many successive elementary reaction-steps with intermediary products and the reaction equation of this mechanism should be given in the determining elementary step with the slowest rate. In a thin gas, molecules will collide with each other and thrown back like elastic balls and some of them will have higher speeds by the collisions than others and are energized and as such even may get such a high speed that they are called to be activated giving a reaction at the collision by a change of the electron structure and kernel rearrangement. Because 2 molecules are involved in the collision the reaction can be expected to be of the second order or bimolecular. For instance:

$A + A \xrightarrow{k} P$ or: $dP/dt = kA^2$ (2.4.1.2)

It is not very probable that in a thin gas, 3 molecules will collide at the same time, in the right directions and reaction orders of 3 and more are not very probable. The order 3 is more probable in a liquid as a result of two successive bimolecular reactions within a very short time. Mostly however first order reactions occur at higher concentrations as will be shown below. The occurrence of first order reactions is evident for elementary reaction steps of decomposition and of isomerization having the form of:

$A \xrightarrow{k} B + C$ respectively: $A \xrightarrow{k} A'$ giving both: $-dA/dt = k \cdot A$

In general, the order follows from the mechanism of a collision equilibrium:

$A + A \underset{k_1}{\overset{k_2}{\rightleftharpoons}} A + A^*$ followed by the chemical reaction: $A^* \xrightarrow{k_3} P$

where A* is an activated molecule. Now both reactions will have the rate of the slowest determining step. Thus the rate of the shift of the equilibrium dA*/dt is equal to the rate of the product formation dP/dt or:

$k_1 \cdot A^2 - k_2 \cdot AA^* = k_3 \cdot A^*$ or:

$$\mathbf{A}^* = \frac{k_1 A^2}{k_3 + k_2 A} \quad \text{and} \quad dP/dt = k_3 \cdot A^* = \frac{k_3 k_1 A^2}{k_3 + k_2 A} \qquad (2.4.1.3)$$

For small concentrations A in dilute solutions or gasses, $k_2 \cdot A << k_3$ and the rate:

$dP/dt = k_1 \cdot A^2$ follows the second order reaction.

At higher concentrations A, as is the case in solids, $k_2 \cdot A >> k_3$ and the reaction rate:

$dP/dt = (k_3 k_1 / k_2) \cdot A$ (2.4.1.4)

shows a first order reaction.

For solids, because of the high density, also for relative small concentrations a first order reaction equation always occurs as can be seen from the following mechanism.

$A + A \underset{k_1}{\overset{k_2}{\rightleftharpoons}} A + A^*$ due to the exchange of vibrational energy,

$A + N \underset{k_4}{\overset{k_5}{\rightleftharpoons}} N + A^*$ due to the exchange of energy with not reacting mole-

cules N, that are not able to jump, and:

$A^* \xrightarrow{k_3} P$

In total there is no accumulation of the intermediate product A* and:

$dA^*/dt = 0 = k_1 \cdot A^2 - k_2 \cdot AA^* + k_4 \cdot AN - k_5 \cdot NA^* - k_3 \cdot A^*$ or:

$$A^* = \frac{k_1 A^2 + k_4 AN}{k_3 + k_2 A + k_5 N} \qquad (2.4.1.5)$$

and for smaller values of A and always high values of N is: $A^* \approx (k_4/k_5) \cdot A$ and:

$$dP/dt = k_3 A^* \approx (k_3 k_4/k_5) \cdot A \qquad (2.4.1.6)$$

and there is a first order rate equation for solids similar to eq.(2.4.1.4). And also when k_3 is not much smaller than $k_5 \cdot N$, there is a first order reaction.

When k_3 is much higher than $k_5 \cdot N$, is:

$$dP/dt = k_3 A^* \approx k_4 \cdot AN \qquad (2.4.1.7)$$

also a first order reaction in A, because N can be regarded to be constant. Mostly diffusion, eq.(2.4.1.7) is determining and not the chemical reaction at the interface, eq.(2.4.1.6).

Because of the applied constant boundary conditions, transformations occur at a constant rate. This steady state also occurs when the number of sites for the reaction is constant as for instance for the reaction of gases at the boundary of a glowing wire. Determining for diffusion in solids is the number of free spaces, where molecules may jump in. This number of holes like lattice defects, dislocations, etc., can be constant following from the minimum energy of formation of these holes. This constant number of holes A_0 will be divided among A and A* in the last mechanism and eq.(2.4.1.5) becomes with $A_0 = A + A^*$ or $A = A_0 - A^*$:

$$A^* = \frac{k_1 A^2 + k_4 AN}{k_3 + k_2 A + k_5 N} \approx \frac{k_4 N(A_0 - A^*)}{k_3 + k_5 N} \quad \text{or:} \quad A^* = \frac{k_4 N A_0}{k_4 N + k_5 N + k_3} \qquad (2.4.1.8)$$

giving a rate of:

$dP/dt = k_3 \cdot A^* \approx [k_3 k_4/(k_5 + k_4)] \cdot A_0$ or: $dP/dt \approx k_4 \cdot NA_0$, similar to eq.(2.4.1.6) and eq.(2.4.1.7), however, showing zero order reactions.

The first order reactions thus may reach a steady state, explaining the quasi zero order reactions of transformations. At the end of the reaction, near equilibrium, when A_0 is not limiting any more, the reaction again becomes of the first order.

For liquids, the behavior is a bit more complicated. The molecules do not move free, as in a thin gas, but interact with their neighbours and collide many times against their neighbours (about 150 times at 293 K) before diffusing away to the next spot where the same will be repeated. If the activation energy is low, a few collisions will lead to a reaction and the speed of the reaction is determined by the speed of diffusion. When the activation energy is high, diffusion is not limiting any more for the speed of product formation and the speed of the reaction is lower and thus determining. The mechanism is:

$$A + B \underset{k_{-d}}{\overset{k_d}{\rightleftarrows}} [AB] \xrightarrow{k_1} P$$

Again the speed of the shift of the equilibrium is equal to the speed of the product formation or:

$v = k_d \cdot AB - k_{-d} \cdot [AB] = k_1 \cdot [AB]$ or: $[AB] = \frac{k_d AB}{k_1 + k_{-d}}$ and $v = dP/dt = k_1[AB]$ or:

$$v = \frac{k_1 k_d AB}{k_1 + k_{-d}} \qquad (2.4.1.9)$$

leading to a second order reaction.

When $k_1 >> k_{-d}$, diffusion is determining or:

$v = k_d \cdot AB$ (2.4.1.10)

and when $k << k_{-d}$, the chemical reaction is determining or:

$v = (k_1 k_d / k_{-d}) \cdot AB \quad (\approx k_1 AB)$ (2.4.1.11)

Mostly diffusion is determining and eq.(2.4.1.10) will apply. However, wood is not a liquid with free moving molecules that may show a second order reaction and a mechanism with an intermediate product (given above by [A,B]). Transformation models of wood thus should not be based, as done, on extrapolation of models of dilute liquid solutions and thin gasses with higher order reactions because the behavior then cannot be made consistent.
As mentioned before, transformations are analyzed by using the empirical equation, eq.(2.4.1.1). This equation can be written in general:

$$-\frac{1}{a}.\frac{dA}{dt} = kA^{n_a}B^{n_b}C^{n_c} \qquad (2.4.1.12)$$

With the ratio of the initial concentrations: $A_0 : B_0 : C_0 = a : b : c$, and with a conversion of X, is: $A = A_0 - X$; $B = (A_0 - X)(b/a)$; and $C = (A_0 - X)(c/a)$, and substitution of these values in eq.(2.4.1.12) gives:

$$-\frac{1}{a}.\frac{dA}{dt} = k(A_0 - X)^{n_a}.(\frac{b}{a}(A_0 - X))^{n_b}.(\frac{c}{a}(A_0 - X))^{n_c} = k'(A_0 - X)^{n_t},$$

where $n_t = n_a + n_b + n_c$. Thus in general applies:

$$-\frac{dA}{dt} = k''A^n \qquad (2.4.1.13)$$

The solution of this equation is for n = 1: $\ln(\frac{A_0}{A}) = k''t$

and for $n \neq 1$: $k''t = \frac{1}{n-1}.((1-y)^{1-n} - 1).\frac{1}{A_0^{n-1}}$

With: $A = A_0 \cdot (1 - y)$, with y = fractional conversion, the solution is at a certain value of y:

$$k''t_y = \frac{1}{n-1}.((1-y)^{1-n} - 1).\frac{1}{A_0^{n-1}} \qquad (2.4.1.14)$$

or: $\log(t_y) = \log(f(n,k'',y)) - (n-1)\cdot\log(A_0)$ (2.4.1.15)

making it possible to determine the order "n" of the "reaction" at regarding a constant value of y, doing tests with mutual different values of A_0. However, as will be shown later, this experimental value of $n = n_a + n_b + n_c \approx 1$ applies for all processes in wood. This lowest overall order n = 1, shows that there is one speed determining step and that there are no mechanisms with intermediate products. Further, the slightly lower value of the order than one, at higher concentrations, indicates that series reactions are acting (and not concurrent reactions).
Based on these results it is possible and convenient to obtain general solutions of the often complex reactions of the transformations by a sinus series expansion of the potential energy surface (as is discussed in [2]). Based on the symmetry conditions of the orthogonal components there is a not changing, thus steady state, intermediate concentration in the successive steps causing a behavior like one elementary symmetrical reaction for each component [2].

2.4.2. Kinetics of phase transformations

A number of phases may be involved in a transformation and may interact in many ways.

Typical transformations are given by the following overall phase changes, written in symbols of the phases:

$\alpha \longrightarrow \alpha' + \beta$ (2.4.2.1)

where the matrix α and the product phase α' have the same structure but different compositions. While the β phase nucleates and grows, solutes drain out of the matrix until α becomes α';

$\alpha \longrightarrow \beta,$ (2.4.2.2)

that may represent a change of the bond structure;

$\gamma \longrightarrow \alpha + \beta$ (2.4.2.3)

where the product consist of two phases which nucleate and grow as a composite.

On quenching an alloy the precipitation reaction eq.(2.4.2.1) may occur. During this transformation, considerable movement of atoms must take place so that a new lattice is created in place of the old one and the solute is redistributed in order to create the composition difference between the phases.

Eq.(2.4.2.2) may represent a polymorphic transition, showing no compositional changes. Atomic movements are still required for the creation of the new lattice.

Eq.(2.4.2.3) may represent an eutectoid transformation. This reaction requires diffusion and partitioning of elements and may show several processes at the same time with comparable activation energies. Considerable atomic movements are required to achieve the differences in structure and changes in composition.

As discussed before, only the first order reaction according to the type of transformation similar to eq.(2.4.2.2) is possible for wood polymers and need to be discussed. In general may apply in this case, for different probabilities of jumps in forwards and backwards directions, the first order reaction equation:

$$\partial N / \partial t = C_f N_f - C_b N_b = (kT/h)\cdot[N_f \cdot \exp(-E_f/kT) - N_b \cdot \exp(-E_b/kT)] =$$
$$= \frac{2kT}{h} \cdot \sqrt{N_f . N_b} \cdot \exp\left(-\frac{E_f + E_b}{2kT}\right) \cdot \sinh\left(\frac{E_b - E_f + kT.\ln(N_f / N_b)}{2kT}\right) \qquad (2.4.2.4)$$

$\partial N/\partial t = 0$ at equilibrium. Thus $\sinh(x) = 0$ or $x = 0$. Thus at equilibrium is:

$N_{fe} / N_{be} = \exp((E_f - E_b)/kT)$ (2.4.2.5)

and eq.(2.4.2.4) can be written:

$$\frac{\partial N}{\partial t} = \frac{kT}{h} \cdot \sqrt{N_{fe} \cdot N_{be}} \cdot \exp\left(-\frac{E_f + E_b}{2kT}\right) \cdot \left(\frac{N_f}{N_{fe}} - \frac{N_b}{N_{be}}\right) \qquad (2.4.2.6)$$

In the classical "steady-state" model for nucleation, grow of the embryo follows from successive reactions and thus from the addition of a large number of equations, eq.(2.4.2.6), and only the first and last value of N remain, giving $N_f = N_{fe}$ and $N_b = 0$. According to the classical model, $N_b = 0$ at the critical size of the embryos because then they are not in equilibrium and spontaneously grow into the stable product phase. For $N_b = 0$, eq.(2.4.2.6) turns to eq.(2.4.2.7). This however only is possible for high values of the driving force. Then x is high in sinh(x) and thus: $\sinh(x) \approx \exp(x)/2$ and eq.(2.4.2.4) becomes:

$\partial N/\partial t \approx (kT/h)\cdot N_f \cdot \exp(-E_f/kT)$ (2.4.2.7)

showing only a forward reaction ($N_b = 0$). An implication of the classical steady-state model of nucleation, eq.(2.4.2.7) thus is, that there are high driving forces and the classical model thus can not apply in general also for low driving forces or for behavior near equilibrium.

The same applies for the classical "equilibrium model" of nucleation. According to this model embryos are formed as a result of a large number of bimolecular reactions:

$$O_1 + O_1 \longleftrightarrow O_2$$
$$O_2 + O_1 \longleftrightarrow O_3$$
$$\ldots\ldots\ldots$$
$$O_{n=1} + O_1 \longleftrightarrow O_n$$
$$nO_1 \longleftrightarrow O_n$$

giving for equilibrium: $\exp((E_b - E_f)/kT) = (N_n/N_t)/(N_1/N_t)^n \approx (N_n/N_t) \approx N_n/N_1$,
because: $N_t = N_1 + \sum N_n \approx N_1$ and thus: $(N_1/N_t)^n \approx 1^n \approx 1$.
Thus whatever the reaction order is (2^{nd} order partial, or nth order total), the reaction behaves like a first order reaction with a low concentration of the product, the embryo, $N_n << N_1$, and thus with: $(E_f - E_b) >> kT$. Thus, also the classical equilibrium model of nucleation implies high driving forces and high activation energies at nucleation in order to explain the occurring first order reaction.
For a general description, the nucleation mechanism should show growth of the grains by diffusion at the grain boundaries and thus also should follow the diffusion requirements (in stead of the questionable condition $N_b = 0$ of the classical model). At diffusion the same sites are involved in forwards and backwards jumps, thus: $N_b = N_f = N_t$ and eq.(2.4.2.4) becomes:

$$\frac{dN}{dt} = \frac{2kT}{h} \cdot N_t \cdot \exp\left(-\frac{E_f + E_b}{2kT}\right) \cdot \sinh\left(\frac{E_b - E_f}{2kT}\right) \qquad (2.4.2.8)$$

In this equation is: $E_f = E_f' - \sigma V_f$ and $E_b = E_b' + \sigma V_b$, where σ is the local stress on the sites and V_f and V_b are the activation volumes.
For an isotropic material, or an orthotropic material like wood in the main directions, there is no difference in positive and negative flow and positive or negative shear-strength etc. and: $\sigma_f V_f = \sigma_b V_b = \sigma V$.
Also for an anisotropic material, expansion of the activation energy surface may be symmetrical with respect to the activation work term σV, [2], and no distinction is possible whether a non-symmetrical process, eq.(2.4.2.8), is acting or different symmetrical processes are active. Eq.(2.4.2.8) thus becomes for each process:

$$\frac{dN}{dt} = \frac{2kT}{h} \cdot N_t \cdot \exp\left(-\frac{E_f' + E_b'}{2kT}\right) \cdot \sinh\left(\frac{E_b' - E_f' + 2\sigma V}{2kT}\right) \qquad (2.4.2.9)$$

This rate is zero when $\sinh(x) = 0$, thus when $x = 0$. Thus: $2\sigma_0 V = E_f' - E_b'$ and the sinh-term in eq.(2.4.2.9) becomes: $\sinh[((\sigma - \sigma_0) \cdot V)/kT]$. Thus, the process starts when the stress is above σ_0. For a stress below σ_0, the equilibrium concentration according to eq.(2.4.2.5) applies and $dN/dt = 0$.
For phase transformations, there is a chemical potential and the corresponding σ_0, as driving force, is positive and the sinh-term in eq.(2.4.2.9) is, when no external stress σ is applied and the internal stress, as usual, is negligible:
$\sinh[((\sigma_0 + \sigma) \cdot V)/(kT)] \approx \sinh[(\sigma_0 \cdot V)/(kT)]$.
A phase transformation of a single component system cannot be caused by a compositional gradient and only the strain-energy gradient by an applied external stress determines the flux. Then $E_f' = E_b' = E'$ and eq.(2.4.2.9) becomes:

$$\frac{dN}{dt} = \frac{2kT}{h} \cdot N_t \cdot \exp\left(-\frac{E'}{kT}\right) \cdot \sinh\left(\frac{\sigma V}{kT}\right) \qquad (2.4.2.10)$$

as applies for creep of materials by self-diffusion [2].
When there are structural changes, N_t in eq.(2.4.2.10) is not constant and as discussed in [2] at 3.5, the concentration term in the equation is more general:
$N_a \cdot 2\lambda A/\lambda_1$
where 2λ is the jump distance of the activated unit; A, the cross-section of that unit; λ_1 the distance between the activated sites, and N_a, the number of these sites per unit area. Then $N_a/\lambda_1 = N_t$ is the number of activated elements per unit volume. The activation volume is: $V_a = 2\lambda A$, and the work by the local stress f on the unit is: $fV_a/2 = f\lambda A$.
The equivalent work by the part σ, of the total mean technical macro stress σ_t, that acts at the site is σ times the unit area thus is:
$\sigma \cdot 1 \cdot 1 \cdot \lambda = N_a f \cdot \lambda A$ or: $f \cdot \lambda A = \sigma\lambda/N_a = \sigma V$,
where $V = \lambda/N_a$ is used in eq.(2.4.2.9) and eq.(2.4.2.10).
With $C = (2kT/h) \cdot \exp(-E'/kT)$, eq.(2.4.2.10) is general, also for structural changes:
$d(N_a 2\lambda A/\lambda_1)/dt = C \cdot (N_a 2\lambda A/\lambda_1) \cdot \sinh(\sigma\lambda/N_a kT)$ (2.4.2.11)
If the structure λA is constant, eq.(2.4.2.11) is analogous to eq.(2.4.2.10):
$dN_t/dt = C \cdot N_t \cdot \sinh(\sigma\lambda/N_a kT)$
and when the maximal concentration of sites is reached: $N_t = N_{tm}$ (or N_a is constant and λ_1 is minimal) this equation becomes (as eq.2.4.1.8):
$dN_t/dt = C \cdot N_{tm} \cdot \sinh(\sigma\lambda/N_a kT)$,
showing a constant rate. In eq.(2.4.2.11), A and $1/\lambda_1$ are mathematically the same in the equation and A can be taken to be constant, as is mostly the case, and when not, any change of A can be accounted by an equivalent change of $1/\lambda_1$ and eq.(2.4.2.11) becomes:
$d(N_a\lambda/\lambda_1)/dt = C \cdot (N_a\lambda/\lambda_1) \cdot \sinh(\sigma\lambda/N_a kT)$ or:
$d\ln(N_a)/dt + d\ln(\lambda)/dt + d\ln(1/\lambda_1)/dt = C \cdot \sinh(\sigma\lambda/N_a kT)$ (2.4.2.12)
It appears that each parameter, or each term at the left side of the equation, may dominate at different time ranges. Writing this equation like:
$d\ln(N_a)/dt + d\ln(\lambda)/dt - C \cdot \sinh(\sigma\lambda/N_a kT) = -d\ln(1/\lambda_1)/dt$,
it is seen that the right and left side of the equation have different variables and there should be a separation constant C_1. This constant however will be small because $d(\ln(1/\lambda_1))/dt = C_1$ can be about zero in some time range (e.g. at the delay time). Thus the change of $1/\lambda_1$ will be due to a separate process and need not to occur in combination with the change of the other 2 variables in the same equation and eq.(2.4.2.12) thus splits into two equations eq.(2.4.2.13) and (2.4.2.14):
$d(\ln(1/\lambda_1))/dt = d\ln(N_a'/\lambda_1)/dt = C' \cdot \sinh(\sigma'\lambda'/N_a' kT)$ (2.4.2.13)
and: $d\ln(N_a)/dt + d\ln(\lambda)/dt = C \cdot \sinh(\sigma\lambda/N_a kT)$ (2.4.2.14)
with constant λ' and N_a' in eq.(2.4.2.13).
Eq.(2.4.2.14) applies when the left hand side of the equal sign is positive, as is the term at the right hand side. When the left hand side is negative, a minus sign should be used before the term at the right hand side. This means that absolute values of the variables should be used. Eq.(2.4.2.14) also can be written:
$-d\ln(1/N_a)/dt + d\ln\lambda/dt = C \cdot \sinh(\sigma\lambda/N_a kT)$ or:
$d\ln(\lambda/|N_a|)/dt + d\ln|\lambda|/dt = C \cdot \sinh(\sigma\lambda/N_a kT)$ or:
$|d\ln(\lambda/N_a)/dt| = C \cdot \sinh(\sigma\lambda/N_a kT) = |-d\ln(N_a/\lambda)/dt|$ (2.4.2.15)

and it is seen that mathematically N_a and $1/\lambda$ are the same variables and often one can be regarded to be constant while any change can be accounted by a compensated change of the other parameter.
$d(N_a'/\lambda_1)/dt$ and $d(N_a/\lambda)/dt$ of eq.(2.4.2.13) and (2.4.2.15) are relative increases of the number of sites and may replace the concentration rate dN/dt of eq.(2.4.2.10).
A further simplification of eq.(2.4.2.10) can be made for high values of $E' >> kT$. Then the temperature dependent term kT/h can be replaced by a constant one and can be written as: $(kT_d/h)\cdot(T/T_d)$, where T_d is the Debye temperature or some other mean temperature and: kT_d/h is the Debye frequency ν_d, or some other mean frequency ν, T/T_d can be written as: $T/T_d = \exp(-\ln(T_d/T)) = \exp(-\ln(1 + (T_d - T)/T) \approx \exp(-(T_d - T)/T)$ and because: $E' = H' - S'T$, the term $\exp(-E'/kT)$ becomes:

$$\frac{T}{T_d}\cdot\exp\left(-\frac{E'}{kT}\right) \approx \exp\left(-\frac{H'+kT_d - S'T - kT}{kT}\right) \approx \exp\left(-\frac{H''-S''T}{kT}\right)$$

and because $kT_d << H'$ and $k << S'$, the enthalpy H' and entropy S' need hardly be corrected when kT/h is replaced by υ_d or by a chosen mean value υ. Eq.(2.4.2.10) thus becomes:

$$\frac{dN}{dt} = 2\nu N_t\cdot\exp\left(-\frac{E'}{kT}\right)\cdot\sinh\left(\frac{\sigma\lambda}{kTN_a}\right) \qquad (2.4.2.16)$$

For the usually described transformations, the driving forces σ (which should be obtained empirically, as the other variables) are mostly very low near the equilibrium temperature. For instance for grain growth this is two orders lower than that for precipitate coarsening or that of recrystallization by cold working or of polymorphic transformations (per one ^{0}C) or of solidification or melting (per degree C) and this group of driving forces is again 3 orders lower than that for diffusion in solid solutions (being 0.7.RT = 1.4 kcal/mol for dilute solutions at 1000 K) what again can be one order lower than the driving force for some chemical reactions like the formation of inter-metallic compounds or 2 orders lower than that of a chemical reaction like e.g. oxidation. At the low transformation stresses (and driving forces), the behavior may become quasi Newtonian because: $\sinh(\varphi\sigma) \approx \varphi\sigma$ and the rate is about linear dependent on the driving force or stress σ. In general, Newtonian behavior only is possible for small spherical molecules (see appendix I). Then, and because of a high concentration of vacancies at the temperatures near "melting", this concentration is not any longer proportional to the initial stress as in the non-linear case. Further, not only the stress, but also the activation volume is small at the occurring vacancy mechanism.
For low values of the driving force: $E_b - E_f << 2kT$, eq.(2.4.2.8) becomes:

$$\frac{dN}{dt} = \frac{E_b - E_f}{h}\cdot N_t\cdot\exp\left(-\frac{E_f + E_b}{2kT}\right) = \frac{2\Delta E}{h}\cdot N_t\cdot\exp\left(-\frac{E'}{kT}\right) \qquad (2.4.2.17)$$

with $E_b = E' + \Delta E$ and $E_f = E' - \Delta E$, or becomes analogous to eq.(2.4.2.10):

$$\frac{dN}{dt} = \frac{2\sigma V N_t}{h}\cdot\exp\left(-\frac{E'}{kT}\right) = \frac{2\sigma\lambda}{h\lambda_1}\cdot\exp\left(-\frac{E'}{kT}\right) \qquad (2.4.2.18)$$

because $\sigma V = \sigma\lambda/N_a$ and N_t per unit volume is comparable with N_a per unit area divided by the distance λ_1 or: $N_t = N_a/\lambda_1$ (see [2] or above).
The last 2 equations thus only may apply (at measurable rates) for some (melting) crystalline materials (of round molecules) and not for the (infinite) long molecules in wood.
The rate dN/dt of eq.(2.4.2.18) is constant at constant stress and temperature, showing that λ_1 is constant and also λ is constant or can be taken to be constant because any variation in λ cannot be distinguished from the variation of 1/N in the equation. Eq.(2.4.2.13) thus may

apply for high loading.
The chemical force may act in the same way as an applied stress:
$(E_b' - E_f')\cdot N_t = \Delta E'\cdot N_t/N_a = \Delta E'/\lambda_1 = 2\sigma_c\lambda N_t/N_a = 2\sigma_c\lambda/\lambda_1$,
and also eq.(2.4.2.17) has a constant rate. The chemical force is due to e.g. differences in the crystal structure and composition of the parent and product phases. The influence of the stress, due to the elastic strain energy by the accommodation of the differences in the specific volumes of the parent and product phases and the mismatches at the interfaces, mostly is small in the tests and σ of eq.(2.4.2.18):
$\sigma = \sigma_e + \sigma_c \approx \sigma_c$, nearly is caused by the chemical force σ_c alone.
For higher values of the driving force: $E_b - E_f >> 2kT$, eq.(2.4.8) and eq.(2.4.2.10) are:

$$\frac{dN}{dt} = \upsilon N\cdot\exp\left(-\frac{E'}{kT}\right)\cdot\exp\left(\frac{\Delta E}{kT}\right) \qquad (2.4.2.19)$$

with: $\Delta E = \Delta E'/N = \sigma_c\lambda/N$.

2.5. Empirical relations

The empirical classical nucleation model will discussed in a next chapter. Wood polymers do not show spherulites or folded molecules and thus will not show nucleation as a barrier to growth or decomposition. However, it plays a role in transformations related side bond breaking, thus to moisture content change and e.g. at (re-)crystallization of crystallites and the discussion of nucleation and a derivation of a new right theory is necessary, not only for nucleating polymers, but also because in a RILEM-proposal and EC-reports, the wrong and impossible classical nucleation equation of solidification (needing infinite energy to obtain equilibrium) is regarded to be the basic equation for all transformations and even for all time dependent behavior (like creep). The derivation of the right theory thus is important, also to show that nucleation is just a common example of a structural change process, thus following the kinetic theory of all transport processes.
The discussion of the classical model of nucleation and the derivation of new exact theory as correction, is given in B(2011) and in Section B.4: "A new theory of nucleation".

2.5.1. Parameter estimation and explanation of the empirical relations

All phase transformations need transport of atoms or molecules through the material by diffusion what is determining for the rate of the process. In principle, the molecules jump from free space to the adjacent free space in the direction of the surface of the new phase. What means that the free spaces move in the opposite direction. The study, in general, of the possible movements of these free spaces, as vacancies and dislocations (and segments of wood), will give the information on the kinetics of transformations and especially on the possible forms of the activation volume parameter.
The diffusion flux is caused by the chemical potential gradient due to the composition gradient or may be due to a strain-energy gradient. Because of the similar effect and the possible interaction with stress, the negative gradient of the chemical potential may be regarded as a chemical force on the molecules that can be aided or opposed by the internal and applied stresses. For a single-component system, there is no compositional gradient and the net flux is entirely due to the stresses. Because of the necessary movement of spaces, the mechanisms are the same for phase transformation as melting and for flow by stress, and for stress-rupture and for creep and self-diffusion, as follows from the same activation enthalpy and entropy of all these processes. The easy obtained data of self-diffusion (like creep) thus may give information on the mechanism of the solid-liquid phase transformation. The displacements of the free spaces can be measured indirectly, by measuring

creep or relaxation, but often also can be measured directly by measuring the jump of the spaces due to a stress pulse [1]. The following empirical equations, applying mostly only in a limited range of stresses, are used to describe the mobility of the free spaces as dislocations etc.:
The power law equation:

$$v = v_0 \cdot \left(\frac{\tau}{\tau_0}\right)^n \qquad (2.5.3.1)$$

and the nucleation equation, based on the classical nucleation model (see 2.5.1):

$$v = C_1 . \exp\left(-\frac{D}{\tau}\right) \qquad (2.5.3.2)$$

where v is the free space velocity and τ is the applied stress. The exact theoretical transport kinetics equation can be given in the form:

$$v = 2C_2 \cdot \sinh(\varphi\tau) \approx C_2 \cdot \exp(\varphi\tau) \qquad (2.5.3.3)$$

for high stresses.
In the following fig. 2.5.4, measurements are given that follow these equations. Fig. c follows the exact eq.(2.5.3.3) and cannot be represented by the other 2 equations. Fig. b follows eq.(2.5.3.2) only and fig. a follows the power law eq.(2.5.3.1).
To explain and compare these empirical equations, the following derivation is made.

2.5.2. Derivation of the power law.

Any function f(x) always can be written in a reduced variable x/x_0
$f(x) = f_1(x/x_0)$
and can be given in the power of a function:
$f(x) = f_1(x/x_0) = [\{f_1(x/x_0)\}^{1/n}]^n$ and expanded into the row:

$$f(x) = f(x_0) + \frac{x - x_0}{1!} \cdot f'(x_0) + \frac{(x - x_0)^2}{2!} \cdot f''(x_0) + ...$$

giving:

$$f(x) = \left[\{f_1(1)\}^{1/n} + \frac{x - x_0}{x_0} \frac{1}{n} \{f_1(1)\}^{1/n-1} \cdot f'(1) + ... \right]^n = f_1(1) \cdot \left(\frac{x}{x_0}\right)^n$$

when: $(f_1(1))^{1/n} = (f_1(1))^{1/n-1} \cdot f_1'(1)/n$ or: $n = f_1'(1)/f_1(1)$
where: $f_1'(1) = [\partial f_1(x/x_0)/\partial(x/x_0)]$ for $x = x_0$ and $f_1(1) = f(x_0)$

Thus: $f(x) = f(x_0) \cdot \left(\frac{x}{x_0}\right)^n$ with $n = \frac{f_1'(1)}{f_1(1)} = \frac{f'(x_0)}{f(x_0)}$ (2.5.3.4)

It is seen from this derivation of the power law, eq.(2.5.3.4), using only the first 2 expanded terms, that the equation only applies in a limited range of x around x_0.
Using this approach on eq.(2.5.3.2) gives:

$$v = C_1 \cdot \exp\left(-\frac{D}{\tau}\right) \approx v_0 \cdot \left(\frac{\tau}{\tau_0}\right)^{D/\tau_0} \qquad (2.5.3.5)$$

and using this approach on eq.(2.5.3.3) gives:

$$v = C_2 \cdot \exp(\phi\tau) \approx v_0 \cdot \left(\frac{\tau}{\tau_0}\right)^{\phi\tau_0} \qquad (2.5.3.6)$$

Thus within a short range of stresses around τ_0 there is no difference in fits according to eq.(2.5.3.1), eq.(2.5.3.2) or eq.(2.5.3.3) by the use of the same power law.

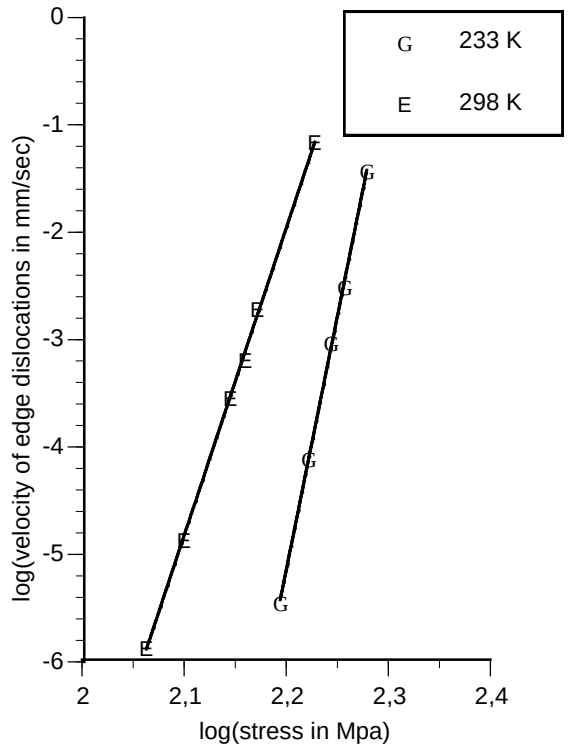

a. edge-dislocation velocity in Fe-Si $_0$ measurements: ––––– eq.(2.5.3.1)

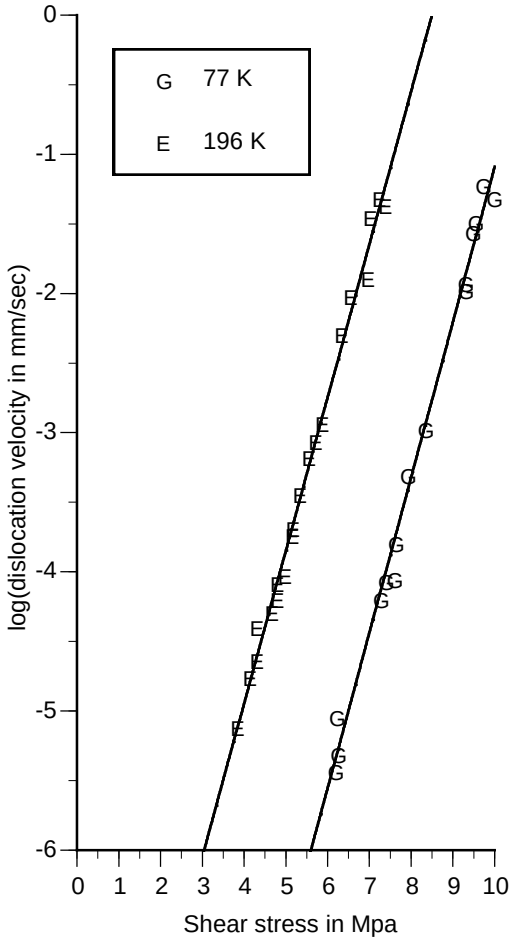

c. dislocation velocity in N_i $_0$ data ––––eq.(2.5.3.3)

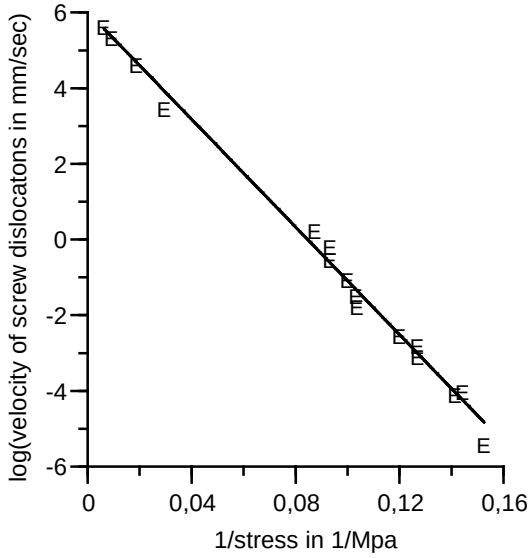

b. screw dislocation velocity in LiF $_0$ data ––––– eq.(2.5.3.2).

Fig. 2.5.4. The stress dependence of dislocation velocity in metals [1]

This can be seen in fig. 2.5.5 a, b and c, at high stress, where, for the same tests on Ge, in a limited high stress range, fitting is possible according to all 3 equations eq.(2.5.3.1) to (2.5.3.3). The power n of eq.(2.5.3.1) can be found from the slope of the double log-plot:

$\ln(v) = \ln(v_0) + n \cdot \ln(\tau/\tau_0)$ (2.5.3.7)

$n = d\ln(v)/d\ln(\tau/\tau_0)$ here, and, similarly according to eq.(2.5.3.5) to eq.(2.5.3.7):

$n = D/\tau_0 = \varphi\tau_0$, and comparison is possible of the constants of the empirical equations with the exact parameter φ of the exact equation.

When over a long range of stresses, eq.(2.5.3.2) applies and the semi log-plot of ln(v) against $1/\tau$ shows a constant slope - D, then the parameter of the exact equation φ is according to: $\varphi\tau_0 = D/\tau_0$, equal to $\varphi = D/\tau^2_0$. This parameter of the nucleation equation will be shown to be right for the nucleation mechanism of the liquid-solid transformation. The semi log-plot of the exact equation, eq.(2.5.3.3) is with $\varphi = D/\tau^2_0$:

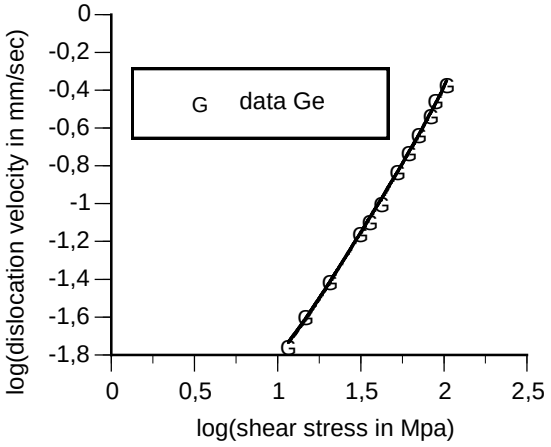

a. dislocation velocity in Ge
□ data; —— theory: sinh- equation
only partly linear (below 7 Mpa)
according to eq.(2.5.3.1)

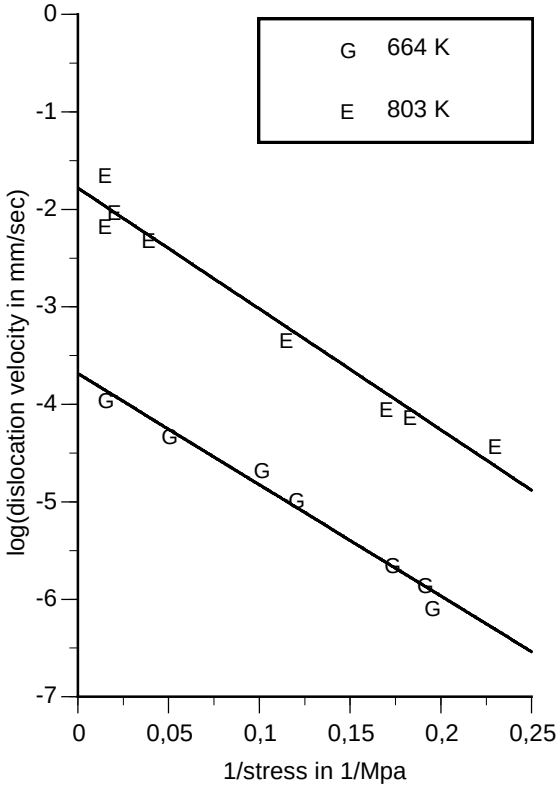

b. dislocation velocity in Ge
□ data; —— eq.(2.5.3.2)

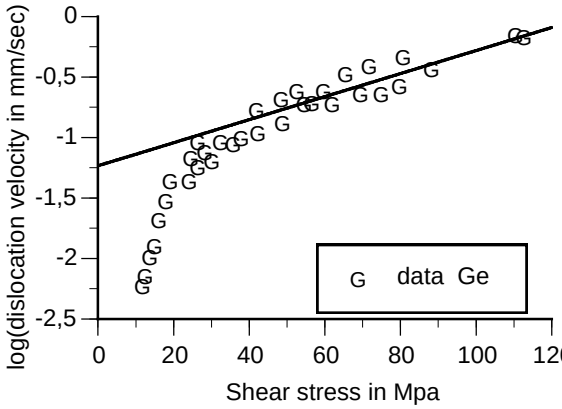

c. dislocation velocity □ data; —— eq.(2.5.3.3), linear at higher stresses.

Fig. 2.5.5. Examples of stress dependency of the dislocation velocity of Ge [1].

$$Ln(v) = \ln(C_2) + \varphi\tau = \ln(C_2) + D\tau/\tau^2_0 \quad (\hat{=} \quad \ln(C_2) + D/\tau_0) \qquad (2.5.3.8)$$

Because the dislocation mobility tests are done with stress pulses that are long enough to get steady state velocities the applied stress τ is equal to the initial applied stress τ_0 and eq.(2.5.3.8) becomes equal to eq.(2.5.3.2) what thus is the equation of the collection of all different pulse tests with different τ_0 and has no meaning for one duration test at constant τ_0. Eq.(2.5.3.8) shows that for stress relaxation (for one duration test, thus not for stress pulse tests) there will be a straight-line $\ln(v) - \tau$ – plot and not a $\ln(v)$ - $1/\tau$ - plot, what is verified by experiments in a sufficient wide stress range. This means that the classical nucleation model (of nucleation of mobile segments by overcoming of point defects) or mod-

els like crystal matrix drag (two-dimensional kink-motion model), all according to eq.(2.5.3.2), are not right and should be rejected because of the evidence of the different behavior at self-diffusion in creep and stress-relaxation experiments that fully can be explained by the activation volume parameter φ of the exact molecular transport kinetics theory which is able to explain all aspects of time dependent behavior. In the same way as for the nucleation equation, that shows a special value of φ, the power law behavior, when it applies over a long range of stresses, represents a mechanism with a special property of the activation volume parameter φ. The constant slope n of the double log-plot of ln(v) against ln(τ) of eq.(2.5.3.1), given in fig. 2.5.4 a, and 2.5.6 a, is equal to $\varphi\tau_0$ and the experimental verification of the constancy of $\varphi\tau_0$ is shown in figure 2.5.6 c. The mechanism with this property of φ is found in many materials as in BCC, FCC and HPC metals and non-metallic crystals and also in e.g. concrete and wood. It was shown in [2], that this property of the activation volume φ, causes the stress-time equivalence and because in wood also in this case the activation volume is independent of the temperature, the time-temperature equivalence also applies for this mechanism.
With the special value of $\varphi = n/\tau_0$, eq.(2.5.3.3) becomes:

$$\ln(v) = \ln(C_2) + \varphi\tau = \ln(C_2) + n\cdot\tau/\tau_0 \qquad (2.5.3.9)$$

and the semi-log-plot of ln(v) against τ (= τ_0) now shows a slope of n/τ_0 that is different for every pulse test value of τ (= τ_0) in the plot, thus a curved line, given in fig. 2.5.6 b. It follows also from eq.(2.5.3.9) that: $d\ln(v)/d\ln(\tau) = \tau\cdot\ln(v)/d\tau = \tau\cdot n/\tau_0$. This is: $\tau_0\cdot n/\tau_0 = n$ for the pulse tests collection of the dislocation mobility tests, where each applied stress τ is equal to the initial applied stress τ_0. Only in this case the constant value n of the slope of the double log-plot may exist in a wide range, as measured (see fig.2.5.4 a). At the same time, for the stress-relaxation tests, (that is one test with one τ_0) at high stresses, the straight semi log-plot: ln(v) - τ - plot applies according to eq.(2.5.3.9), what thus is no contradiction but is fully explained here by the exact theory by the other type of loading.

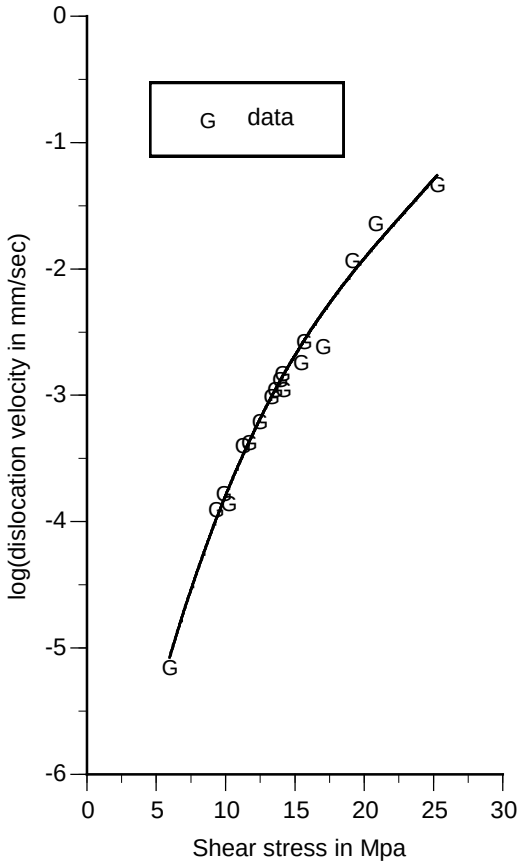

Fig. 2.5.6. b. dislocation velocity in Mo □ data; ––––– low stress sinh-equation

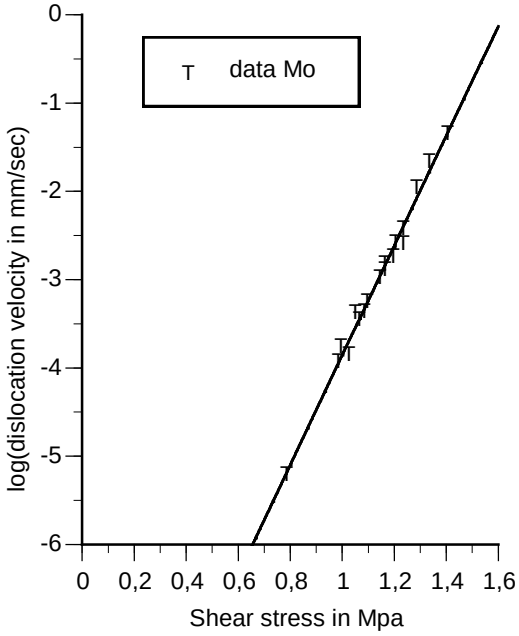

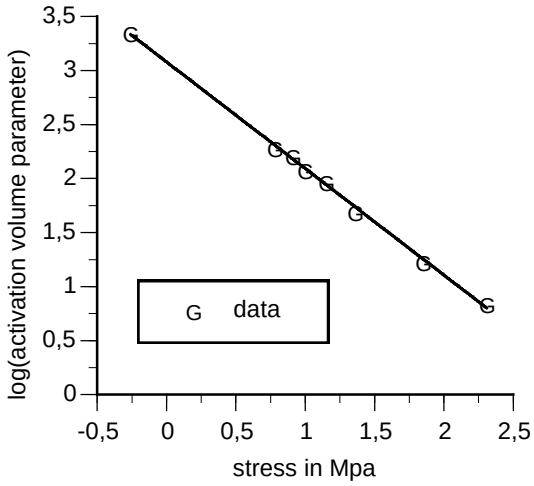

c. activation volume of dislocation movement in Mo; ----sinh-equation

a. activation volume of dislocation movement in Mo: T- data; ––– theory, eq,(2.5.3.1)

Fig. 2.5.6. Dislocation movement in Mo [1].

Fig.2.5.4. c. shows that also a mechanism exists with a constant value of φ in eq.(2.5.3.3). This does not only apply for polycrystalline material like Ni, but also occurs in other materials and in wood, for instance in a species with a wavy grain, as is measured by Kingston and Clarck and applies generally for wood for a dominating mechano-sorptive effect. The empirical laws only apply for high stresses because at low stresses there is no measurable mobility of dislocations and other jumping element, etc.

2.6. Liquid-solid transformations

As known, crystallization is the formation of crystalline solids from liquids. It occurs by nucleation of crystals and the growth of the nucleated particles. Because the theory is extended in B(2011), and in Section B.4, this former Section 2.6 is scratched at this place.

2.7. Short range diffusion

Because the (infinite) long wood-polymers only show structural changes by side bond breaking and not by breaking of primary bonds, transformations by long-range transport of atoms are not possible in wood. The transformations are determined by interface processes and only may show a short- range like transport. Examples are given in 2.2. Although these transformations apply for "Newtonian" substances, similar behavior is sometimes expected to be possible for polymers like wood, as also implicitly follows from the use of eq.(2.7.4). This thus has to be discussed. The short-range transformations show changes in the structure and no compositional changes. They occur by nucleation and diffusional growth. The interface controlled growth follows the kinetic equation as given in B(2011):

$$\frac{dR}{dt} = 2\nu R_c \cdot \exp\left(-\frac{E'}{kT}\right) \cdot \sinh\left(\frac{\Delta E'}{kT}\right) \approx \frac{2R_c}{h} \cdot \exp\left(-\frac{E'}{kT}\right) \cdot \Delta E' \qquad (2.7.1)$$

The growth rate then is constant at a fixed temperature and each dimension of the growing particle of the product phase increases linearly with time. Following [5], the transformation

can be regarded in the time interval $0 < \tau < t$. The increase of the number of nuclei per unit volume during the time $d\tau$ is: $(dN/dt)\cdot d\tau$ where dN/dt is the constant rate of homogeneous nucleation per unit volume. When the isotropic growth is not restrained by other particles, each nucleus, occurring at τ, grows in the time interval τ and t into a sphere of radius: $(dR/dt)\cdot (t - \tau)$. The extended volume V_e of all the nuclei thus is:

$$V_e = \int_0^t \frac{4\pi}{3}\left(\frac{dR}{dt}\right)^3 \cdot (t-\tau)^3 \frac{dN}{dt}\, d\tau = \frac{\pi}{3}\cdot\frac{dN}{dt}\cdot\left(\frac{dR}{dt}\right)^3 \cdot t^4 \qquad (2.7.2)$$

When the growing particles impinge on each other, a common boundary is formed and the growth over this boundary stops while the growth continues in the other directions. At an increase of time dt, the increase of the volume dV is only possible in the untransformed part. Hence: $dV = dV_e\cdot(1 - V)$ or upon integration: $\ln(1 - V) = - V_e$ or with eq.(2.7.2):

$$V = 1 - \exp(-V_e) = 1 - \exp\left(-\pi\frac{dN}{dt}\left(\frac{dR}{dt}\right)^3 \frac{t^4}{3}\right) = 1 - \exp\left(-k^n t^n\right) \qquad (2.7.3)$$

Calling the extent of the reaction Y, eq.(2.7.3) becomes:

$$y = 1 - \exp\left(-k^n t^n\right) \qquad (2.7.4)$$

what is identical to the empirical Johnson-Mehl-Avrami Equation.
Regarded by this derivation thus is not the transient stage of increasing rates, as applies for wood, but only the steady state stage of constant rates dN/dt and dR/dt which is not possible in wood and other cross-linked polymers. Also the end stage approaching equilibrium is not regarded and the equation thus is an approximation for homogeneous steady state behavior only.
Transformations initiated by a fixed number of randomly distributed pre-existing nuclei N_0 with a constant and isotropic growth rate have a V_e of:

$$V_e = N_0\frac{4\pi}{3}\left(\frac{dR}{dt}\right)^3 \cdot t^3 \text{ and thus: } Y = 1 - \exp\left(-4\pi N_0\left(\frac{dR}{dt}\right)^3 \frac{t^3}{3}\right)$$

and n of eq.(2.7.4) is n = 3. In fine-grained materials, nucleation occurs on the randomly orientated grain boundaries and n = 4 in the early stages of the transformation. When the grain boundaries are exhausted, nucleation ceases and there only is growth in one direction perpendicular to the grain boundary and n = 1 at a later stage. There also are other possibilities and possible values of n, mentioned in literature, which are:
For polymorphic transformations and recrystallization n = 4 at homogeneous nucleation and n = 3 for nucleation at pre-existing nuclei. The same values of n apply at randomly distributed heterogeneous nucleation sites. For nucleation at grain corners n = 4 and at a later stage n = 3 and for grain edge nucleation n = 4 and n = 2 at a later stage due to the two-dimensional growth on grain edges. Also for massive transformations therefore n = 2. For order-disorder transformations n = 3 for spherical grains of the ordered phase and n = 2 for disc-shaped ordered grains.

Transformations in wood are coupled with moisture content. At zero moisture content, only damage and decomposition may occur. Swelling is mainly perpendicular to the grain and n = 2 is what maximal can be expected, because there also is no nucleation. However, the moisture content is a linear parameter in the activation energy and volume. This means that the rate equation of a phase change will be volumetric with n = 1.
For reactions between water molecules between layers the behavior can be approximately Newtonian and is for instance:
$dV/dt = - C\cdot V$ or: $\pi\delta d(R^2)/dt = - C\cdot\pi\delta R^2$ or: $dR/dt = - C\cdot R/2$
having as solution: $R = R_0\exp(- C\cdot t/2)$.
Thus as well as the volumetric change as the change of the dimension R is dependent of

time t to the power one, or n = 1. Also at the start of the process, during the delay time, the change has this exponential form, what means that n = 1 during the accelerated and decelerated stage of the transient behavior. Because the transformations in wood, as cross-linked polymer, can not show a stationary stage, n is always n = 1. A measured value of n, different from 1 means that more processes than one are acting and the Johnson-Mehl-Avrami equation thus is a meaningless empirical power law equation for transient behavior and the exact method should be used with the tensor method to describe the behavior in all directions. From the separated measurements in the main material directions as well as the off-axis directions, the volumetric descriptions can be given by these unidirectional data.

2.8. Explanation of the empirical rate equations

All transformations may fit, at low driving forces, the empirical equation:

$$Y = 1 - \exp(-\,k^n t^n) \qquad (2.8.1)$$

where Y is the extent of the reaction thus mostly the fraction of transformed material and k and n are constants. The explanation of this equation is given in 2.7 and is given by eq.(2.7.4). For transient processes the value n looses its meaning and eq.(2.8.1) is nothing more than a power law equation. In any case, eq.(2.8.1) can be the basis for the derivation of other empirical equations for low driving forces. After differentiation and elimination of t, this equation can be seen to follow the differential equation:

$$\frac{dY}{dt} = n\cdot k\cdot(1-Y)\cdot\left(\ln\left(\frac{1}{1-Y}\right)\right)^{1-1/n} \qquad (2.8.2)$$

For small values of Y is: $\ln(1/(1-Y)) = \ln(1 - Y/(1-Y)) \approx Y/(1-Y)$ and eq.(2.8.2) becomes:

$$dY/dt = n\cdot k\cdot(1-Y)^{1/n}\cdot(Y)^{(1-1/n)} \qquad (2.8.3)$$

For large values of Y approaching Y = 1 closely, eq.(2.8.2) becomes:

$$dY/dt = n\cdot k\cdot(1-Y) \qquad (2.8.4)$$

because ln(X)/X approaches 1/X when X approaches infinity, and X = 1/(1 – Y) approaches infinity when Y approaches 1.
Eq.(2.8.4) is equal to eq.(2.8.3), when n = 1 is inserted. This agrees with the result found in 2.7 that at the end of every process n should approach n = 1.
Eq.(2.8.2) can be written:

$$\frac{dY/dt}{(1-Y)^{(1-\delta)}} = kn(1-Y)^{\delta}\cdot\left(\ln\left(\frac{1}{1-Y}\right)\right)^{(1-1/n)} = kn\left[(1-Y)^{\delta/p}\cdot\left(\ln\left(\frac{1}{1-Y}\right)\right)^{(1-1/n)/p}\right]^p$$

and the part between the square brackets can be expanded in the same way as done for eq.(2.5.3.4) giving:

$$\frac{dY}{dt} = \frac{dY'}{dt}\cdot\left(\frac{1-Y}{1-Y'}\right)^{1-\delta}\cdot\left(\frac{Y}{Y'}\right)^p \qquad (2.8.5)$$

$$\text{with: } \frac{dY'}{dt} = kn(1-Y')\left(\ln\left(\frac{1}{1-Y'}\right)\right)^{(1-1/n)} \quad \text{and} \quad p = \frac{Y'}{1-Y'}\cdot\left(\delta - \frac{1-1/n}{\ln(1-Y')}\right) \qquad (2.8.6)$$

Y' is the value of Y around which the expansion of the curve is made. It can be seen from eq.(2.8.6) that $p \approx 1 - 1/n$ when $Y' \to 0$, and $\delta \to 0$ when $Y' \to 1$, as found before. As for all power laws, the powers p and $1 - \delta$ depend on the part of the curve that is fitted, thus on the choice of Y'.
It now is shown, that the often used empirical equation eq.(2.8.5), (used with Y' = 0.5) that

fits the sigmoid curve of the transformations, is the same as eq.(2.8.1).
Equation (2.8.1) also can be written as a power law in time t, using the same expansion as given for eq.(2.5.3.4):

Thus: $1-Y=\left(1-Y_{t_0}\right).\left(\frac{t}{t_0}\right)^{-p}$ (2.8.7)

With: $p = k^n \cdot t_0^n \cdot n$

All empirical equations thus are different forms of the same equation eq.(2.8.1), which only applies for quasi Newtonian behavior and thus not for wood.

2.9. Conclusions about phase transformations

The extrapolation of the qualitative linear viscoelastic models of liquids and soft materials to wood-material, makes a discussion necessary of these models for the consequences. A theoretical derivation and correction of these models, based on the exact theory of molecular kinetics, thus is a first necessity. New theory is derived in chapter 2 about: nucleation and heterogeneous nucleation, (2.5), with the corrected "Tammann Hesse" equation, (2.6), and the explanation of other empirical nucleation equations, (2.5); further about the general diffusion equation of transformations, (2.3); the reaction order, (2.4); the activation volume parameters, (2.5); the power law (2.5); and the empirical power law rate equations, (2.8). As shown in 2, the phase transformation models of liquid-like materials, with proposed linear viscoelastic behavior only may apply for idealized "Newtonian liquids", and certainly cannot apply for a glassy and crystalline material like wood. In general, transformations models based on a free transport of structural molecules, can not be used for wood because the (infinite) long wood-polymers only may show structural changes by secondary side bond breaking. For wood only models based on the short range displacements are possible that only may give a structural change at an interface as a heterogeneous transformation. This diffusion at an interface is shown to follow the reaction equation as given in 2.3.

For wood, only diffusive transformations are possible, because the martensitic transformation will not occur in wood- and wood-products. Even when a martensitic configuration may exist in wood, the elementary crystalline fibrils in wood of 3 nm are too small to be able to build up high enough internal stresses for that transformation. A derivation of a general diffusion equation for all kinds of driving forces, eq.(2.3.5), is given in 2.3, showing that Fick's first and second law are not always applying special cases. Because for wood, diffusion occurs at interfaces, the diffusion equation gets the form of the monomolecular reaction equation, eq.(2.3.10).
It is shown in 2.4 that only first order reactions may occur in wood. A value of the order of one is also measured. The also measured slightly lower value than one indicates that there is another successive reaction. This second reaction can be regarded to be of zero order, because of the nearly constant reactant.
It is shown in 2.4.2 that the classical steady-state model and classical equilibrium model of nucleation are not right. The right basic equations for diffusion and structural changes are derived in B(2011) and in Section B.4. and should be used in stead.

As discussed in 2.5.1, the classical nucleation theory is not right and thus also wrong is, the thereupon based "Tammann Hesse"- equation (with its impossible negative driving force and the need of infinite energy to obtain equilibrium) that even is proposed to be the basic equation for all transformations and even for all time dependent behavior (including creep). The right nucleation theory shows that nucleation is just an example of a common structural change process. The other aspects also are derived as e.g. the explanation of heterogeneous nucleation, without needing the non-existent surface stresses in solids of the

classical theory, and e.g. the value of $\Delta S'/k = 2$ as boundary between the occurrence of a faceted and a diffused interface. It appears that the empirical Tammann Hesse equation, (eq.(2.6.5)), follows from a fit of limited ΔT values. When ΔT approaches zero this Tammann-equation does not apply but the sinh-form of eq.(2.6.3), showing the $dR/dt \approx 2CD(\Delta T)/a'$ for small ΔT values. It thus is necessary to replace the Tammann-Hesse equation by the exact equation, eq.(2.6.3), which follows from the special form of the activation volume parameter.

The "power law" equation is derived in 2.5.2 from first expanded terms of any equation. Thus, every equation can be written as power law-equation. By using the power law form, it is possible to compare and explain the power value n of eq.(2.5.3.4) of the different empirical equations with those of the exact equation, eq.(2.5.3.6), $n = \varphi\tau_0$ to get information on this activation volume parameter. It shows e.g. the special form of $\varphi\tau_0$ for nucleation, eq.(2.5.3.8) and eq.(2.6.3), etc.

To study properties as activation energy and volume of possible transformations in materials, a study of movement the free spaces (the activated sites) is possible that is the same for self-diffusion, creep, flow, rupture and transformations as melting. Creep and stress pulse experiments show all the possible forms of the activation volume parameter (2.5). Creep tests of wood show comparable values as found for other strong structural materials.

The derivation of the empirical Johnson-Mehl-Avrami equation (see 2.7) shows that this equation only applies for the steady state stage of the transformations and thus can not apply for cross-linked polymers like wood which cannot show a steady state stage, and the equation thus is a meaningless power law equation for wood. Also the other empirical rate equations are shown, in 2.8, to be related to this equation and to apply only for fictive Newtonian materials.

3. Thermal analysis of transitions and of decomposition of wood

3.1. Introduction

The general equilibrium theory of molecular transport kinetics, derived in [2], applies, by the same equation, for all time dependent processes. Thus applies for the thermo-mechanical behavior as creep and damage etc. [2], due to external and internal stresses and also applies for the processes due to high temperature alone, and due to the chemical or physical driving forces of transformations as for instance of glass-transition ([2] pg. 88), aging, nucleation, annealing [3], etc. This implies, that the incorrect model of a free volume change [3] to explain glass-transition has to be rejected and also the wrong nucleation theory and rubber-theory, [4], etc., as is discussed at 2 and appendices A and B.

All phenomena are explained precisely by one reaction-equation (correlation close to one for tests on the same specimen), and the differences between the processes are only due to different activation volume parameters.

To find the parameters for transformations, decompositions and some other structural change processes, by thermal analysis, the temperatures should be found where, the driving forces, or changes in bonding or molecular arrangements, will cause an aberration on the rate of temperature change of a specimen when the environment is heated (or cooled); see fig. 3.1. The driving force then is caused by a more or less abrupt change in the heat content. Such processes may exist in wood, occurring only at high temperatures after the first transformation and decomposition. At lower temperatures, the temperature-time and stress-time equivalence make it possible to detect other processes in wood that are too slow to be measured at common temperatures. The changes, occurring by these slow chemical reactions (or analogous physical processes), will depend on temperature, history, stress, etc. and are e.g. known as aging effects (see 4).

The techniques used in thermal analysis are:
- the differential thermal analysis (DTA) in which the temperature difference between a substance and a reference material (with known properties and no transitions etc. in that temperature range) is measured as a function of the temperature while both materials are subjected to a controlled temperature program.

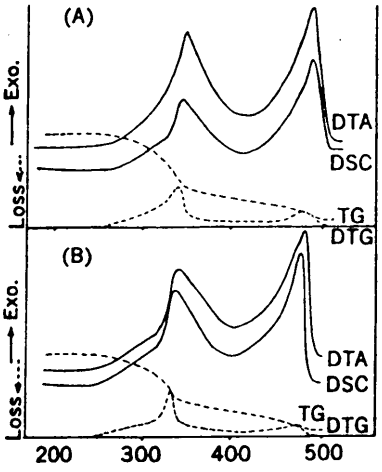

fig. 3.1.a. temperature in ^{0}C

DSC, DTA, TG and DTG
curves of wood (A Hinoki, B Katsura)
measured in air.
Heating rate: 10 ^{0}C-min. See [12].

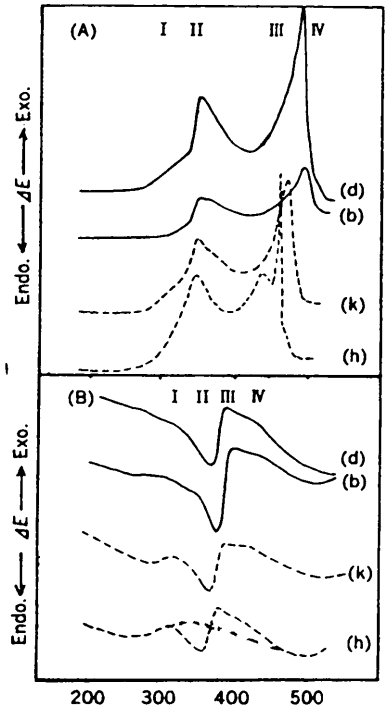

Temperature in ^{0}C

fig. 3.1.b. DSC curves measured in air,A, and in nitrogen B on Hinoki d, Akamatsu b, Buna k, Kusu h.

- the differential scanning calorimetry (DSC), being the same as DTA however instead of the temperature difference, the difference in energy inputs of both materials is measured.
- the thermogravimetry (TG) in which the mass of a substance is measured when subjected to a controlled temperature program (also gas evolution etc. can be measured). The derivative thermogravimetry (DTG) shows the same peaks as the other methods (see fig. 3.1.a).
- the thermodilatometry, in which the dimension of a substance is measured when subjected to the temperature program.
- the thermomechanical (non-oscillatory) and dynamic thermomechanometry where the static modulus and dynamic modulus (with damping) are measured as function of the temperature at a temperature program.
- Other physical properties as sound emission, acoustic wave behavior; optical, electric, magnetic, etc., characteristics also can be used.

3.2. Thermogravimetry of wood.

By thermogravimetry, the decomposition at transformations of wood mostly is determined by measuring the weight loss. However there also is a weight loss by drying or disappearance of filler material at heating and there also is bond breaking without weight loss. For wood, therefore TG as well as DSC is used. The enthalpy found and reported by these methods is only indicative because of:

the gas lost; the combustion of these gasses, determining also the reaction within the specimen; the successive and simultaneous reactions, giving overlapping peaks; the assumed wrong equation and driving force and wrong reaction order, (different from order one) for the determination of the activation enthalpy, assuming also that only one process is acting, giving e.g. apparent changing activation parameters with the extend of the reaction; the structural transitions in wood that only are possible after the previous, or at the same time acting decomposition reactions, etc. The peaks further may result from many influences, some of which are characteristic of the tests and sample holder assembly and not of the sample so that the measurements of all laboratories differ from each other. The wide range of reported activation energies, obtained by the different interpretations, equations and devices, thus is not astonishing. The results thus have no meaning unless they agree with the results of the thermo-mechanical method.

Because of the mentioned influence of the reaction of the gasses with air, the measurements in air have no meaning for the parameter estimation of transformations in wood. This should be done in an inert environment as in nitrogen and only these measurements, as given in fig. 3.1.b, thus should be discussed.
It is seen in fig. 3.1.b that endothermic melting and degradation causes the possibility of exothermic degradation, so that both processes are overlapping. In principle thus only one two-stage process is acting. (The first process creates the sites of the second process).

Important for the thermo-gravimetric analysis is the proof in 2, that all transformations follow one or two first order reactions that are not directly dependent on the overall concentration. This is not known and every analysis in literature is based on one reaction of a broken order or of even a higher order than one, giving wrong results. For wood, values close to order one are measured. The remaining small deviation from this order one indicates that another process is acting. In the past (see e.g. [10]) the fit of the data was done as wavy as possible, even following the small steering deviations. The resulting many very small peaks, (crinkles on the main peak), that are also influenced by the used test procedure and equipment of the thermo-gravimetric tests, were regarded as separate adjacent mechanisms. Mostly out of the many peaks, about 5 peaks where arbitrarily chosen to represent the degradation of: the filler mass and hemicellulose; crystalline cellulose; amorph cellulose; bonding by lignine; lignine products. This arbitrary split of a reaction into many forward reactions, with wrong activation energy parameters, leads to meaningless reaction orders between 0.6 and 4, and not existing enthalpies of the peaks between 38 and 175 kcal/mol. Further, as discussed before, wood is a co-polymer and thus will not show separate transition peaks of the different components. Changing the composition of wood by removing a component then will not result in a disappearance of the peak of that component but will shift the single peak of the co-polymer wood to lower temperatures. For instance, the peak of the DTG-curve, follows from the steepest slope of the TG-diagram of fig. 5.1. Wood does not show the peaks (steepest slopes) of the components and the peak of holocellulose (what is wood with removed lignin) shifts to a lower temperature. Thus, possible other peaks are due to enforced testing and damage and should not be associated with transformations of components, as is done e.g. in [16] by the multiple transitions model (of Huet).

Regarding gas evolution of wood powder, (i.e. of a destroyed chain structure, inferior to the structure of wood) the following description can be found in literature [7]:
At high temperatures, there always are chemical reactions also with air causing decomposition and pyrolysis. Below 100 ^{0}C (the boundary where bonded water is freed), only drying occurs and chemical reactions in filler material can be neglected up to about 150 ^{0}C. At that temperature, there is no disintegration but volatilization of wood extractives and probably of some low molecular weight lignin filler material. Between 150 and 200 ^{0}C the gas

formation starts of mainly CO_2 and CO, showing carbohydrate disintegration (probably by pyrolysis of filler material and non-structural lignin and hemicellulose). Above 200 ^{0}C, organic acids may evolve from the side groups of hemicellulose. Lignin degrades to produce aromatic compounds and a variety of low molecular gases. Above 280 ^{0}C the CO_2 and CO production goes down (thus showing the end of a peak) and combustible Carbohydrates (C_nH_m) are formed and the reaction becomes exothermic. Above 500 ^{0}C dissociation is noticeable by the start of strong hydrogen (H_2) formation that dominates above 700 ^{0}C. However, higher transition temperatures are found for less degraded test-material than the used milled powders.

3.3. Thermogravimetric analysis

The kinetic analysis is based on the general forward reaction equation eq.(2.4.1.12):

$$-\frac{1}{a}.\frac{dA}{dt} = kA^{n_a}B^{n_b}C^{n_c}$$

what is shown there to be, with $A = A_0 - X$:

$$-\frac{1}{a}.\frac{dA}{dt} = k'(A_0 - X)^{n_a+n_b+n_c}$$

with the conversion X and thus in general applies:

$- dA/dt = k''A^n$

The concentration A in this equation may be replaced by other linearly related variables as pressure or volume during a gas reaction or the loss in weight in a pyrolysis reaction. The equation can be written:

$\ln(- dA/dt) = n\cdot\ln(A) + \ln(k'') = n\cdot\ln(A) + \ln(\nu\cdot\exp(- E/kT)) = n\cdot\ln(A) + \ln(\nu) - E/kT$ and plotting $\ln(- dA/dt)$ versus 1/T for different temperatures at the same value of A, a straight line plot is obtained with a slope:

$d(\ln(- dA/dt))/d(1/T) = - E/k$,

giving the activation energy E. The order n of the reaction is supposed to follow from the slope of the straight line of $\ln(- dA/dt)$ versus $\ln(A)$ by:

$n = d(\ln(- dA/dt))/d(\ln(A))$.

However, this is not right because E also is dependent of A. As shown before the order of the reaction is always n = 1.

The basic kinetic transport equation for a forward and backward reaction, e.g. eq.(2.4.2.11), is, with reactant N and λA_a as activation volume, with constant λ_1:

$$- d(N\lambda A_a)/dt = 2\nu(N\lambda A_a)\cdot\exp(- E/kT)\cdot\sinh((\Delta E + f_e\lambda A_a)/kT) \qquad (3.3.1)$$

For Newtonian liquids, discussed in 2, $\sinh(x) \approx x$. For noticeable transformations in wood the driving force is high and $\sinh(x) \approx \exp(x)/2$ and eq.(3.3.1) becomes:

$$- d(N\lambda A_a)/dt = 2\nu(N\lambda A_a)\cdot\exp(- E/kT)\cdot\exp((\Delta E + f_e\lambda A_a)/kT) \qquad (3.3.2)$$

For a first order transformation there is an enthalpy and entropy change ΔE and the work of the (chemical) driving force is: $\Delta E = \Delta H - T\cdot\Delta S = f\lambda'A_a - f\lambda''A_aT$, while the work due to the stress of the surrounding elastic material on the activated site, $f_e\lambda A_a$, mostly is negligible. For decomposition at high temperatures, the product phase is determining for the driving force and because work is done at the surface of the product causing a molecular step increase of the product, the work $f\lambda A_a$ is, integrated, any moment, proportional to the amount of product, thus to the loss of weight, or to the concentration of sites of the product: $N_0 - N$ per unit volume. Eq.(3.3.2) thus becomes:

$$- d(N\lambda A_a)/dt = 2\nu(N\lambda A_a)\cdot\exp(- E/kT)\cdot\exp((c\cdot(N_0 - N)\cdot\lambda A_a)/kT) \qquad (3.3.3')$$

or because $N\lambda A_a$ is proportional to the active weight per unit volume w, this equation becomes general in the relative weight $W = w/w_0$:

$$- dW/dt = \nu\cdot W\cdot\exp(- E/kT)\cdot\exp(c_1\cdot(1 - W)/kT - c_2\cdot(1 - W)/k) \qquad (3.3.3'')$$

where $\lambda = \lambda' - \lambda''T$, by the enthalpic and entropic component of ΔE, is inserted. This equation can be given in the extent of the reaction: $y = (w_0 - w)/w_0 = 1 - W$:

$$- d(1 - y)/dt = dy/dt = \nu\cdot(1 - y)\cdot\exp(- E'/kT)\cdot\exp(c_1 y/kT - c_2 y/k) \qquad (3.3.3)$$

With the dynamic method, by heating the specimen at a constant rate, it is possible to detect all existing transition peaks successively.

Heating a specimen at a heating rate $1/\alpha$, the time t of the increase of the absolute temperature from zero to T, follows from $t = \alpha T$ and the rate of weight loss is:

$$dW/dt = dW/\alpha dT = - dy/\alpha dT$$

This leads for the first order reactions in wood to:

$$dy/dt = dy/\alpha dT = \nu\cdot(1 - y)\cdot\exp(- E/kT)\cdot\exp(c_1 y/kT - c_2 y/k) \text{ or:}$$

$$dy/dT = \alpha\nu\cdot(1 - y)\cdot\exp(- E/kT)\cdot\exp(c_1 y/kT - c_2 y/k) \qquad (3.3.4)$$

At the top of the peaks of the rate plot, thus at the maximal rate, is: $d^2y/dT^2 = 0$ or:

$$\alpha\cdot\nu\cdot\exp(- E/kT)\cdot\exp(c_1 y/kT - c_2 y/k)\cdot[- dy/dT - (1 - y)\cdot d(E/kT)/dT +$$
$$+ (1 - y)\cdot d(c_1 y/kT - c_2 y/k)/dT] = 0, \text{ or:}$$

$$- dy/dT = (1 - y)\cdot d(E/kT)/dT - (1 - y)\cdot d(c_1 t/kT - c_2 y/k)/dT \qquad (3.3.5)$$

In this equation is $d(E/kT)/dT = d((H - ST)/kT) = - H/kT^2$

and: $d(c_1 y/kT - c_2 y/k)/dT = (c_1/kT)\cdot dy/dT - c_1 y/kT^2 - (c_2/k)\cdot dy/dT$

and eq.(3.3.5) becomes:

$$dy/dT\cdot(1 - (1 - y)\cdot c_1/kT + (1 - y)\cdot c_2/k) = (1 - y)\cdot(H/kT^2 - c_1 y/kT^{2)} \quad \text{or:}$$

$$\frac{1-(1-y)\cdot c_1/kT+(1-y)\cdot c_2/k}{H-c_1 y}\cdot\nu\cdot\exp\left(-\frac{E}{kT}+\frac{c_1 y}{kT}-\frac{c_2 y}{k}\right)=\frac{1}{\alpha kT^2}$$

or in molar quantities, where R is the gas constant:

$$\ln\left(\frac{1-(1-y)\cdot c_1/RT+(1-y)\cdot c_2/R}{hN_a(H'-c_1 y)}\cdot\nu\cdot\exp\left(\frac{S}{R}-\frac{c_2 y}{R}\right)\right)-\frac{H'}{RT}+\frac{c_1 y}{RT}=\ln\left(\frac{1}{\alpha RT^2}\right)$$

Because the left term is not noticeable dependent on the peak-temperature T and on the peak value y, is: $c_2 T >> c_1$ and $c_1 << H'$ and $c_2 << S$, thus is:

$$\ln\left(\frac{1+(1-y)\cdot c_2/R}{hN_a H'}\cdot\nu\cdot\exp\left(\frac{S}{R}-\frac{c_2 y}{R}\right)\right)-\frac{H'}{RT}+\frac{c_1 y}{RT}=\ln\left(\frac{1}{\alpha RT^2}\right) \qquad (3.3.6)$$

and testing at different rates α, in a sufficient small range of 1/T to neglect the differences of the peak values y at the different peak-temperatures, T gives:

$$\frac{d\left(\ln\left(1/\alpha RT^2\right)\right)}{d\left(1/T\right)}=-\frac{H-c_1 y}{R}\approx-\frac{H}{R} \qquad (3.3.7)$$

For wood and wood-products, the term $c_1\cdot y$ in this equation will not have a negligible influence on the mean value H as is shown below.

In [12], thermogravimetric and differential scanning calorimetry measurements of wood are given (see fig. 3.1). It can be seen from the data in fig. 3.1.b in nitrogen that there is an endothermal melting peak of possible melting and endothermal decomposition of the crystallites, immediately followed by exothermic decomposition that overlaps the melting. The onset of the exothermal process may even start before endothermic melting (as given by curve k in (B) of fig. 3.1.b) and it is clear that both processes interact and are overlapping making it impossible to locate the true peaks. The shoulders (peak I and IV) have no meaning, not only because the intensity is too small for a noticeable contribution, but because the base-line of the graph is wavy instead of horizontally, as in all other investigations in the past. Thus only peak II and III give the occurring endothermic and exothermic reactions, showing about the same activation energy because of the overlapping. The found enthalpies by the DSC-method, $H - c_1 y$ (eq.(3.3.7)) of the peaks, at about $y = ½$, are 43 to

49 kcal/mol. The TG-method, did mainly show the second process with lower values of 23 to 30 kcal/mol for the equivalent peaks. All these enthalpy values are comparable with those obtained by thermomechanical measurements at lower temperatures of creep- and strength tests (see e.g. chapter 9.1 of [2]). The lower TG-values of the enthalpy with respect to the second process, measured in [13], is also due to a too high heating rate with respect to the long delay time of the processes. This second process was found in [13], by more precise (non-dynamic) isothermal thermo-gravimetric measurements in that temperature region. The measurements were done at different temperatures, in an inert environment, using flowing nitrogen. Eq.(3.3.4) can be written for this case:

$$\ln\left(\frac{dy}{dt}\right) = \ln\left(\nu\cdot(1-y)\exp\left(\frac{S}{k}-\frac{c_2 y}{k}\right)\right) - \frac{H-c_1 y}{kT} \qquad (3.3.8)$$

showing a straight-line plot of ln(dy/dt) versus 1/T, at the same conversion: y, at the different temperatures (see fig. 3.2). Eq.(3.3.8) is always applied in literature with the assumption that $c_1 = c_2 = 0$, and not with the order n = 1, thus according to eq.(3.3.9).

$$\ln\left(\frac{dy}{dt}\right) = \ln\left(\nu\cdot\exp\left(\frac{S}{k}\right)\right) + n\cdot\ln(1-y) - \frac{H}{kT} \qquad (3.3.9)$$

what wrongly leads to changing values of H and n and a value of n, different from n = 1. In table 3.1, the measured activation energies according to eq.(3.3.9) for each value of y are given with the theoretical values of eq.(3.3.8) that is drawn through the points y = 0.4 and 0.8. In fig. 3.3 the measurements are given. The good fit of the theory for cotton shows that clearly one process is acting. It can be seen by the kinked lines of pine craft of fig. 3.3a, (even the line of 342 ^{0}C shows a kink) that 2 processes are acting. This also is shown in table 3.1, where the dominating process, at the end of the reaction, shows a constant activation energy of 35.4 kcal/mol while the first process has the same properties as for cotton. Further, it also follows from the apparent value of the reaction order n, when one process is assumed to act instead of two. For bleached pine kraft, n of eq.(3.3.9) is measured to be:
n = 0.39 (0.95) at 268.1 ^{0}C
n = 0.48 (0.84) at 285.7 ^{0}C and
n = 0.70 (0.84) at 303.7 ^{0}C,

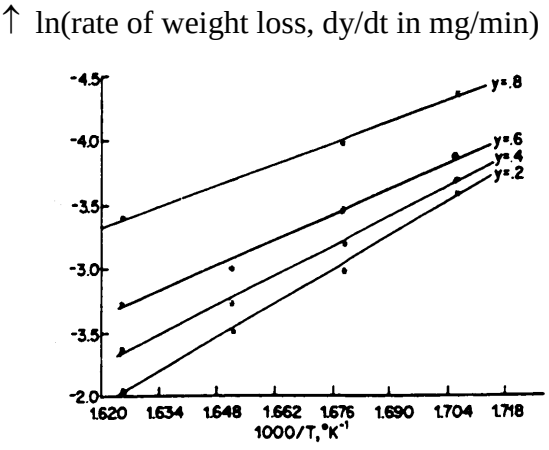

fig. 3.2. Isothermal differential logarithmic plot of rate of weight loss dy/dt in mg/min. vs inverse temperature for bleached pine kraft pulp [13]

Table 3.1. Measured and theoretical activation energies for cotton linters pulp and for bleached pine kraft.

Extent of the Reaction: y	Activation energy in kcal-mol cotton measured	cotton theory	pine kraft measured	
0.1	42.8	39.1	56.3	
0.2	36.9	36.9	51.3	
0.3	33.9	34.6	45.7	
0.4	32.3	32.3	41.9	
0.5	29.4	30.0	37.8	
0.6	27.5	27.7	36.4	
0.7	25.1	25.4	35.4	⎤
0.8	23.2	23.2	35.0	⎥ mean 35.4
0.9	20.2	20.9	35.8	⎦

thus showing at least two processes to be present of order zero and of order one. The values in brackets are for the plots at conversions above 0.6, showing mainly the influence of the second process thus mainly the influence of one process and thus showing the order approaching one. For Cotton linters, the true order n = 1 was measured, showing that only one process is acting.

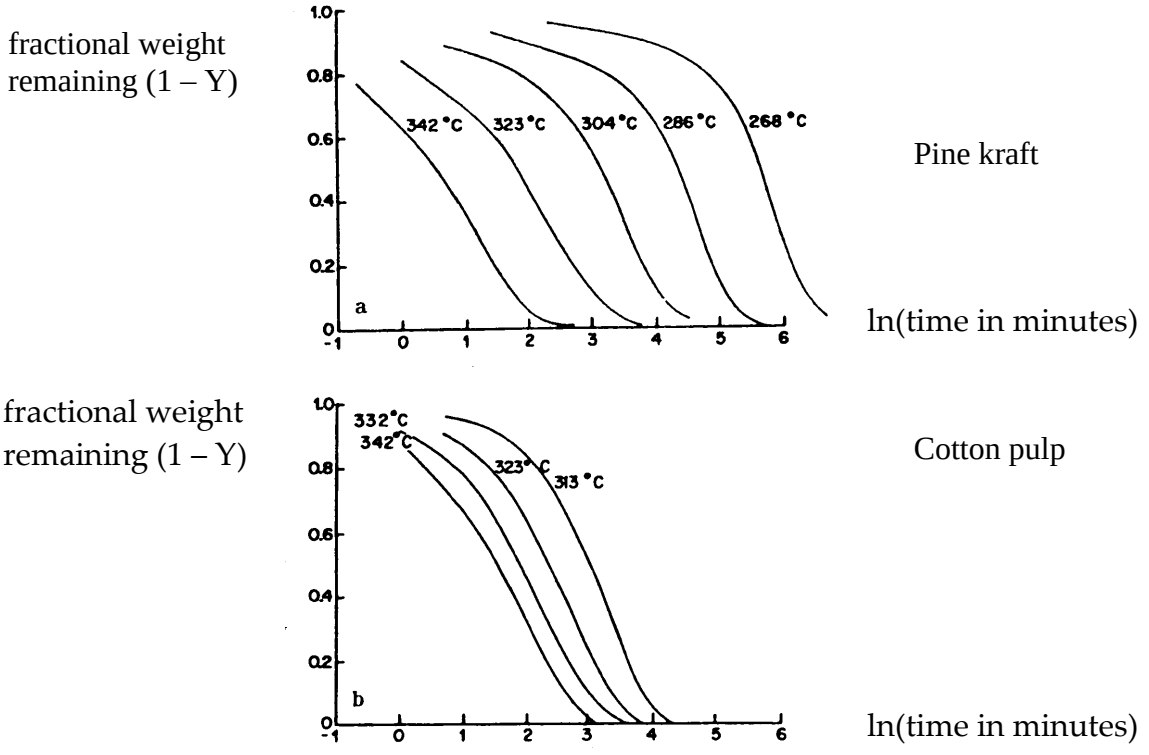

fig. 3.3. Measurments of a) bleached pine kraft and b) cotton linter pulp [13].

The solution of the theoretical equation eq.(3.3.8) may show a long delay time, before the process becomes noticeable. It appears that for wood during this delay time an other (first order) process is acting, (that produces the sites of the second process), with a nearly

constant reactant, and thus can be regarded as a quasi zero order reaction. This system was confirmed, by the thermo-mechanical method in [2], to be present for creep and damage processes in wood at low temperatures.

3.4. Powder collapse method

Conclusions, in literature, about "low" transition temperatures of wood and the constituents of wood, as cellulose, lignin and hemicelluloses, are also based on the investigations by the powder collapse method, what thus need to be discussed.
A powder of the material is compressed under constant load in a glass capillary and the thermal softening point is determined as the temperature at which the powder collapses into a solid plug. This temperature is dependent on the applied stress thus is not a real glass transition temperature. Further, friction of the powder particles is due to formation of a new type of side bonds at the former broken bonds by grinding and the collapse is due to this type of side bonds only. By the isolation of the components of wood, the physical and chemical properties may change strongly. Cellulose is strongly degraded by the common delignifying agents. However by nitration, with help of non-degrading acids, undegraded cellulose nitrate can be obtained. But, as mentioned before, this gel has, as other cellulosic products, totally different properties from in situ wood cellulose.
Also lignin changes, not only physically, by isolation with solvents. For instance, Periodate lignin (showing still a high softening temperature $T_S \approx 200\ ^0C$ in the powder collapse test) has lost methoxyl groups. This change also depends on the type of solvent. For instance, liquid ammonia reduces the plastization temperature of isolated lignin from:

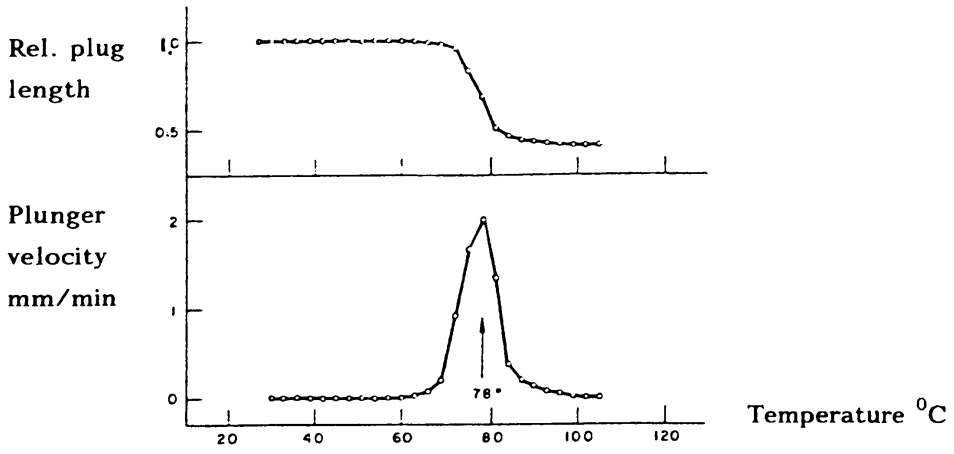

fig. 3.4. Relative plug length and plunger velocity vs. temperature for aspen dioxane lignin (m.c. 7.2 %) in the powder collapse test [11].

+ 125 ^{0}C to - 30 ^{0}C and enters in the cellulose crystallites modifying the lattice. Milled wood lignin is chemically the closest to native lignin. However, the molecular weight is only 11000 while native lignin has an undetermined high molecular weight.
The low value of the molecular weight of isolated lignin and hemicellulose has influence on the softening temperature. Spruce dioxane lignins (obtained by dioxane as solvent), showing the lowest lignin softening temperature T_S, shows an increase of this temperature from $T_S = 126\ ^0C$ at a molecular weight of M = 4300 to $T_S = 176\ ^0C$ at a molecular weight of M = 85000. From these powder collapse tests, the following tendency of the influence of M on T_S can be derived:

$T_S \approx 400 + 5.8 \cdot 10^{-4} \cdot M$ (with M < 190000 and T_S in degree Kelvin), (3.4.1)

predicting a molecular weight of M = 190000 to be the value, where above the chain length has no further influence on T_S in the powder collapse tests, because: T_S < 510 K = 240 ^{0}C. This follows from tests on dry wood powder, showing only one softening peak at about 220 to 240 ^{0}C, the same as for lignin, the lignin-hemicelluloses complex, as well as for cellulose. This is confirmed by tests on pulps (cellulose), holocellulose (= cellulose + hemicellulose) and birch wood with removed xylan (thus removed hemicelluloses), showing all the same high value of T_S in the dry state. The reason of one and the same T_S for all components and co-polymers is certainly due to the collapse of the grain structure by side-bond failure and degradation of the locally high loaded grain particles by splitting of the OH-side bonds making plastization possible. The high weight loss (~ 35%) at the high testing temperatures shows that decomposition is an accompanying phenomenon of this softening. This behavior of the wood powder test agrees with the results discussed later concerning the modulus of elasticity, the strength, thermal expansion, and the specific heat, all indicating that dry wood does not show a transition up to the high temperature of degradation. Because from wood extracted lignins and hemicelluloses are polymers with a low molecular weight (m.w.), the moisture dependency of the softening temperature T_S' is comparable with all other types of low m.w. polymers giving:

$T_S' \approx T_S - 550 \cdot \omega$ ($\omega < \omega_S$, for extracted lignins and hemicelluloses) (3.4.2)

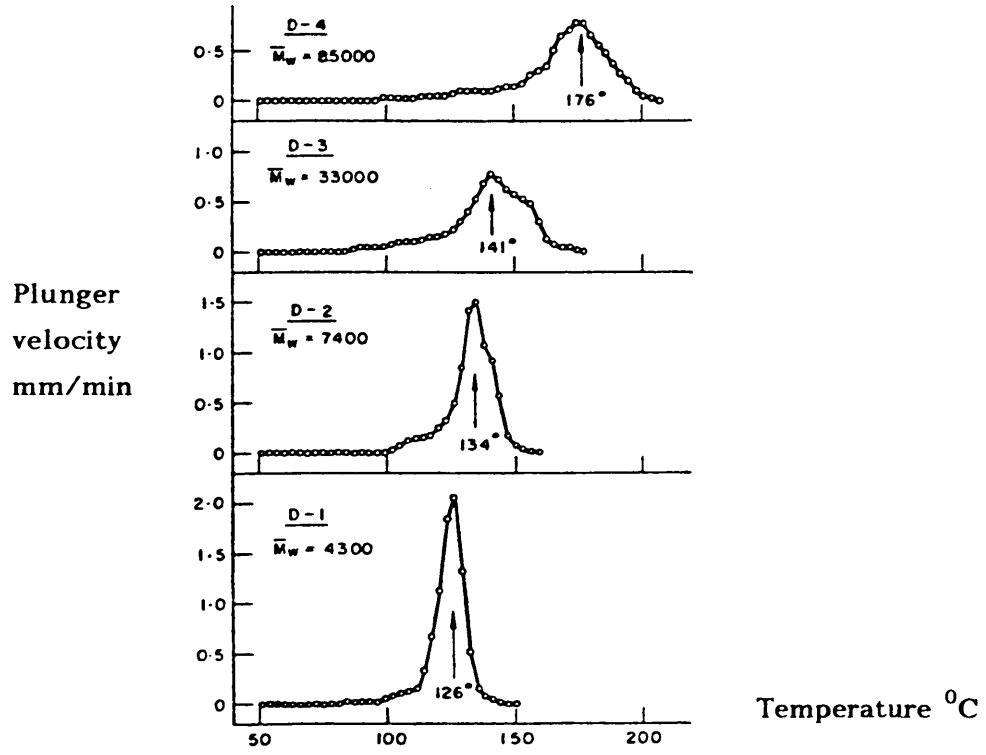

fig. 3.5. Influence of increasing molecular weight on the softening temperature of spruce dioxane lignins [11].

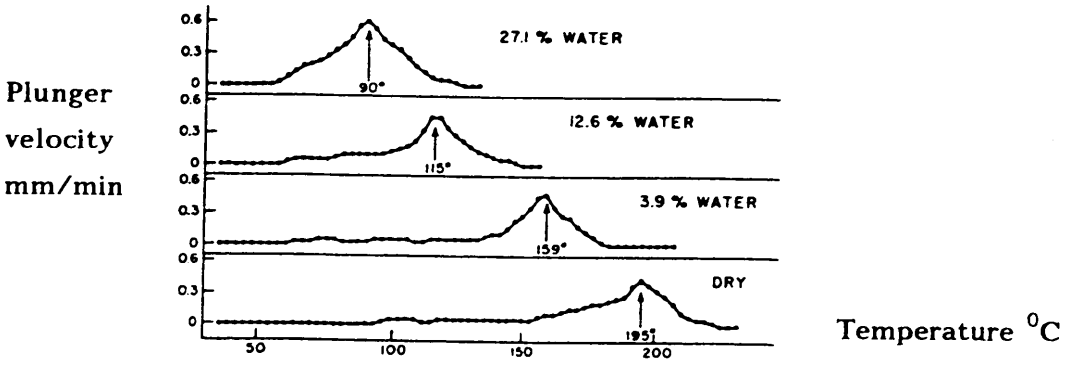

fig. 3.6. Influence of moisture content on the softening temperature of spruce dioxane lignins [11].

explaining the measured low transition temperatures of the components (fig. 3.6). Contrary to the general assumption in literature, the layers containing lignin and hemicelluloses don't show a behavior according to heterogeneous blending, by showing the same transition temperatures for the mixtures as for the separate components. If this was the case, the transition temperatures would be 20 ^{0}C and 70 ^{0}C for wet (resp. hemicellulose- and lignin-) layers and would be 150 ^{0}C and 210 ^{0}C for the dry state, as is measured for these components by N. Takamura, according to eq.(3.4.2) and similar to fig.(3.6). This is not occurring for wet intact wood powder and also dry wood only shows one transition temperature 220 ^{0}C, showing bonded chains to be present in the powder grains. The mixture thus behaves homogeneously similar to solutions, or alloys or copolymers, thus showing bonded

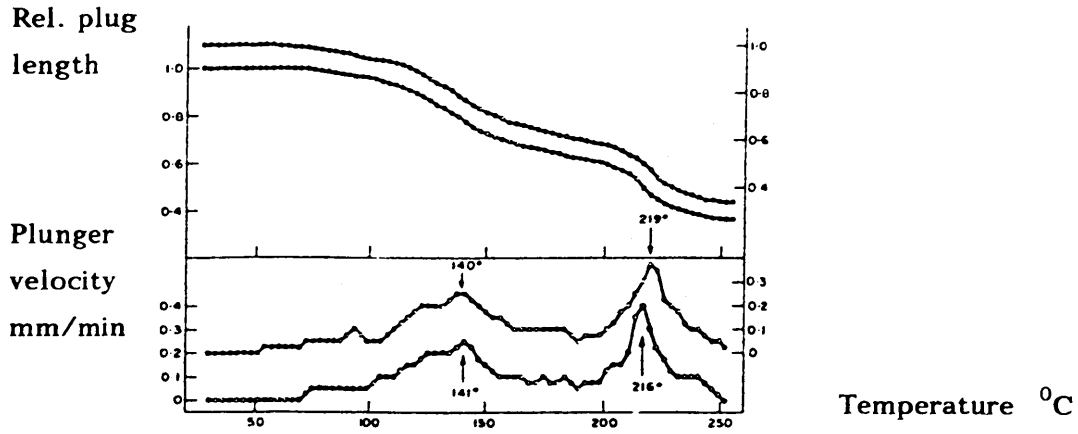

fig. 3.7. Twin curves, of the two softening points in wet spruce wood powder (Relative air humidity above 95%) of the non-structural filler material (140 ^{0}C) and of the wood co-polymer (219 ^{0}C) [11].

lignin and hemicellulose chains. The additional peak at 140 ^{0}C in Fig. 3.7 of wet spruce powder at 23% m.c. (R.H. of the air above 95%) is due to the moisture dependence of the activation volume of loose filler material, thus due to the relatively short polymers in the powder. This influence is confirmed by tests on wet kraft pulp (cellulose) powder that may show a similar just noticeable transition peak (around 140 ^{0}C) as for wood powder, when there is a higher pentosan (a non-structural linear hemicellulose) content. The powder collapse tests show the importance of the molecular weight and moisture content on the softening temperature. Because of the low molecular weight and frictional bonds, the behavior is not comparable with that of solid wood.

3.5. Dielectric properties

Dielectric dispersion, may sometimes give information on the mechanical behavior of materials. For wood however, this is not the case. The dielectric behavior, only may show mechanical properties when the side bonds are dipoles and dipole motion is possible by rotation of side groups. Several polymers for instance of the methacrylate series do show this by the same activation energies of ~ 24 kcal/mol, for dielectric relaxation and for mechanical relaxation. For wood, this is not possible because in cellulose the OH-groups are symmetrical attached and are dielectric neutral. The straight cellulose chains in wood prevent non-symmetrical binding of water, contrary to the cellulose types of plants (cotton, starch, etc.) where this is possible. Lignin also is neutral because of the random orientation of the OH-groups. Dielectric measurements show other processes than found by mechanical testing and the much lower activation energy indicates that it only gives information on the special water-structures at the free surfaces of wood that still are present in dry wood, and determine only apparent dielectric properties of wood. The dielectric constant of water: $\varepsilon_w = 81$, while ε of wood is about: $\varepsilon = 2$. For the lightest wood species $\varepsilon \approx 1$ and ε of these species may approach $\varepsilon_w = 81$, when saturated with water. As expected from the dependency of the activation energy on the moisture content, and as is measured, the logarithmic blending rule applies for the influence of the moisture content on ε. In the neighbourhood of a peak in the dielectric loss tangent: tan(δ) however, the influence of water is higher than according to this rule, showing an additional resonance behavior, e.g. at the peak in fig. 2 of [16]. This resonance peak, around 10^7 Hz is the same for wood, cellulose and lignin (see fig 6.125 of [9]), and is also found in other materials as in paper and rubbers and even in dielectric neutral materials, because ions at grain boundaries and pores may provide with water molecules the same structures as found in wood. This peak disappears when the water is removed and it also disappears in pressed wood, (see fig. 6.123 of [9]), because then the pores are closed by the pressing, reducing the free surfaces. Thus the

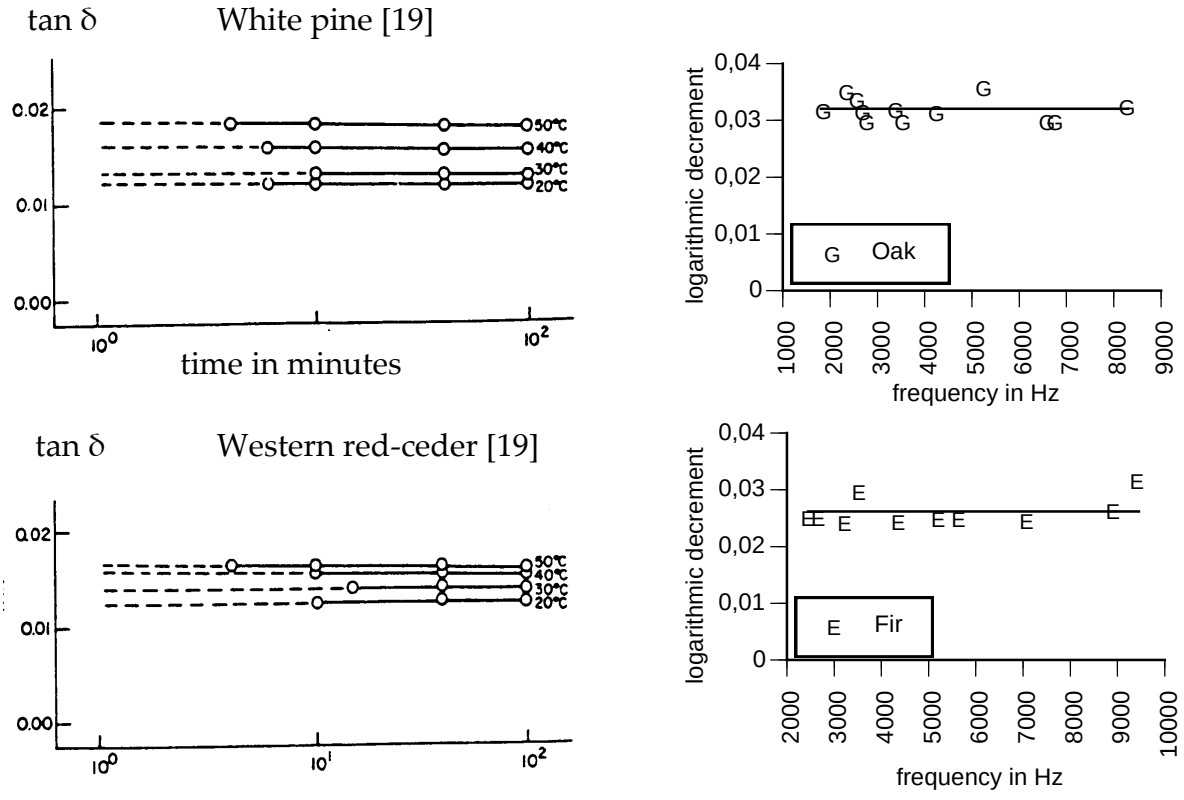

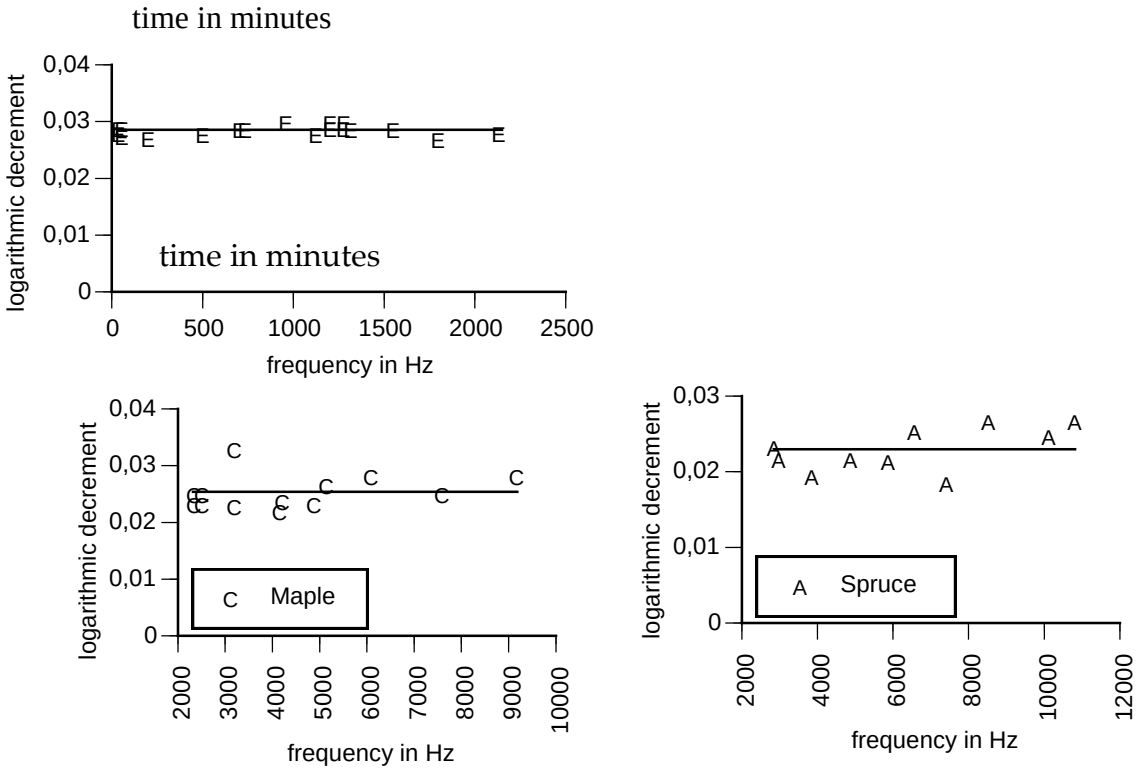

fig. 3.8. Internal friction.

peak around 10^7 Hz has no influence on the mechanical properties and has nothing to do with a transformation, as is stated in [16] and in mentioned EC and RILEM publications, but is simply the resonance peak at the eigen frequency of the water dipole resonator. This mechanism thus only can be noticed at this high frequency of 10^7 Hz. The high frequencies also cause heating of the water by molecular friction due to the oscillations what is used for kiln drying of steam permeable species of wood.
The measured overall dielectric tan(δ), outside the peak value, of "dry" wood is totally different in the different investigations. In the investigation of Brake and Schutye of oven dried wood at 20 ^{0}C, see fig. 6.123 of [9], a decrease of tan(δ) with increasing frequencies between 10 and 10^5 Hz is measured, while the investigations of Kroner (see the older German publication of [9] of real dry wood) there is strong increase of tan(δ) up to the top near 5.10^6 Hz. In fig. 2 of [16], there is a decrease until 10^3 Hz and an increase above 10^3 Hz (indicating that this 'dry' wood has a m.c. of about 4%. The real, right value of tan(δ) of wood follows from mechanical testing, showing (as common for glasses) a, constant, loss tangent, tan(δ), and logarithmic decrement Δ (≈ π·tan(δ)), at common temperatures, in the whole, technical frequency range of about 10^{-5} to 10^4 Hz, (see fig. 3.8), depending on the loading level. Only at very high loading levels, additional damage peaks may occur.
This constant value of tan(δ) is explained by the theory (see [2], pg. 96 to 100), as a consequence of the special property of the activation volume. The same property explains the time-stress and time-temperature equivalence of processes in wood.

4. Aging of wood

4.1. Measured aging

For the structural use of wood, transformations play no role. At common temperatures, loading levels and moisture contents there is no indication of any transformation and there

thus also is no aging or change of crystallinity, chemical changes, or change of concentration of flow units (determining creep etc.) during very long times. Long term loaded wood

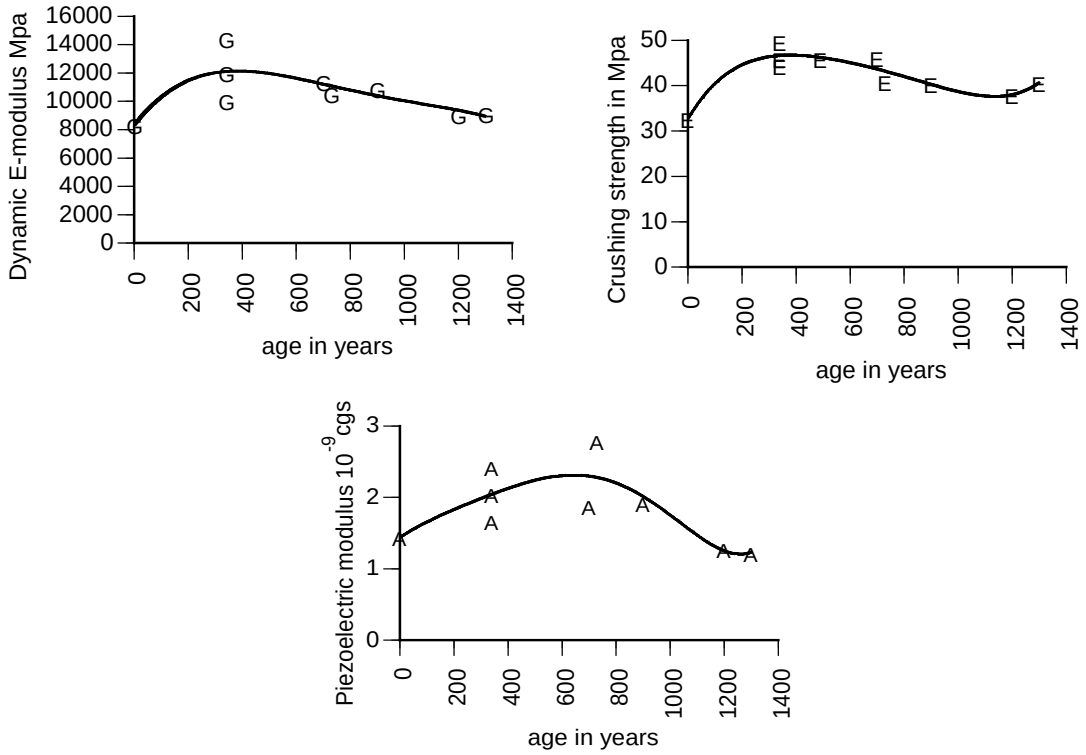

fig. 4.1. Change of strength, dynamic Young's modulus and piezoelectric modulus with time of old Japanese cypress wood [9]

(Hinoki) of old Japanes temples, did show an increase of strength during the first 400 years and then a slow decrease during the next 1000 years, due to a process of increase of crystallinity and a slower process of decomposition of cellulose (see fig. 4.1.). This follows from a piezoelectric shear modulus that shows the same behavior and from the X-ray diffraction patterns being sharper for 350 years than for 8 years old wood and being diffuse for 1400 years old wood, indicating the decrease of crystallinity although the strength and stiffness still was higher than for 8 years old wood. Aging of wood at normal conditions and low stresses thus is extremely slow and the changes at common times are not noticeable. If not neglected, a net strength increase, at low or zero stresses, could be accounted for of about 1 % in 10 years (during the first 400 years) at common temperatures (indicating the common creep value of the activation volume parameter of this kinetic process of n = 33).

4.2. Measured accelerated aging of wood

Accelerated "aging" tests at high temperatures (115 to 175 ^{0}C, at a moisture content of about 5%) are e.g. given in [14]. The rate of deterioration of wood, by isothermal heating during some time, was measured by the decrease of weight, the decrease of the modulus of elasticity and the decrease of strength. The decrease of bonds is proportional to the weight loss and the loss of strength. The "strength" or work to failure $f \cdot \lambda A$, thus is proportional to the residual bonds thus proportional to the residual weight w (or energy in the DSC-method) and thus to the concentration of the reactant.
The strength reduction equation, eq.(3.3.2), thus becomes:

$$-\frac{d(N\lambda A)}{dt} = \nu N\lambda A \cdot \exp\left(-\frac{E'}{kT}\right)\cdot\exp\left(\frac{cN}{kT}\right) \qquad (4.1)$$

with E' = E - ΔE and f·λA = cN or in general:

$$-\frac{dW}{dt} = \nu W.\exp\left(-\frac{E'}{kT}\right).\exp\left(\frac{c_1 W}{kT} - \frac{c_2 W}{k}\right) \qquad (4.2)$$

or given in the extent of the reaction: $y = (w_0 - w)/w_0 = 1 - W$:

$$-\frac{d(1-y)}{dt} = \frac{dy}{dt} = \nu\cdot(1-y)\exp\left(-\frac{E'}{kT}\right)\cdot\exp\left(\frac{c_1(1-y)}{kT} - \frac{c_2(1-y)}{k}\right) \qquad (4.3)$$

Integration gives:

$$y = 1 - \frac{E_1^{-1}\left(E_1\left(c_1/kT - c_2/k\right) + \nu t\exp\left(-E'/kT\right)\right)}{c_1/kT - c_2/k} \qquad (4.4)$$

where E_1 is the exponential integral and E_1^{-1} is the inverse of the exponential integral.
Eq.(4.4) only applies as long as the driving force is high. Integration of the general sinus-hyperbolicus equation that also applies in the end state gives as solution a row of exponential integrals. However, for very low driving forces a simple approximate solution is possible for fitting and parameter estimation.
Eq.(4.4) shows that damage increase at the start can be very small and may suddenly increase to failure at the end of the lifetime.
For comparison with test results and analysis in literature, an approximate solution of eq.(4.3), called integral method, based on a constant driving force, has to be used. Thus:

$$\int\frac{dy}{1-y} = \nu\cdot\exp\left(\frac{-E'}{kT}\right)\cdot\exp\left(\frac{c_1(1-y/2)}{kT} - \frac{c_2(1-y/2)}{k}\right)\cdot\int dt$$

where for each value of y, the mean driving forces $c_1(1 - y_m)$ and $c_2(1 - y_m).T$ are used, according to the always so applied integral method of literature.
Integration of the last equation then gives:

$$-\ln(1-y) = t\cdot\nu\cdot\exp\left(\frac{-E'}{kT}\right)\cdot\exp\left(\frac{c_1(1-y/2)}{kT} - \frac{c_2(1-y/2)}{k}\right)$$

with $y_m = y/2$, so that:
$\ln(\ln(1/(1-y)) = \ln(t) + \ln(\nu\cdot\exp(S/k)) - H/kT - c_2(1 - y/2)/k + c_1(1 - y/2)/kT$
This can be written:
$\text{Log}(t) = \log(\ln(1/(1-y))) - \log(\nu\cdot\exp(S/k) + (H/kT + c_2(1 - y/2)/k +$
$- c_1(1 - y/2)/kT)/2.3$
The time t is in seconds, when written in days t_d , the equation becomes:
$\text{Log}(t_d) = -4.94 - \log(\nu\cdot\exp(S/k)) + \log(\ln(1/(1-y))) + 0.4343c_2(1 - y/2)/k +$
$+ 0.4343(H/k - c_1(1 - y/2))/T \qquad (4.5)$
To fit this equation, two measured points y = 0.1 and y = 0.5 of [14] are used:
$\text{Log}(t_d) = -4.94 - 9.8 + \log(\ln(1/(1-y))) + 2.02(1 - y/2) +$
$+ 0.4343(16736 - 3074(1 - y/2))/T$ or:
$\text{Log}(t_d) = -14.74 + \log(\ln(1/(1-y))) + 2.02(1 - y/2) + (5933 + 667.5\ y)/T$
$= C_1 + C_2/T$ for each value of y.
From this fit follows: H/R = 16.736 or: H = 2·16.736 = 33.5 kcal/mol.
The apparent values for y = 0.1 and 0.5 are: 2·(16.74 - 0.95·3.07) = 27.6 kcal/mol.
resp. 2·(16.74 - 0.75·3.07) = 28.8 kcal/mol.
For the loss of weight and reduction of the modulus of elasticity at y = 0.05 (the 95 % survival boundary), activation enthalpies of 28.9 kcal/mol resp. 29.3 kcal/mol follow from the data. The measured values predict a 5% loss of the weight at 30 ^{0}C after 20000 years. For a

5% loss of the modulus, at 30 ^{0}C, 32000 year is predicted. A 5% loss of the strength will occur in 1300 years at 30 ^{0} C because of the low activation energy at the start. These reductions, by heating alone as driving force, are orders lower than the reduction found in 4.1, according to the descending branch of aging at normal climatic conditions with changing temperatures and moisture contents and at the common low stress-levels of old buildings. In [10] results of isothermal thermo-gravimetric measurements are given, between 93.5 and 280 ^{0} C with the Arrhenius plot, based on the first order reaction equation:
dW/dt = - kW, that may apply outside the delay time. The given plot shows an activation

Table 4.1. Measured and theoretical activation energy parameters of wood

	C_1		C_2	
y	measured	theory	measured	theory
0.05	13.94	14.06	5925	5966
0.1	13.80	13.80 ----	6000	6000 ---- chosen fit
0.2	13.75	13.57	6063	6067
0.3	13.55	13.47	6150	6134
0.4	13.45	13.42	6202	6200
0.5	13.39	13.39 ----	6267	6267 ---- chosen fit

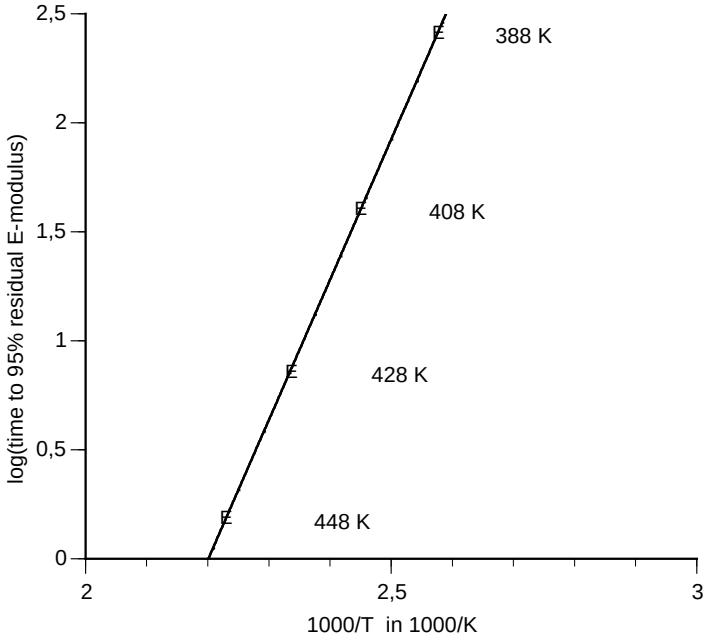

fig. 4.2. Time to attain 95 % residual modulus of elasticity, depending on temperature T (in degrees Kelvin) of 6 species of each 7 specimen [14]. Similar perfect straight lines, according to eq.(3.2), apply for the residual weight and residual modulus of rupture.3.35 years at 100 ^{0} C).

enthalpy of 28,3 kcal/mol. Reported for boards is 29.5 kcal/mol.
These results confirm the found values above of [14].

Also mentioned in [10] is the occurrence of a second process in thick specimens (see fig. 4.3). This process with a higher activation energy than the first process occurs at lower temperatures, showing that there is a high internal stress. The same also was found in [2] (pg. 79) for relaxation at 40 ^{0}C of wet wood and for the compression strength ([2], pg. 51)

and for creep ([2], pg. 54) at room temperature. The same activation energy of about 41 kcal/mol was also found by the DSC-method (see 3.3, lowest peak).

Determining for aging, at common temperatures, are the damage processes due to mechanical loading and not the transformations due to the chemical forces. Based on the data of the temples, mentioned above, the 95% lifetime prediction thus should be based on 2

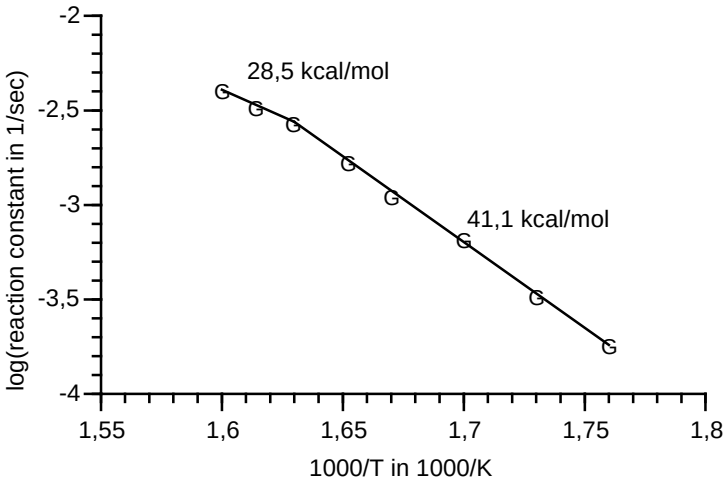

fig. 4.3. Arrhenius plot of thermal degradation of yellow pine [10].

dominating processes due to loading. One process of a strength decrease and one process of strength increase (by the increase of crystallinity due to loading). The high glassy value and the exact fit according to the Arrhenius law, even at higher temperatures (115 ^{0} to 175 ^{0} C) of the modulus of elasticity, shows the main constituents of wood to be, still then, in the glassy state.

5. Transformations and decomposition of wood

5.1. Introduction

At a phase transformation, the free energies of 2 coexisting phases at the transformation temperature are the same, but when the first derivatives of their free energies are not the same, above and below the equilibrium temperature, there is a latent heat, or a discontinuity of the enthalpy, the entropy and volume, what is known as a first order transformation. When these first derivatives are continuous, but the second derivatives of the free energies are different below and above the transformation temperature, showing then thus discontinuities in the thermal expansion coefficient, the heat capacity (specific heat) and the compressibility, the transformation is known as a second order transformation (e.g. a glass-rubber transition).

5.2. First order transformations

Examples of first order transformations of wood-material are the changes as:
melting, crystallization, depolymerization, degradation, dehydration and some types of plasticize and hardening. Transformations of wood components are mentioned e.g. in [7], but are based on highly degraded material. Wet hemicellulose is therefore supposed to soften at about 55 ^{0}C and lignin at 120 ^{0}C and there also are other structural changes in this temperature range. First, the structure of lignin is altered and then transverse shrinkage of wood-components begins (at 70 ^{0}C) and next the lignin starts loosing weight. As a transi-

tion temperature of cellulose 210 ^{0}C is given. The changes in the range 120 to 210 ^{0}C are: initial decomposition of lignin and degradation of hemicellulose; hemicellulose starts to decrease and cellulose begins to increase (by the reaction with hemicellulose); bonded water is freed (140 ^{0}C); Lignin "melts" and begins to re-harden; rapid weight loss of hemicellulose and then of the lignin; cellulose dehydrates. Above 210 ^{0}C, cellulose crystallinity decreases and recovers; cellulose decomposition and weight loss starts above 280 ^{0}C (formation of Carbohydrates); crystalline ordering changes (at about 225 ^{0}C) crystallites start to melt also above 280 ^{0}C; dissociation starts above 500 ^{0}C and dominates above 700 ^{0}C; hemicellulose completely degrades; wood is carbonized.
The mentioned transformation temperatures have no general meaning because in [12] much higher temperatures are given (see fig. 5.1), indicating higher molecular weights of the sample material.
Wood does not follow these transformations of the degraded components. As shown before, wood is not a heterogeneous composition and will not show transformations of the components, but is a homogeneous composite and shows one intermediate transition point (see e.g. fig. 5.1) of the co-polymer depending on the composition. It can be seen in fig. 5.1, that the bend down of line 1 of wood, the onset of the transition peak of wood, (that is proportional to the slope of the line), is not influenced by the onset and transformation of the components. The composite wood shows a higher crystalline melting point than is mentioned for the components. The dynamic DTA and DSC tests, [12], did show the endothermic melting peak to be at about 380 ^{0}C, a higher crystalline melting point than

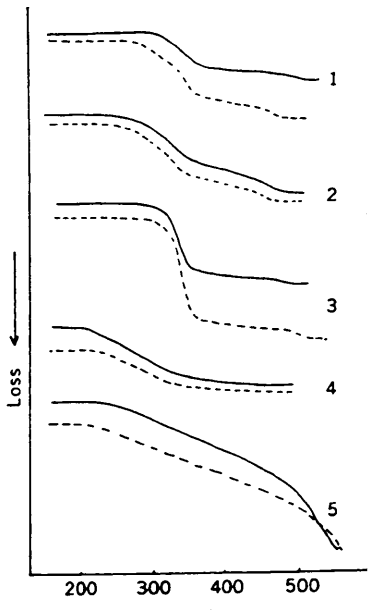

1. wood
2. holocellulose
3. cellulose (α - cell. C)
4. hemicellulose (extracted with 10 % NaOH)
5. lignin (dioxane lignin)

——— Akamatsu;
- - - - - - Buna.

Temperature (^{0}C)

fig. 5.1. TG curve of wood and wood components [12].

is mentioned for the components, occurring at the high temperatures where also depolymerization and degradation occurs (failure of the chain oxygen linkages).
Decomposition thus is necessary to get "melting" and this "melting"-process can better be regarded as a process of endothermic decomposition.
It can be concluded that first order like transformations of wood only occur at high temperatures and have a not noticeable influence on time dependent behavior at common temperatures (as also follows from 4).

5.3 Second order transformations

Second order transformations, that may show at the transition temperature a "step increase" of the thermal expansion coefficient, the heat capacity and the compressibility, should e.g. be detectable for wood by a fall down of the modulus of elasticity. For a real glass-rubber transition, the stiffness (or rigidity) diminishes more than 3 orders (and the strengths more than 2 orders). However wood, as highly oriented, cross-linked, filled and crystalline composite can be expected to show a leather transition and to remain elastic (potential-elastic, not rubber-elastic) and only may show a reduction of the stiffness of less than one order in the stiff direction.

5.3.1. Change of the thermal expansion coefficient

The thermal expansion coefficient α can only be measured for dry wood, because else temperature changes cause changes of m.c. and cause higher deformations than by thermal expansion. The measurements on dry wood of Schaffer, between 0^{0} and 270^{0} C, did not show a sudden increase of the thermal expansion coefficient. Dry wood thus does not show a transformation up to the highest temperatures of degradation.

5.3.2. Change of the heat capacity

The heat capacity of wood, or specific heat (as ratio of the capacity to the capacity of water at 15^{0} C), is known e.g. between 0^{0} and 110^{0} C [9]. It is independent of the species and specific gravity. It slightly increases with temperature and the dependency of the moisture content follows the additive rule of the specific heats c of the water content and of dry wood content:

$c_m = \omega \cdot c_w + (1 - \omega) \cdot c_0 = \omega + (1 - \omega) \cdot 0.324 = 0.324 + 0.676 \cdot \omega = (\omega_0 + 0.324)/(1 + \omega_0)$

where ω is the moisture content based on the wet weight and ω_0 on the oven-dry weight; c_0 is the specific heat of dry wood and $c_w = 1$, is the specific heat of water. There thus also is no indication of any "discontinuity" (or quick change) in this temperature range (nor due to water). The usually assumed glass-transition of wet wood around 50^{0} to 80^{0} C thus is not indicated. Around this temperature, a common second relaxation process may become noticeable, after a long delay time, at sufficient high stresses, by the time-stress equivalence, (see fig. 4.3 and [2] pg. 79). The glass state, determining this mechanism, is confirmed by the perfect Arrhenius plot of the damping peaks (or loss modulus peaks) at thermodynamically loading (comprising the whole moisture content range).
For a glass transition, a WLF-type equation should apply instead of the Arrhenius equation. Wet wood thus also does not show a transformation (below 110^{0}C).

5.3.3. Change of the strength and modulus of elasticity

According to the constant temperature dependency of the modulus of elasticity, dry wood (m.c. = 0) does not show any transformation up to the highest temperatures where degradation occurs. The same follows from the constant temperature dependency of the strength for the ultimate load bearing bonds. The compression strength at 0 % m.c. is measured between -180^{0} to $+280^{0}$ C to be linearly dependent on the temperature. This linear decrease with the temperature of the strength is due to the positive constant entropy term of the activation energy what is common for glassy behavior. The same applies for the bending strength, measured between -180^{0} and $+130^{0}$ C, and for the tensile strength, measured between $+20^{0}$ and 280^{0} C. One investigation (of Schaffer), did show a kink in the straight lines for the modulus of elasticity, the compression- and the tensile strengths around $+200^{0}$ C, showing the influence of damage by the initial quick m.c. change. The

common decrease of the strength with the moisture content is a property of the activation volume. This effect is recoverable, as for most moisture dependent properties (at sufficient low stresses).
The moisture content has no influence on the tensile strength at low temperatures (- 180 ^{0} to ~ + 20 ^{0} C). As discussed in [2] pg. 51, there is a change of the dominating strength determining process at – 8 ^{0} C, where below the determining process shows an activation

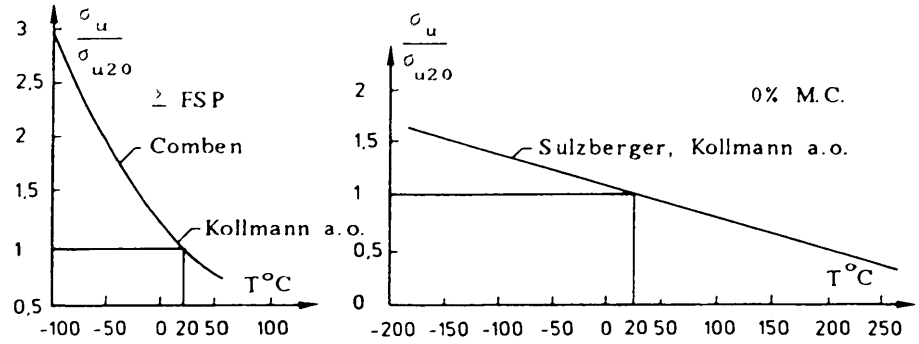

fig. 5.2. Compressive strength // [12] of wood in the whole temperature range according to theory and measurement (see [2] pg. 52).

volume that is not dependent on the m.c. for tension and follows $\lambda_0 \approx \lambda_1 \cdot \omega_m \cdot T_0$ for compression, explaining the curved decrease of the compression strength at a m.c. above fiber saturation (given e.g. between – 100 ^{0} and + 20 ^{0} C in fig. 4.5.3, and between 20 ^{0} to 100 ^{0} C in fig. 4.5.1 of [2]), and shows no "step" change of the strength or "sudden" change of the temperature dependency in this temperature range thus shows no transformation. The same follows from the shear strength, measured for wet wood e.g. between 20 ^{0} and 170 ^{0} C, and from the strengths perpendicular to the grain measured up to 100 ^{0} C. The modulus of elasticity also is measured, in the temperature range of - 150 to + 280 ^{0} C, to be linearly dependent on the temperature for dry wood (m.c. ~ 2 %).

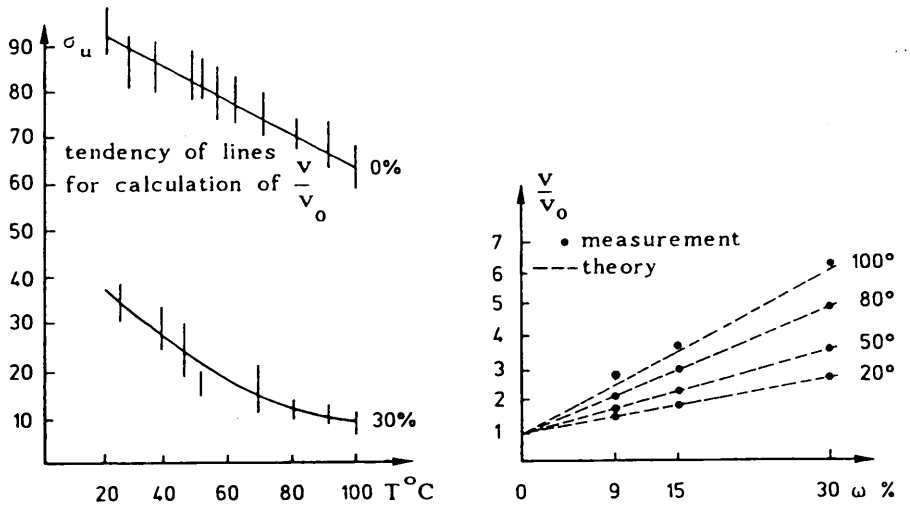

fig. 5.3. Compression strength and activation volume

Because the modulus of elasticity is proportional to the activation energy (by the form of the energy barrier), the linear temperature dependence is caused by the constant positive entropy term (see [2] pg. 33). This predicts a similar m.c. dependency as for the strength

(see 5.3.3 and [2]).
Thus, the strength and modulus of elasticity don't indicate, in common circumstances, a transformation of load bearing bonds in the whole temperature and moisture content ranges of un-degraded wood.

5.3.4. Changing loading, moisture content and temperature

Softening of wood is possible at high temperatures and moisture contents (m.c.) due to high loading. The influence of m.c. is known from manufacturing densified wood. Pressing wood of 26 % m.c. at 26 ^{0} C is as easy as pressing wood of 6 % m.c. at 160 ^{0} C. By the time-stress equivalence, the softening temperature of wood is also strongly reduced by high loading.
A type of a leather-like transformation of wet wood is possible by a cycling load or (see [2]) by a cycling m.c. change. This is not a real glass-transition that only depends on its transition temperature, but may occur at any temperature and is dependent on the loading level that should be above the long-term strength. The transformation is not possible for tension in grain direction and at low moisture contents, but is measured in compression (Y.M Ivanov) and in torsion (Becker and Noack) and the other loading cases [2].
Repeated compressional loading of small clear compression specimens (1x1x2 cm^3) at a stress level above the long-term strength did show, besides the visco-elastic strain, a strong increase of the elastic strain. Thus, a strong decrease of the modulus of elasticity. This elastic strain may become of higher order with respect to the initial strain, when pure central loading of the specimen remains possible in the test. If this is no longer possible, instantaneous compressional failure occurs. The applied stress is thus a fatigue load of the repeated central loading. The behavior is according to a damage equation or to a structural change equation like eq.(6.5.23) of [2], and there is a delay time and an exponential increase of the elastic and viscoelastic strain. Visco-elastic strain is caused by side bond breaking and bond reformation in a shifted position. The mechano-sorptive effect is a special form of this mechanism where there is a alternate shrinking and swelling with slip in adjacent layers by the moisture content changes, what is fully explained in [2] chapter 7 for all histories of high moisture content changes. At high stresses, there thus is an additional

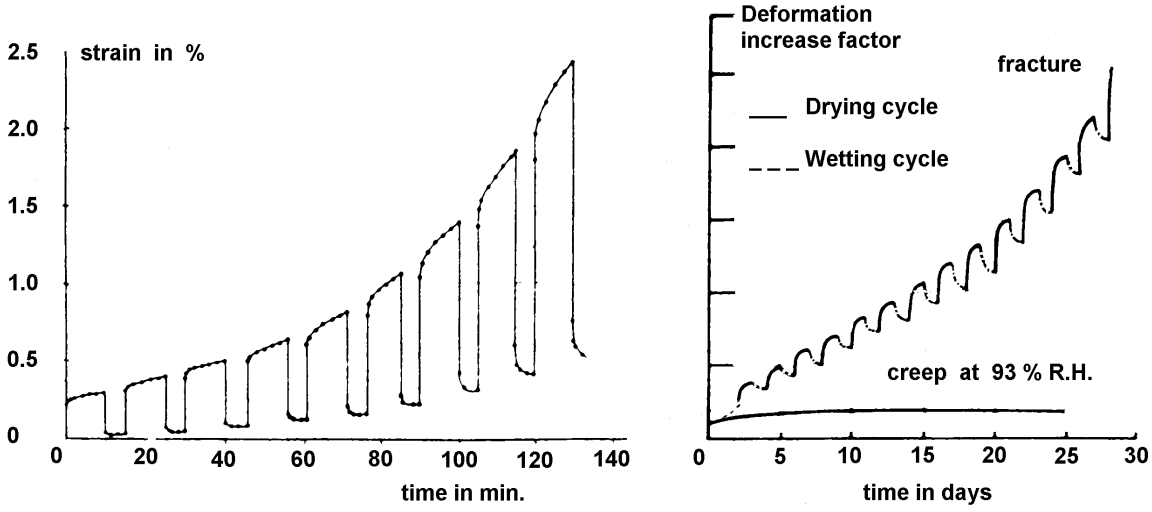

fig. 5.4. High elastic strain and mechanosorptive strain ([18]-left, [17]-right)

effect of high visco-elasticity and of diminished bond reformation causing the decrease of the modulus of elasticity due to damage by fatigue.
An other way to obtain a high elastic strain is given in chapter 8 of [2]. Creep and relaxation compression tests on small clear specimens at a high stress level, with small changing moisture contents, did show, in the delay time before the high elastic state in compression, a strong increase of the activation volume and thus a much higher compressional creep and already a high elastic state for bending movement of the compression specimen. This shows that side bond breaking starts only in certain planes and changing moisture content tests should be done in combined bending and compression for parameter estimation.
For wood, the high elastic state is the result of a strength mechanism, decreasing the side bonds and it is not a glass transformation, at a specific temperature, although the deformation is partial recoverable. The real glass transition is discussed in B(2010), Section B.3.

6. Conclusions

Conclusions about phase transformations discussed in chapter 2, are given in 2.9.
Based on the theory of molecular kinetics, a discussion and theoretical derivation and correction is given in 2 of the old qualitative linear rheological models. As a consequence, new theory in 2 is derived about: nucleation and heterogeneous nucleation (2.5), with the right "Tammann Hesse" (2.6), and other empirical nucleation equations (2.5); the general diffusion equation of transformations (2.3); the reaction order (2.4); the activation volume parameters (2.5); the power law (2.5); and the empirical power law rate equations (2.8).
- Conclusions about transformations in wood, discussed in 3 to 5, are as follows:
- The activation enthalpy, found by thermogravimetry, is only indicative because of: the gas lost; the combustion of these gasses, determining also the reaction within the specimen; the successive and simultaneous reactions, giving overlapping peaks; the assumed wrong equation of only one process and wrong reaction order (different from order one); the structural transitions in wood that only are possible after the previous, or at the same time acting decomposition reactions; the strong influence of the molecular weight and dimensions of the sample and of the heating rate; the neglect of the strong influence or the extend of the reaction y on the enthalpy H, so that H – cy is measured and reported to be H; the many influences causing peaks that are characteristic of the test and sample holder assembly and laboratory and not of the sample.
A thermo-mechanical verification of the found enthalpies thus is always necessary.
- Thermo-gravimetric and differential scanning calorimetric measurements of wood in nitrogen show that there is a peak, at about 380 ^{0}C, of endothermic melting and degradation of the crystallites and at the same time a peak of exothermic decomposition and depolymerization that interacts and overlaps the melting. The apparent activation enthalpies of both peaks are 43 to 49 kcal/mol, according to the DSC-method. From the TG-method, lower values from 23 to 30 kcal/mol for the equivalent peaks are found, showing, that there is a process of weight loss and a process of bond breaking without weight loss.
- Isothermal TG measurements just below 380 ^{0}C, did show that two processes are acting, and by the changing driving force, due to the extent of the reaction, of one of the processes, an apparent changing total activation energy between 35.4 and 56.3 kcal/mol was found, see table 3.1. The lower value agrees with the value found at still lower temperatures of the accelerated aging process of 4.2. The lower enthalpy values of 23 to 30 kcal/mol, of the dynamic TG method with respect to 35 to 56 kcal/mol of the isothermal TG method is also due to a too high heating rate with respect to the long delay time of the processes.
- The found enthalpy values from thermogravimetry agree with those obtained by thermo-mechanical methods of creep and strength as given in [2].

- It can be concluded that first order transformations of wood only occur at high temperatures and have a not noticeable influence on time dependent behavior at common temperatures as also follows from chapter 4.
- The powder collapse tests show the important influence of the molecular weight and moisture content on the softening temperature. Because of the low molecular weight of the degraded sample material and the other type of bonds, the behavior is not comparable with that of wood.
- It is clearly shown that wood is not a heterogeneous composition but a co-polymer, (a homogeneous composite), and thus will not show separate transition peaks of the different components, but one intermediate transition point. Thus, cellulose-, hemicellulose- and lignin- peaks, etc. don't exist in wood.
- Thus, peaks due to previous testing; water movement; temperature history and damage etc.; should not be associated with transitions of components, as is done.
- Dielectric dispersion gives no information on the mechanical behavior of wood because wood is dielectric neutral. The dielectric measurements only give information on the special loose water-structures at the free surfaces of pores etc. in wood, as also follows from the low activation energies.
- The internal friction thus does not show the multi-peaked dielectric behavior of the "multi-transitions model", but the real, right value of internal friction, following from mechanical testing, shows a constant loss tangent, $\tan(\delta)$, and constant logarithmic decrement Δ ($\approx \pi \cdot \tan(\delta)$), at common temperatures, in the whole, technical frequency range of about 10^{-5} to 10^{+4}, (depending on the loading level). This constant value of $\tan(\delta)$ is explained by the theory (see [2], pg. 96 to 100), as a consequence of a property of the activation volume. The same property also explains the time-stress equivalence.
- Measured aging on wood of temples, loaded between 400 to 1300 years, did show a negligible decrease of strength and stiffness during 1300 years, despite of loading and climate changes. Accelerated "aging" tests at high temperatures did show a still smaller decrease, because there was no mechanical loading. Also for this structural change process, the time-stress equivalence applies.
- For the structural use of wood, transformations play no role. At common temperatures, loading levels and moisture contents there is no action of any transformation and there thus also is no aging effect or change of crystallinity, chemical changes, or change of concentration of flow units (determining creep). There also is no indication of second order transformations because there is no sudden change on a temperature plot of: the thermal expansion coefficient; the heat capacity; the strength and the modulus of elasticity. The only process that matters is the damage process at high loading. Stress is the only driving force then, because the chemical driving forces are negligible.
- Softening of wood is possible at higher temperatures and high moisture contents, by high changing loading or by changing moisture content at sufficient high loading. Preliminary tests and parameter estimations are given in [2]. More investigations are necessary to obtain the parameters of this special mechano-sorptive effect. Because unprotected wood in buildings undergoes the maximal moisture content change during the year, the mechano-sorptive effect, together with the softening effect at higher loading and by long term cycling, is determining for creep and safety and is the only effect that needs to be investigated further.
- Conclusions about the new rubber theory are given in appendix I - 4.
- Conclusions about new theory of glass transition and annealing are given in Section ab.3.
- All aspects of strength and time dependent behavior of materials are fully explained by the acting physical and chemical processes, thus by statistical mechanics and reaction kinetics. The correlation of the theory with the measurements is about one, for the processes

in each specimen (each given structure). It thus is a deception to use the old qualitative linear rheological model of liquids and soft solids, which even do not apply for these soft materials and only locally and meaninglessly may fit some data, and thus is not able to predict behavior.

References

[1] Deformation kinetics. A.S. Kraus, H. Eyring, 1975, John Wiley & Sons.
[2] Deformation and damage processes in wood. T.A.C.M. van der Put, Delft University Press, NL, called B(1989a). Final extended version is Section B.1.
[3] Annealing of amorphous solids. T.A.C.M. van der Put, Delft Progr. Rep., 15 (1991/1992) pg. 55-63. Final version is Section B.3.
[4] Explanation of "rubber theory" or flexible chain models by the exact theory of molecular deformation kinetics, COST 508. T.A.C.M. van der Put, Rep. 25.4-95-07/ME-01 Stevinlab., 1995. See also final vision in Section B.2.
[5] Phase transformations in materials. A.K. Jena, M.C. Chaturvedi, Prentice Hall.
[6] Non-Crystalline Solids, ch. 12: Non-Newtonian Relaxation in Amorphous Solids, ed. V.D. Frechette, Wiley, New York, 1960
[7] Influence of Heat on Creep of Dry D.-fir. E.L. Schaffer , Forest Prod. Lab. Madison Wisconsin.
[8] Viscoelastic properties of polymers. J.D.Ferry, London, John Wiley & Sons.
[9] Principles of Wood Science and Technology. F.F.P. Kollmann, W.A. Cote, 1968 Springer-Verlag, Berlin, New York (and the older German version).
[10] Untersuchungen uber die thermische Stabilitat nativer hochpolymerer Werkstoffe ... usw., Dissertation von N. Christoph, Univers. Hamburg 1966.
[11] Thermal Softening of Lignin, Hemicellulose and Cellulose, D.A.I. Goring, Pulp and Paper Magazine of Canada, dec. 1963.
[12] Differential Scanning Calorimetry of Wood and Wood components, T. Arima, Research reports in memory of the 10th anniversary of the Founding, 1981, Dep. of Forest Products of the University of Tokyo.
[13] Thermogravimetric analysis of pulps. R.D. Cardwell, P. Luner, Wood Science and Technology vol. 10, nr. 2, 1976 p. 131 - 147.
[14] Accelerated Aging. M.A. Millett, C.C. Gerhards, Wood Science vol. 4, no 4, 1972 p. 193 - 201.
[15] Theory of Non-Newtonian Flow, T. Ree and H. Eyring, Journal of Applied Physics Vol. 26, Nr. 7, july 1955,
[16] On viscoelastic modelling of multi-transition effect in wood. S. Hayanov, P. Zeiter. COST 508 meeting in Limerick 1993. See also publications of C. Huet, e.g. in the EC-MA1B report
[17] Moisture Content Changes and Creep of Wood, R.F.S. Hearmon, J.M. Paton, Forest Products Journal of August 1964.
[18] Behavior of Wood and Synthetic Materials under Repeated Load, Y.M. Ivanov, RILEM-symposium Mexico-City, Mexico, Sept. 1966.
[19] The Influence of Temperature on Creep in Wood, R.W. Davidson, Forest Products Journal of August 1962.

APPENDIX I

Replacement of the classical phenomenological 'Rubber Theory" by the exact equilibrium theory of molecular deformation kinetics

1. Introduction

Although linear viscoelasticity does not exist for structural materials, there is, due to the standard computer applications, still a fall back to models based on linear behavior and on linear spectra of relaxation times based on the flexible chain theory. These models are extrapolated to the totally different, non-linear cases of rubbers, glasses and crystalline materials and even are supposed to be able to describe transformations. Even the free chain model of Zimm [16] is proposed as such for the glassy and crystalline material wood, although it only may apply for flow of very dilute solutions. Wood remains glassy and does not show a real glass transition or real melting below its high temperatures of decomposition. A real glass transition temperature of wood thus does not exist. For wood, the process of side bond reduction, causing softening, is only possible at combined high temperatures, high moisture contents, and high loading, close to the level of damage and decomposition.

That spectra of relaxation times cannot exist is shown before in publications and at COST-workshops. Besides the theoretical impossibility of such an existence, also the simple test of e.g. zero relaxation, after a relaxation test, shows that only one non-linear deformation kinetics process is acting within a very wide time or frequency range. Zero relaxation occurs when the applied strain and stress are lowered to such a level that the internal stress on the mobile sites is zero. This proves the impossibility of the existence of a spectrum [2] that predicts that there always is relaxation at any strain that is applied. This

further shows that none of the other methods (chain models, power laws, general functions, etc.), based, or implicitly based, on the existence of spectra, is able to explain or predict any behavior and thus is nothing more than an arbitrary, only partial applicable fitting procedure.

For valid conclusions on wood behavior, it is necessary to show when, and for what material, there is any possibility of assumptions of linearity or chain-like behavior and thus any applicability of the phenomenological rubber theory. This is done here by a simple derivation of this "theory" to show its basic suppositions and the consequences. Because this analysis leads to a rejection of this "theory", the real explanation of rubber behavior by the exact physical theory, (statistical mechanics and limit analysis of equilibrium theory [2] of deformation kinetics), also has to be discussed. This general theory is shown, in many publications, to explain fully all aspects of time dependent behavior without the need of the invalid extrapolation of the free chain model of a very dilute solution to dense rubbers and without the need of an incorrect and inconsistent phenomenological model of increase of free volume as cause of` glass transition [3], [2], etc.

From the given derivations it is shown that the explanation of rubber behavior by deformation kinetics removes the existing serious contradictions of the, therefore rejectable, chain models. Of course, these models, based on the behavior of isolated flexible molecules, only were supposed to apply for liquid-like behavior in the terminal zone of very dilute uncross linked polymers and can not apply for undiluted material in the glass-, or in the plateau zone, nor for cross-linked networks and thus certainly not for structural materials like wood.

2. Discussion of the classical rubber theory

2.1. Basis hypothesis of the theory (Rouse; Zimm; etc.)

The “rubber” theory is based on the Brownian motion of isolated flexible chains at higher temperatures above glass transition, thus deals with very dilute solutions where a separated long molecule is surrounded by solvent. The driving force of these Brownian motions is the thermal energy that is regarded to be opposed by viscous forces of the hydrodynamic resistance of the solvent. At dynamic loading, the force in phase of the Brownian displacements causes energy storage and in phase with the velocity causes energy dissipation. At very high frequencies (many orders above the measuring frequency of the rubber state), there will mainly be bond stretching or elastic behavior (glassy rigidity), while for low frequencies there is time for chain movement within a period showing the mentioned strain and velocity in phase with the stress (in rubber behavior).

The theory however does not deal with the behavior at higher frequencies and short-range relationships and the prediction of this theory of infinite rigidity and infinite loss at infinite high frequencies is invalid. The theory is limited to the low frequency chain statistics that any point on the chain backbone separated by 50 or more chain atoms will be related to each other in space according to a Gaussian distribution of vectors (distance according to a random walk). The root-mean-square distance, s, between 2 points separated by q monomeric units (q > 50 chain atoms) is:

$$s = a\sqrt{q}\ ,$$

where "a" is about the monomer distance. Distortion of these 2 distance points by a shear stress in the solvent will be opposed by the restoring force due to the diffusion back to this configuration by the Brownian motion resulting to a spring constant of: $3kT/qa^2$, (the "entropy spring" of a chain segment in liquids and soft solids), where 3kT is the mean thermal energy (T = absolute temperature; k = Boltzmann’s constant). By Rouse it is as-

sumed, as model, that the friction along the chain can be concentrated on these distance points (called segment junctions) in order that only the movements of these points have to be regarded. It thus is assumed that there is no hydrodynamic interaction for smaller motions between the junctions (limiting the model to low frequencies). The motions of all

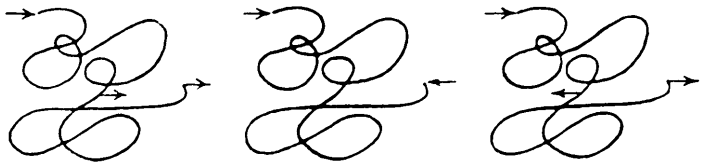

fig. 2.1. characteristic modes of motion of a flexible chain molecule

segment junctions can be expanded into modes (like a vibrating string) and each mode corresponds to a discrete contribution to the relaxation spectrum H, from which all experimental visco-elastic functions can be derived, leading, according to Rouse, to:

$$H = mkT \sum_{p=1}^{N'(\leq N/5)} \tau_p \qquad (1)$$

predicting a line spectrum, where τ is a relaxation time; N is the number of junctions of each molecule of q monomers, and "m" is the number of polymer molecules per cc, or, with ρ = polymer density; M = molecular weight; N_0 = Avogadro's number: $m = \rho N_0/M$.
To keep the series in eq.(1) convergent, p must be smaller than about $p < N/5$.
Then, using this bound, the term: $\sin^2(p\pi/2(N+1))$ in the Rouse model can be approximated by: $\sin^2(p\pi/2(N+1)) \approx (p\pi/2N)^2$ and τ_p becomes:

$$\tau_p = a^2 q^2 N^2 \varsigma_0 / \left(6\pi^2 p^2 kT\right) \qquad (2)$$

where, ς_0 is the friction coefficient per monomer. Thus per junction the friction is $q\varsigma_0$ (where the friction is assumed to be concentrated on the junctions by the Rouse model).
The magnitudes of "q", "a" and "N" need not to be known. However: Nq = Z,
the degree of polymerization of the polymer, what is known and q (> ~ 50) determines the high-frequency limit of application of the random walk statistics of the model.
Because the influence of the short relaxation times is ignored in the model, the applicability and verification of the theory only is possible for behavior after longer times (or at lower frequencies).

2.2. Relaxation spectra

Linear visco-elastic behavior always can be described by mechanical models involving Hookean springs and Newtonian dashpots. For a single linear visco-elastic Maxwell element the shear rigidity is:

$$G(t) = G_i \exp(-t/\tau_i) \qquad (3)$$

giving for n parallel elements:

$$G(t) = \sum_{i=1}^{n} G_i \exp\left(-t/\tau_i\right) \qquad (4)$$

Increasing the number without limit, a continuous spectrum results with the infinitesimal contribution Fdt or $Hd(\ln\tau)$ with $H = F\tau$ on the $\ln(\tau)$ scale, giving:

$$G(t) = G_e + \int_{-\infty}^{\infty} H.\exp\left(-t/\tau\right) d\left(\ln(\tau)\right) \qquad (5)$$

where $G_e = 0$, for this case of uncross-linked polymers.
For dynamic loading the complex stress-strain ratio: G* = G' + iG'' gives for:

$$G'(\omega) = \sum_{i=1}^{n} G_i \omega^2 \tau_i^2 / (1 + \omega^2 \tau_i^2) \quad (6)$$

and for G'':

$$G''(\omega) = \sum_{i=1}^{n} G_i \omega \tau_i / (1 + \omega^2 \tau_i^2) \quad (7)$$

The dissipative effects of alternating stress also can be described by the ratio of stress in phase with the strain rate $d\gamma(t)/dt = i\omega\gamma_0 \cdot \exp(i\omega t)$, divided by the strain: $\gamma(t) = \gamma_0 \cdot \exp(i\omega t)$ or: $\eta^* = G^*/i\omega = \eta' - i\eta''$, where $\eta' = G''/\omega$ and $\eta'' = G'/\omega$.
Because τ_i in eq.(3), (4), (6) and (7) is: $\tau_i = \eta_i / G_i$, η' may approach the steady- state flow viscosity η because according to eq.(7): $\eta' = (G''/\omega)_{\omega \to 0} = \sum G_i \tau_i = \sum \eta_i = \eta$

$$\eta'(\omega) = \sum_{i=1}^{n} \eta_i / (1 + \omega^2 \tau_i^2) \quad (8)$$

This of course only applies for polymers showing a steady-state flow viscosity.
In the same way as done for G(t) is for an infinite Maxwell model:

$$G' = G_e + \int_{-\infty}^{\infty} \left(H\omega^2\tau^2 / (1 + \omega^2\tau^2)\right) d\left(\ln(\tau)\right) \quad (9)$$

$$G'' = \int_{-\infty}^{\infty} \left(Hw\tau / (1 + \omega^2\tau^2)\right) d\left(\ln(\tau)\right) \quad (10)$$

$$\eta' = \int_{-\infty}^{\infty} \left(H\tau / (1 + \omega^2\tau^2)\right) d\left(\ln(\tau)\right) \quad (11)$$

The steady-flow viscosity for an uncross-linked polymer follows from this equation by: $\omega = 0$ or:

$$\eta = \int_{-\infty}^{\infty} H\tau \cdot d\left(\ln(\tau)\right) \quad (12)$$

Substitution of eq.(1) in (12) and using eq.(2) gives:

$$\tau_p = 6(\eta - \eta_s)/(\pi^2 p^2 mkT) \quad (13)$$

where η is the total viscosity and η_s is the viscosity of the solvent and because m is known from the molecular weight, time dependent properties are known from easily measurable quantities.

2.3. Relaxation spectrum of Rouse

Inserting eq.(1) in eq.(5), (6) and (8) gives:

$$G(t) = mkT \sum_{p=1}^{N/5} \exp(-t/\tau_p) \quad (14)$$

$$G'(\omega) = mkT \cdot \sum_{p=1}^{N/5} \omega^2\tau_p^2 / (1 + \omega^2\tau_p^2) \quad (15)$$

$$\eta'(\omega) = mkT \cdot \sum_{p=1}^{N/5} \tau_p / (1 + \omega^2\tau_p^2) \quad (16)$$

For low frequencies, $(\omega\tau)^2 << 1$, wherefore the theory applies, eq.(15) becomes:

$$G'(\omega)/\omega^2 = mkT. \sum \tau_p^2 = mkTc_1 \quad (15')$$

and eq.(16):

$$G''(\omega)/\omega = \eta' = mkT. \sum \tau_p = mkTc_2 \quad (16')$$

giving finite values of c_1 and c_2 by the convergent series, e.g. by using eq.(2), what is possible by the sufficient small upper value of $p < N/5$.
From eq.(15') and eq.(16') follows in this region:

$$\text{Log}(G') = C_1 + 2\cdot\log\omega \qquad (15'')$$

and: $\text{Log}(G'') = C_2 + \log\omega \qquad (16'')$

and the derivation shows that always, for all uncross-linked polymers, the slope of the logarithmic plot of G' is 2 and is 1 for the loss modulus G''.

As can be seen in fig. 2.6.1 and 2.6.2, this never applies. The reason is that converging of the series only may apply at a steep descent, thus in the terminal zone for uncross-linked polymers by the cut off to N/5 used in τ_p and by the limiting longest relaxation time due to the limiting value of η'.

The limiting forms at moderately short times or higher frequencies depend on the model. According to eq.(2), τ_p has, according to Rouse, the form of: $\tau_p = c_3/p^2$, giving for eq.(15), with $x = p/\sqrt{\omega c_3}$:

$$G'(\omega) = mkT\int\left(1/(1+p^4/\omega^2c_3^2)\right)dp = mkT\sqrt{\omega c_3}\cdot\int_b^\infty\left(1/(1+x^4)\right)dx = mkTc_4\sqrt{\omega}, \qquad (15''')$$

leading to a slope of 1/2 at a double log-plot (see fig. 2.3).

In general, with the arbitrary power law $\tau_p = c_3/p^\alpha$, is found in the same way:

$G' = mkTc_4(\omega)^{1/\alpha}$.

This gives with α = 1.5 the Zimm value of the slope, (see 2.4).

Except for the 3 longest relaxation times of the line spectrum eq.(1), being too far apart, the other contributions to the spectrum are closely enough spaced to approximate this as a continuous spectrum leading to:

$$H = (aqNm/2\pi).(\zeta_0 kT)^{1/2}\cdot\tau^{-1/2} \qquad (17)$$

or, in terms of steady-flow viscosity:

$$H = \left(\sqrt{6}/2\pi\right)\cdot\left(mkT(\eta-\eta_s)\right)^{1/2}\cdot\tau^{-1/2} \qquad (18)$$

where N, as too high value, is inserted as upper value of p in stead of N/5. This result thus is not right and because of the limitation of N/5 and the applicability for $\tau < \tau_{p=3}$, (corresponding to H > 1.5mkT), eq.(17) and (18) only may apply over about 3 decades of time scale (or 1.5 decades of H-values), as confirmed by the measurements, what is far too less for an explanation of the total behavior.

2.4. Hydrodynamic interaction, or extension of Zimm

Zimm introduced hydrodynamic interaction between the moving sub-molecules based on the calculation of steady-flow viscosity of dilute solutions. This leads to a different expression for τ_p than given by eq.(1), that however can be written analogous to eq.(13):

$$\tau_p = 6(\eta-\eta_s)/(\pi^2\lambda_p^2 mkT) \qquad (19)$$

where λ_p are numeric values whose first few values (p = 1, 2, 3, 4) are:

1.2, 2.1, 2.9, 3.67, (in stead of the 1, 2, 3, 4 -values in the Rouse equation) leading to somewhat smaller values by eq.(19) than given by eq.(13) and leading to a continuous spectrum of:

$$H = (a^2qNm/5)\cdot(kT)^{1/3}\cdot\eta_s^{2/3}\cdot\tau^{-2/3} \qquad (20)$$

showing a slope of – 2/3 on logarithmic scales.

Alternatively, eq.(19) can be given, comparable to eq.(13), like:

$$\tau_p = 0.7\cdot6\cdot(\eta-\eta_s)/(\pi^2 p^\alpha mkT) \qquad (19')$$

where $\alpha \approx 1.6$ for the first 4 terms, descending to $\alpha \approx 1.5$ for high values of p.

Although the Zimm theory should provide a better calculation (at high molecular weights)

of the intrinsic viscosity (= the limiting value of the viscosity η when the polymer concentration approaches zero), visco-elastic data of e.g. dilute solutions of polystyrene etc., in the range and conditions where the theory applies (e.g. in the terminal zone), don't show a behavior according to the Zimm theory but do show a behavior close to the Rouse eq.(18) despite the neglect of hydrodynamic interaction and internal viscosity (= intramolecular steric effects) in this Rouse equation. The explanation of this apparent contradiction is given by the deformation kinetics approach that is able to describe the whole behavior precisely. As will be shown in 3.3, the determining deformation kinetics equation of the visco-elastic behavior at longer times can be expanded into a row which is identical to the row of the Rouse equation. Thus, the Rouse line spectrum represents one special non-linear process. There thus is no restriction of an application to only dilute solutions, as is the basis of the chain models. This single process explains why at zero relaxation, after a relaxation test, the spectrum is not present. Because the "spectrum" only exists as expanded terms of one process, it does not exist when this single process is not acting (as in the zero relaxation test, see 3.4).

Thus diffusion of activated segments is the basic mechanism that explains the behavior and the chain model should be rejected because it strictly only should apply for separated chains in dilute solutions, according to the assumed basic mechanism, while it shows a better experimental agreement for undiluted polymers outside the basic assumptions of this chain model.

The explanation of the Rouse equation as an expansion of one non-linear deformation kinetics process also explains why this line spectrum (that seems physical improbable, but exists as terms of the row expansion of the exact equation) gives better results than a continuous spectrum (that does not exist). Further, it explains why the theory also can be applied to undiluted polymers, using only one friction coefficient for all types of coordinated motions. These motions, represented by the separate terms, are in fact the expanded terms of one process with one relaxation time, thus one friction coefficient.

In the same way, the slip of the entanglement couplings, showing a second bond breaking deformation kinetics process, can be represented by a group of modes (= expanded terms) with another friction coefficient as is applied in the chain models by using a second ladder network behind the first.

The experimental determination of H for undiluted polymers shows a slope between – 1/2 to over – 2/3. However, the slope is mostly closer to – 1/2 in the time scale where the theory should be applicable (the terminal zone at steady-flow-viscosity) and thus is not – 2/3 as predicted by Zimm. The steeper slope, occurring at shorter times, certainly can not be explained by the Zimm theory because η_s, the solvent viscosity in a dilute solution, now, by the absence of solvent, would presumably represent an effective local viscosity far smaller than the real macroscopic viscosity.

In the range where the slope of the curve of $\log(G')$ against $\log(\omega)$ is 2/3, applies: $\log(G') = \log(G_1') + 0.67\log(\omega/\omega_1)$.

Because $G'' \approx (\pi/2) \cdot dG'/d(\log(\omega))$, and therefore:

$d(\log(G'))/d(\log(\omega)) \approx (2/\pi)\tan(\delta)$ is: $(2/\pi)\tan(\delta) \approx 2/3$, or $\tan(\delta) \approx 1$ and $G' \approx G''$.

This last relation may apply near the midpoint of glass-transition and explains why the slope here is about 2/3 and not at the terminal zone as predicted by the Zimm-model. The Zimm model further only could be right for very dilute solutions approaching the limiting value of zero concentration. The different measured slopes show in reality that still an other additional process is acting. This again shows that an explanation or a description cannot follow from chain models or arbitrarily power law models.

2.5. Ladder networks

In dilute solutions, polymer molecules can be represented by springs (with spring constant $3kT/(qa^2)$) moving in a viscous medium (with friction coefficient ζ_0). This model is analogous to the ladder network in electrical network theory. When the lumped springs and dashpots are uniformly distributed along the length, the mechanical model becomes exactly analogous to an electrical model of an inductive transmission line, for which the

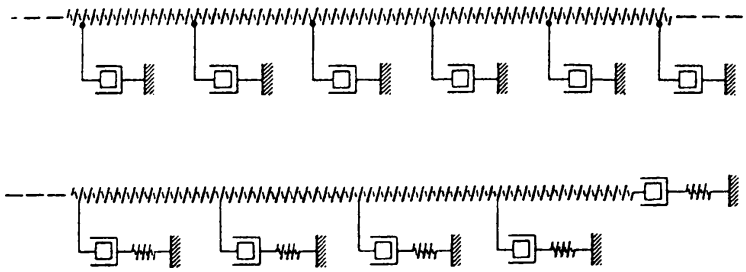

Fig. 2.5.1. Ladder networks of Blizard (above) and Marvin (below).

frequency dependence of the impedance (= complex relaxation modulus G*) is well known giving for an undiluted polymer with molecular weight M:

$$G^* = G' + iG'' = (C_1 / M)\left((iC_2M^2\omega)^{1/2}\coth(iC_2M^2\omega)^{1/2} - 1\right) \quad (21)$$

At high frequencies, eq.(21) gives the limiting value:

$$G' = G'' = C_1(C_2\omega / 2)^{1/2} \quad (22)$$

identical with the Rouse theory and at low frequencies the limiting values are:

$$G' = C_1C_2^2M^3\omega^2 / 45 \quad (23)$$

$$G'' = C_1C_2M\omega / 3 \quad (24)$$

also according to the Rouse theory, when: $C_1 = \rho RT / 2$ and $C_2 = a^2\zeta_0 / (6M_0^2kT)$, where ρ = polymer density, R = gas constant, M_0 = M/Z = monomeric molecular weight.
Using additional springs below the dashpots (see fig. 2.5.1), Marvin obtained a slightly different G* leading to the same eq.(22) at high frequencies and slightly different values at low frequencies. However there is an abrupt change from eq.(22) to the properties of a single Maxwell element as limiting value of the glass value of G. The spectrum thus is a triangle, giving only a qualitative description of the behavior neglecting also the flat plateau at small times. As to be expected for this liquid-like behavior, there hardly is an influence of side group packing which differs greatly between tested ethyl and dodecyl ester.

A thorough study in the past of ladder networks with both lumped and distributed parameters, has shown that a continuous dynamic modulus function as eq.(21) corresponds to a discontinuous relaxation spectrum with discrete lines, so that the series expressions eq.(6) to (8) or (14) to (16) are equivalent to eq.(21). This confirms again the explanation of the behavior according to the Rouse model being a row expansion of the deformation kinetics equation of one process.

2.6. Modified spectra for cross-linked networks

It should be emphasized that the theory for isolated flexible molecules is not supposed to apply for viscoelastic behavior in the glassy, or in the plateau zones, nor for cross-linked networks and is not able to describe this behavior. This of course is evident because short chain units cannot be randomly coiled and have the Gaussian distribution of configurations

and thus cannot behave as entropy springs. This also follows from fig. 2.6.1, where the storage modulus is given of all typical polymeric systems, above glass transition (except curve IV), with the uncross-linked polymers on the left and the cross-linked on the right. The glassy state, curve IV and the cross-linked polymers, curve V, VI and VII, and even the uncross-linked polymers curve I to III, don't show the steep slope 2 as predicted by the free chain model, eq.(15").

Thus, chain models don't apply for solids and thus certainly not for structural materials, also not above glass transition.

The storage modulus $G'(\omega)$ is about the mirror image of the relaxation modulus G(t) with respect to the modulus axis $G'(\omega) = G'(1/t) \approx G(t)$. Thus the behavior after long times is the same as at low frequencies. In the same way, a first impression of the creep compliance J(t) follows from a mirror image reflected in the time axis: $J(t) \approx 1/G(t)$. For the same reason that $G'(\omega)$ resembles G(t) plotted backwards, $J'(\omega)$ resembles J(t) reflected in the compliance axis. For uncross-linked polymers, this applies for the recoverable part:
$J(1/t) \approx J(t) - t/\eta$.

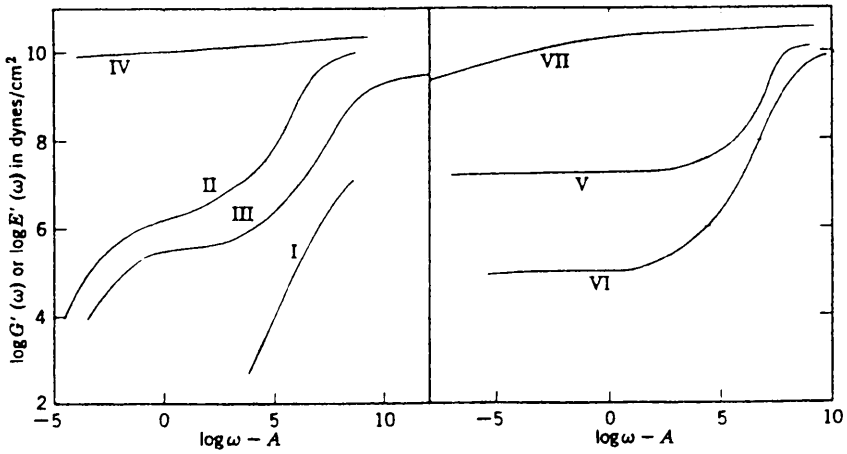

Fig. 2.6.1. *Storage modulus* G' of all typical polymeric systems [8]. The arbitrary horizontal shifts A of: I to VII are: -3; -1; 0; -7; 0; 0; 2. The deformation is shear except for curves V and VII, which are extension.

The types of polymers of fig. 2.6.1 to 2.6.3 are:

I: a low-molecular-weight polyisobutylene, the only one type that approaches the best the limiting behavior of quasi-linear visco-elasticity.

II: and III: uncross-linked polymers of high molecular weight (long chains) that by its lengths will have a probability of local side bonding connecting the chains, what is called entanglement coupling in the classical model. Curves II and III show the glass transition in 2 stages by the 2 types of bonds. The first stage of descent of the curve, at high frequencies or short times, is regarded to show motion of chain segments between the entanglement coupling points. The nearly horizontal plateau zone, is regarded as an "equilibrium" modulus that is reached, showing the rubber like elasticity, as also is seen for the lightly cross-linked networks V and VI at low frequencies or long times. The bond breaking of the bonds between the chains, is regarded in the classical model as slipping of the coupling points showing the second stage of a steep descent of the curve, representing the terminal zone. Type III (poly-n-octyl methacrylate) has large side groups, decreasing the modulus.

At long times or low frequencies and at equilibrium in the plateau zone G or G' should

vanish according to the classical theory because of the resumption of random average configurations by the macromolecular coils in the deformed state. This is not the case and also G" in fig. 2.6.2 , (similar to H of fig. 2.6.3), shows still finite values. Further, at high frequencies, the perfect elastic behavior is predicted by the classical theory and G" should become zero. It is seen in fig. 2.6.2 that this is not the case, but that on the contrary, G" increases enormously and becomes many orders higher at high frequencies showing the same values as for crystalline material VII or amorphous material in the glass state IV (showing thus the same time dependent processes).

IV: The glassy state of an amorphous polymer with high molecular weight, (the only one here below glass transition) that only shows local readjustments as is explained by deformation kinetics [2]. These processes explain the time dependent behavior as creep of structural materials (like wood, concrete, steel, etc.).

V: A lightly vulcanized rubber providing a lightly cross-linked network.

VI: A soft gel, that, as V, is lightly cross-linked but now by crystallites as links. At long times, or low frequencies, the lightly cross-linked networks V and VI, are regarded to approach an "equilibrium" rubber-like shear modulus. However fig. 2.6.2 shows that this is not true because G" and H of V and VI don't vanish. Thus the plateau zone represents a common process of he same type as found in the glassy and crystalline polymers IV and VII, what is explained by deformation kinetics [2].

VII: A highly crystalline polymer with a matrix of crystallites (that shows no change of crystallinity). As mentioned before, the rather flat spectra H of IV, VII and V and VI at long times (see fig. 2.6.3) can not be explained by linear spectra but are explained by one non-linear deformation kinetics process. It is easy to show by a test that spectra do not really exist (see 3.4) but that the spectral lines are the expanded terms of one non-linear process (see 3.3).

The plots of H in fig. 2.6.3 show similar shapes to those of G" in fig. 2.6.2, reflected in the modulus axis. (In the same way the retardation spectrum L resembles the loss compliance J" reflected in the compliance axis).

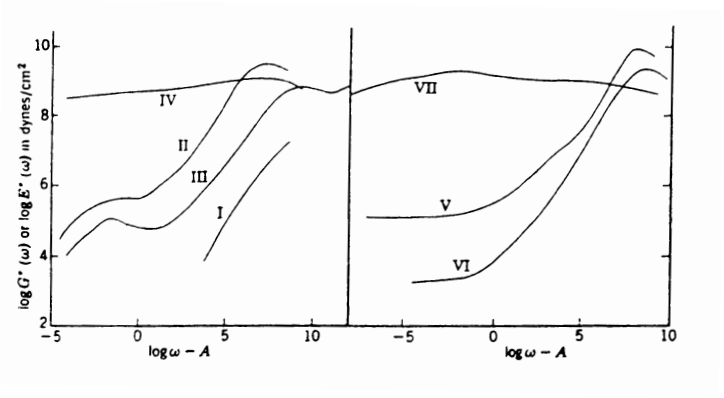

fig. 2.6.2. *Loss modulus* G" of the 7 polymers described above [8]

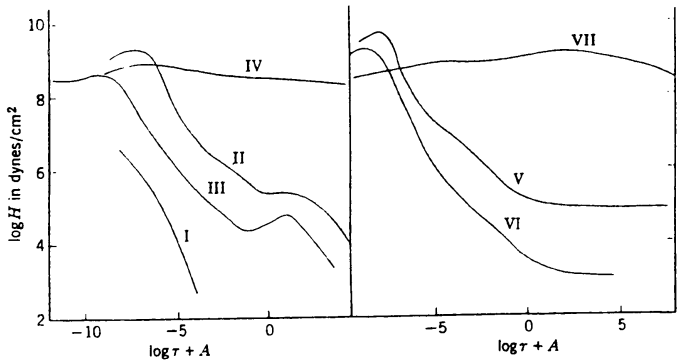

fig. 2.6.3. The *relaxation spectrum* "H" of the 7 polymers described above

Several modifications of the series of H (for cross-linked networks) by several characteristic modes of several types of linked strands (using bond rotations instead of the simplified model of entropy springs) and networks (or series of networks) only give qualitative descriptions of the behavior at transition, e.g. with square root (Rouse; Bueche), linear, and square dependence of J'' on t, all roughly in accordance with the applied range of measurements. However, real fits of the whole behavior are not possible by the chain and power law models. This is evident because the very long relaxation times can not be explained by extrapolation of the model to (impossible) motions of large groups of strands of large dimensions, while physics, shows, [2], that the behavior is explained by the very local movement of small flow units (segmental jumps, or dislocations movements in crystals, etc.).

3. Explanation of rubber behavior by deformation kinetics

3.1. Introduction

The properties of liquid-like materials usually are determined at flow of the material. For cross-linked polymers that are not able to flow, creep- or relaxation tests can be done for a first parameter estimation. The deformation kinetics equations, explaining these processes, are given in [2]. By a simple test of zero relaxation after a relaxation test (see 3.4), it can be shown that only one non-linear process is acting in a wide time interval of many decades and thus a spectrum of relaxation times does not exist.
Thus none of the used other methods (as free chain models, power laws, general functions, etc.), that are based, or implicitly based, on the existence of linear spectra, is able to explain this behavior. Thus the apparent relaxation spectrum, (that is nothing more than the derivative of the measured G or G' curve), is explained by one non-linear process in [2]. It will be shown in 3.3, that the Rouse spectrum is identical to a row-expansion of such a non-linear molecular kinetics process, that is not a structural change process or a transformation.

3.2. Stress relaxation

According to [2], the constitutive equation for this case is identical to that of a system of parallel non-linear Maxwell elements. Mostly the relaxation times of the elements are far apart and all Maxwell elements act like springs, with spring constant K_2, and only one is noticeable as such during the test providing a non-linear three-element model with one Maxwell element and a parallel spring [2] (see fig. 3.4) .

The total stress is $\sigma = \sigma_v + \sigma_2$, where $\sigma_2 = K_2\varepsilon$ is the stress on the free spring and σ_v is the stress on the Maxwell element: $\sigma_v = K_1(\varepsilon - \varepsilon_v)$, thus $\sigma_2 = K_2\varepsilon = \sigma - \sigma_v$. Above glass transition, all Maxwell elements may flow and the stress after relaxation after long time approaches its minimum value. The strain rate $\dot{\varepsilon}$ of the viscous strain ε_v of one process (= one Maxwell element given in Fig. 3.4) follows:
$\dot{\varepsilon} = \dot{\varepsilon}_1 + \dot{\varepsilon}_v = 0$, because for relaxation $\dot{\varepsilon}$ = 0 or:

$$\dot{\varepsilon} = \frac{\dot{\sigma}_v}{K_1} + D\cdot\sinh(\phi\sigma_v) = 0 \qquad (25)$$

or:

$$\dot{\varepsilon}_v = D\cdot\sinh(\phi K_1(\varepsilon - \varepsilon_v)) \qquad (26)$$

$$\text{or: } d\varepsilon_v\cdot\left(e^{-\phi K_1(\varepsilon-\varepsilon_v)} + e^{-3\phi K_1(\varepsilon-\varepsilon_v)} + e^{-5\phi K_1(\varepsilon-\varepsilon_v)} + ...\right) = \frac{D}{2}dt \qquad (27)$$

giving as solution:

$$\frac{e^{-\phi\sigma_v}}{\phi K_1} + \frac{e^{-3\phi\sigma_v}}{3\phi K_1} + \frac{e^{-5\phi\sigma_v}}{5\phi K_1} + \ldots - \frac{e^{-\phi\sigma_{v0}}}{\phi K_1} - \frac{e^{-3\phi\sigma_{v0}}}{3\phi K_1} - \frac{e^{-5\phi\sigma_{v0}}}{5\phi K_1} - \ldots = \frac{Dt}{2} \qquad (28)$$

As will be shown below, eq.(28) may be interpreted as terms of a spectrum that is a similar line spectrum as the Rouse theory, explaining the better results in rubber theory by using this line spectrum than by using a continuous spectrum. (Although a line spectrum is physically impossible, it does exist as expanded terms of the physical right equation).
Eq.(28) can be written:

$$\frac{1}{\phi K_1}.\operatorname{arccoth}(e^{\phi\sigma_v}) - \frac{1}{\phi K_1}.\operatorname{arccoth}(e^{\phi\sigma_{v0}}) = \frac{Dt}{2} \qquad (29)$$

$$\text{or: } -\sigma_v\phi = \ln\left(\tanh\left(\frac{D}{2}t\phi K_1 + \operatorname{arctanh}\left(e^{-\phi\sigma_{v0}}\right)\right)\right)$$

$$\text{or: } -\sigma_v\phi \approx \ln\left(\tanh\left(\frac{D}{2}t\phi K_1 + e^{-\phi\sigma_{v0}}\right)\right) \qquad (30)$$

or at the start of the process when $\tanh(x) \approx x$:

$$-\sigma_v\phi \approx \ln\left(\frac{D}{2}t\phi K_1 + e^{-\phi\sigma_{v0}}\right) \approx \ln\left(1 + \frac{D}{2}t\phi K_1.e^{\phi\sigma_{v0}}\right) - \phi\sigma_{v0} \qquad (31)$$

$$\text{or: } \sigma_v\phi \approx \sigma_{v0}\phi - \ln\left(1 + \frac{t}{t'}\right)$$

At longer times eq.(31) becomes:

$$\sigma_v\phi \approx \sigma_{v0}\phi - \ln(t/t') \qquad (\text{or: } \sigma\phi \approx \sigma_0\phi - \ln(t/t')) \qquad (32)$$

where t' is the delay time ($t' \approx 2/(De^{\phi\sigma_{v0}}\phi K_1)$) showing the linear line on log-time scale. Further an extension of this straight line to σ_v = 0, shows that the intersect with this time axis gives $t'' = 2/(D\phi K_1)$, being the relaxation time based on the straight part of the line. Thus: $\ln(t''/t') = \phi\sigma_{v0}$.
For very long times eq.(30) becomes:

$$-\sigma_v\phi \approx \ln\left(\tanh\left(\frac{D}{2}\phi K_1 t\right)\right)$$

giving the curve of σ_v approaching σ_v = 0, or: $\varepsilon_v \to \varepsilon_{v\infty} = \varepsilon$ (in this case of a symmetrical energy barrier of activation).

3.3. Explanation of the Rouse spectrum

It is easy to show by the simple test of zero relaxation (see [2] or 3.4) that a spectrum as physical reality does not exist. However, the really acting single non-linear process can be expanded mathematically into a row, showing in some tests the same behavior as if there is a line spectrum (i.e. the expanded terms).
As given before, the integration of eq.(26) gives:

$$\frac{e^{-\phi\sigma_v}}{\phi K_1} + \frac{e^{-3\phi\sigma_v}}{3\phi K_1} + \frac{e^{-5\phi\sigma_v}}{5\phi K_1} + \ldots - \frac{e^{-\phi\sigma_{v0}}}{\phi K_1} - \frac{e^{-3\phi\sigma_{v0}}}{3\phi K_1} - \frac{e^{-5\phi\sigma_{v0}}}{5\phi K_1} - \ldots = \frac{D}{2}(t - t_0)$$

This equation shows that the time t_e to reach the end state of total relaxation, or $\sigma_v = 0$, is:

$$t_e = \frac{2}{nD}\left(1 + \frac{1}{3} + \frac{1}{5} + \frac{1}{7} + ...\right) \rightarrow \infty$$

where $n = \phi K_1$. Thus, the time to reach equilibrium in the end state is infinite. The Rouse equation for the relaxation time also shows an infinite sum of the row of relaxation times and cut offs of this row are used to have a converging row.
Because the first term of the Rouse row provides the main contribution to the spectrum and the viscosity, eq.(28) should be comparable with the Rouse equation at $t = t_r$, the relaxation time of Rouse. With $t_0 \approx 0$ and thus omitting the small terms (with $\phi\sigma_{v0}$) this eq.(28) becomes:

$$\left(\frac{e^{-\phi\sigma_v}}{\phi K_1} + \frac{e^{-3\phi\sigma_v}}{3\phi K_1} + \frac{e^{-5\phi\sigma_v}}{5\phi K_1} + \ldots\right)\cdot\frac{2}{D} = t_r = \sum_{p=1}^{N/5}\tau_p \quad \text{with} \quad \tau_p = \frac{c_3}{p^2} \quad \text{(see at eq.(15''))}$$

Thus:

$$\frac{e^{-\phi\sigma_v}}{\phi K_1}\cdot\left(1 + \frac{e^{-2\phi\sigma_v}}{3} + \frac{e^{-4\phi\sigma_v}}{5} + \ldots\right) = \frac{c_3 D}{2}\left(1 + \frac{1}{2^2} + \frac{1}{3^2} + \ldots\right) \qquad (38)$$

giving: $c_3 = 2/(D\phi K_1 e^{\phi\sigma_v}) = t''/e^{0.14} = t''/1.15$ or the longest relaxation time of Rouse is proportional and of the same order of the relaxation time t''of the falling curve as can be expected. Further is:

$$1 + \frac{e^{-2\phi\sigma_v}}{3} + \frac{e^{-4\phi\sigma_v}}{5} + \ldots = 1 + \frac{1}{2^2} + \frac{1}{3^2} + \ldots$$

or in general: $\phi\sigma_v = \left(\ln\{p^2/(2p-1)\}\right)/(2p-2)$, for every: p = 2, 3, 4, 5, ..., giving:

p	2	3	4	5
$\phi\sigma_v$	~ 0.14	~ 0.14	~ 0.14	~0.13

or $\phi\sigma_v \approx 0.14$ because the first few terms determine nearly the total behavior.
The value of $\phi\sigma_v$ quickly decreases at a small change of the power of the row. For instance for a 5% difference, when the power is 1.9 in stead of 2, $\phi\sigma_v \approx 0.11$,

p	2	3	4	5
$\phi\sigma_v$	~ 0.11	~ 0.12	~ 0.11	~0.11

according to: $\phi\sigma_v = \left(\ln\{p^{1.9} / (2p-1)\}\right) / (2p-2)$, for every: p = 2, 3, 4, 5, …
For a power of 1.7, $\phi\sigma_v$ is about 0.05 and at the power of 1.6, close to the Zimm value, the weighted mean value of $\phi\sigma_v$ is very small close to equilibrium and data show that there is a steeper slope, approaching the Zimm value at the longest times, near equilibrium, by the lower $\phi\sigma_v$. Thus the chosen cutoff of the spectrum explains the success of the use of power laws in the terminal zone. For linear visco-elasticity, a similar expansion is not possible and the Rouse spectrum thus cannot represent a linear process.

3.4. The non-existence of spectra of relaxation times

The response of a stress relaxation test cannot be described by a linear visco-elastic process or by a spectrum of (infinite) linear relaxation processes. It is necessary to use the exact description. As solution of the exact equation, an expansion of the potential energy barrier can be used, leading to a line spectrum of elementary non-linear reactions. However, the spectral values of the "lines" are so far apart from each other, that they act as separate processes and not as a spectrum. In any experiment therefore, only one or two elementary processes are detectable. According to the constitutive equations, these two processes can be represented by a system of parallel (non-linear) Maxwell elements. Because the relaxation times are far apart, only one or two Maxwell elements are noticeable in a test, while others (if present) flow too fast to be loaded or flow too slow to be noticeable and thus act as springs, within the time range of the test.
The whole relaxation behavior, including the delay time (of no decrease of stress) at the start, the linear stress decrease on the log-time scale and the bend off to equilibrium at the end of a process can be represented by one non-linear Maxwell element and a parallel spring (fig. 3.4) with a non-linear dashpot according to deformation kinetics, representing one relaxation time. If the straight relaxation line (on log- time scale) is kinked, there is a second process acting with a long delay time [2].

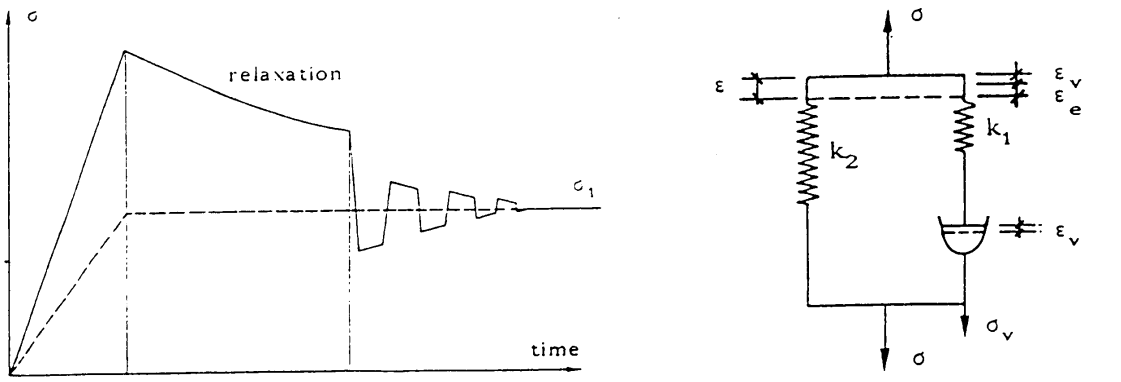

Fig. 3.4. Zero relaxation by zero internal stress [2]

To show that there is only one relaxation time acting in a long time range and not a spectrum, the following test was done in [2]. In a relaxation test on wood, after a few hours of relaxation at the working strain level, (enough for a parameter estimation), the internal stress was made zero by reducing the load on the specimen to a level of about 0.6 times the initial strain (depending on the time of testing and to be found by a searching procedure see fig. 3.4 and [2]). At this stress level, the stress on the dashpot (and spring of the Maxwell element) is zero in fig. 3.4 and the total stress (in the free spring) remains perfectly constant showing no further relaxation or change during the next 24 hours (the time of this

test in [2]). This behavior is not possible if there exists a continuous spectrum. The stress always should change then. But also a discrete spectrum cannot explain this behavior. In order to explain e.g. the measured constant value of the loss tangent or relaxation spectrum of wood and of other glasses, by a discrete linear viscoelastic spectrum, the adjacent relaxation times τ can not differ more than by one order: $\tau_{i+1} \leq 10\tau_i$ (see [2], pg. 97). The zero relaxation test however shows that loading one order of time longer than the first relaxation period (of the first element) does not show any change of stress, while it should have been of the same relative order. This perfect constancy of the stress shows the next relaxation time to be many orders higher than the first one (in stead of one order higher) and there thus is no contribution of a spectrum or a line spectrum.

3.5. Viscosity equations

When a material may show viscous flow, the direct measurement of the viscosity is appropriate for parameter estimation. At flow, all sites are used and there is no change of the concentration and the stress is constant and the rate of change of the elastic strain is zero. Thus in eq.(25) is $\dot{\sigma}_v = 0$ and $\dot{\varepsilon} = \dot{\varepsilon}_v$.

For no structural change, eq.(26') applies or:

$$\dot{\varepsilon} = \frac{\dot{\sigma}_v}{K_1} + A \cdot \sinh(\phi\sigma_v) = A_1 \cdot \sinh(\phi_1\sigma_1) \tag{39}$$

If there are more processes acting (visualized as a system of parallel non-linear flowing Maxwell elements) the total stress σ is: $\sigma = \sigma_1 + \sigma_2 + \sigma_3 + ...$, or:

$$\sigma = \frac{1}{\phi_1}\operatorname{arcsinh}\left(\frac{\dot{\varepsilon}}{A_1}\right) + \frac{1}{\phi_2}\operatorname{arcsinh}\left(\frac{\dot{\varepsilon}}{A_2}\right) + \frac{1}{\phi_3}\operatorname{arcsinh}\left(\frac{\dot{\varepsilon}}{A_3}\right) + \ldots$$

The viscosity then is: $\eta = \sigma / \dot{\varepsilon}$ or:

$$\eta = \frac{\operatorname{arcsinh}(\dot{\varepsilon}/A_1)}{\dot{\varepsilon}\phi_1} + \frac{\operatorname{arcsinh}(\dot{\varepsilon}/A_2)}{\dot{\varepsilon}\phi_2} + \frac{\operatorname{arcsinh}(\dot{\varepsilon}/A_3)}{\dot{\varepsilon}\phi_3} \tag{40}$$

Because relaxation times of the processes are far apart from each other, only a few terms, are noticeable together in the viscosity equation. All very small values of the variable "x" in arcsinh(x) act as one Newtonian process and all very large values are not noticeable. For very large values of x is: (arcsinh(x))/x ≈ 0 and these processes thus are not acting. Because of this eq.(40) applies for no more than 3 processes. For very small values of x is: (arcsinh(x))/x = 1 and processes with this property act as Newtonian or are quasi Newtonian in the range of measuring.

Eq.(40) then becomes:

$$\eta = \frac{1}{\phi_1 A_1} + \frac{\operatorname{arcsinh}(\dot{\varepsilon}/A_2)}{\dot{\varepsilon}\varphi_2} + \frac{\operatorname{arcsinh}(\dot{\varepsilon}/A_3)}{\dot{\varepsilon}\varphi_3} \tag{40'}$$

It further is possible that the second term may be non-linear, as given in eq.(40'), for high strain rates $\dot{\varepsilon}$, while it may become quasi Newtonian at low rates, being $1/(\phi_2 A_2)$. For larger values of x, $\operatorname{arcsinh}(x) \approx \ln(2x)$ and eq.(40") thus becomes:

$$\sigma \approx \frac{1}{\phi_1 A_1}\dot{\varepsilon} + \frac{\operatorname{arcsinh}(\dot{\varepsilon}/A_2)}{\phi_2} + \frac{1}{\phi_3}\ln\left(\frac{2\dot{\varepsilon}}{A_3}\right) \tag{40"}$$

As will be shown below, eq.(40') and (40'') hold for solutions and for finely milled rubbers, while eq.(40) holds for solid plastic systems. Linear visco-elastic behavior thus does not exist for structural materials, even not above glass transition, as follows from eq.(40).

3.6. Solutions of high polymers

The equations above should contain, for a solution, one extra term of the flow units of the solvent molecules. The solvent molecules generally flow more easily than the high polymer solute molecules. Thus, dilute solutions only will show one process of shearing of the solvent molecules. If this solvent is Newtonian, then real linear behavior can be expected to be possible and measurable.

Eq.(40') becomes for solutions:

$$\eta = \frac{1}{\phi_0 A_0} + \frac{1}{\phi_1 A_1} + \frac{\operatorname{arcsinh}(\dot{\varepsilon}/A_2)}{\dot{\varepsilon}\phi_2} + \frac{\operatorname{arcsinh}(\dot{\varepsilon}/A_3)}{\dot{\varepsilon}\phi_3} \qquad (40''')$$

where $\eta_0 = 1/\ \phi_0 A_0$ is the viscosity of the solvent.

The following quantities are often used for solvents:

The relative viscosity η_{rel} is by definition: $\eta_{rel} = \eta/\ \eta_0$

The specific viscosity is given by: $\eta_{sp} = \eta_{rel} - 1$

The intrinsic viscosity is defined as: $\eta_{int} = \eta_{sp} / c$, where c is the concentration.

The limiting intrinsic viscosity $[\eta]$, (for low concentration approaching zero), is:

$[\eta] = \lim(\eta_{int})_{c\to 0}$

The inherent viscosity, η_{inh}, is defined as $(\ln(\eta_{rel}))/c$.

For small terms and very small concentrations, this is equal to $[\eta]$ according to:

$$\frac{1}{c}\ln\left(\frac{\eta}{\eta_0}\right) = \frac{1}{c}\ln\left(1 + \frac{1}{\phi_1 A_1 \eta_0} + \frac{\operatorname{arcsinh}(\dot{\varepsilon}/A_2)}{\dot{\varepsilon}\phi_2\eta_0} + \frac{\operatorname{arcsinh}(\dot{\varepsilon}/A_3)}{\dot{\varepsilon}\phi_3\eta_0}\right) \approx$$

$$\approx \frac{1}{c}\left(\frac{1}{\phi_1 A_1 \eta_0} + \frac{\operatorname{arcsinh}(\dot{\varepsilon}/A_2)}{\dot{\varepsilon}\phi_2\eta_0} + \frac{\operatorname{arcsinh}(\dot{\varepsilon}/A_3)}{\dot{\varepsilon}\phi_3\eta_0}\right) \approx (\eta_{int})_{c\to 0} \approx [\eta] \qquad (41)$$

what holds for low concentrations and small relative viscosities of the groups or:

$$\sum \frac{\operatorname{arcsinh}(\dot{\varepsilon}/A_i)}{\dot{\varepsilon}\phi_i\eta_0} << 1 \qquad (42)$$

These equations can be used as first approximations for parameter estimation. At the end the exact equations for η_{inh} and η_{sp} should be used:

$$\frac{\ln(\eta_{rel})}{c} = \frac{1}{c}\ln\left(1 + \frac{1}{\phi_1 A_1 \eta_0} + \frac{\operatorname{arcsinh}(\dot{\varepsilon}/A_2)}{\dot{\varepsilon}\phi_2\eta_0} + \frac{\operatorname{arcsinh}(\dot{\varepsilon}/A_3)}{\dot{\varepsilon}\phi_3\eta_0}\right) \qquad (43)$$

and: $$\ln(\eta_{sp}) = \ln\left(\frac{1}{\phi_1 A_1 \eta_0} + \frac{\operatorname{arcsinh}(\dot{\varepsilon}/A_2)}{\dot{\varepsilon}\phi_2\eta_0} + \frac{\operatorname{arcsinh}(\dot{\varepsilon}/A_3)}{\dot{\varepsilon}\phi_3\eta_0}\right) \qquad (44)$$

For small rates, if applicable, eq.(43) becomes:

$$\frac{\ln(\eta_{rel,0})}{c} = \frac{1}{c}\ln\left(1 + \frac{1}{\phi_1 A_1 \eta_0} + \frac{1}{\phi_2 A_2 \eta_0} + \frac{1}{\phi_3 A_3 \eta_0}\right) \qquad (43')$$

and at high rates:

$$\frac{\ln(\eta_{rel,\infty})}{c} = \frac{1}{c}\ln\left(1 + \frac{1}{\phi_1 A_1 \eta_0}\right) \qquad (43'')$$

In materials and wood science, there still is a belief (against facts) in the existence of linear visco-elastic relaxation spectra (thus spectra being independent of the stress, ignoring e.g. the time-stress equivalence). To discuss the consequences of such an assumption it first is necessary to study the cases where there is a possibility of existence of any Newtonian behavior as for liquids, soft solids and crystals or metals near melting. Further solutions can be regarded for stages between the liquid- and the solid state. Of course, the solvents of

these solutions should behave as Newtonian (thus should consist of short bulky rotational molecules) in order to have any possibility of linear behavior.

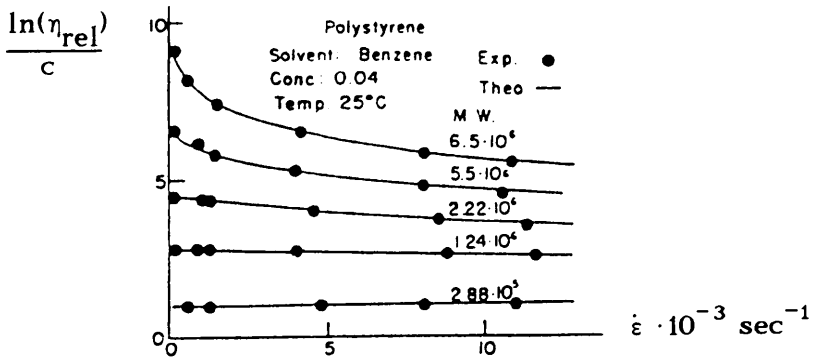

Fig. 3.6.1. The effect of molecular weight of polystyrene solved in benzene, c = 0.04 g/100 cc; temperature 25 0 C; $\eta_0 = 6.01 \cdot 10^{-3}$ poise [17]. The theoretical curves are according to eq.(43).

In fig. 3.6.1, measured viscosities by a capillary viscometer are given of a dilute solution. It is seen by the straight line parallel to the $\dot{\varepsilon}$ - axis, that only the shortest chain, with molecular weight of $0.288.10^6$, behaves as (quasi) Newtonian (with $\eta_{rel}/c = 1.08$ cm^3/g), within the strain rate interval of the measurement. At the molecular weights of $1.24.10^6$ to $2.22.10^6$, two types of flow units are present, one linear and one non-linear as follows from the negative slope, which increases with increasing molecular weight. Three types of flow units are acting at the fractions with molecular weights of $5.5.10^6$ to $6.5.10^6$ as follow from the sharp increase of the curvature at low values of $\dot{\varepsilon}$, that increases at increasing molecular weight. For the fit of the curve in fig. 3.6.1, of the solution of polystyrene with molecular weight $6.5.10^6$ the parameters are: $1/\phi_1 A_1 \eta_0 = 0.168$; $1/A_2\eta_0 = 0.0795$; $1/A_3\eta_0 =$ $= 1.57$; $1/\phi_2 = 2{,}01$ N/m^2; $1/\phi_3 = 0.00129$ N/m^2.

Comparable results are found for other solutions. For a polystyrene solution in cyclohexane, for instance, two types of flow units are present at a molecular weight: m.w. = $2.4.10^6$ and three types at m.w. = $5.2.10^6$ at 65 ^{0} C, while this occurs at m.w. = $5.2.10^6$, respectively m.w. = $9.2.10^6$ at 35 ^{0} C. At 35 ^{0} C there only are 2 types of flow units acting (below the highest tested m.w. = $9.2.10^6$, while at 65 ^{0} C the third kind of flow unit acts above m.w. = $5.2.10^6$.

As can be seen in fig. 3.6.1, Newtonian behavior only is possible, in the given strain rate range, in dilute solutions of low molecular weight solutes in Newtonian solvents. At increasing molecular weight the probability of formation of stronger types of bonds increases. This also is the case for higher concentrations and when molecules unfold in poor solutions at higher temperatures. <u>These stronger bond types are not acting through the Newtonian solvent and thus are non-Newtonian.</u>

In fig. 3.6.2., the influence of the concentration on η_{inh} is given for the highest m.w. and highest temperature tested, thus showing the influence on all three kinds of flow units. The equation of η_{inh} is given by eq.(43) and the parameter estimation of the fit shows that the terms $1/A_i\eta_0$ are independent of the concentration:

$$\frac{1}{A_i\eta_0} = \frac{A_0\phi_0}{A_i} = \frac{(kT/h)N_0 \exp(-E'_0/kT)\cdot(\lambda_0/N_0kT)}{(kT/h)N_i \exp(-E'_i/kT)} =$$

$$= \frac{\lambda'_0}{N_0 k} \exp\left(\frac{-(E'_0 - E'_1)}{kT}\right) \qquad (45)$$

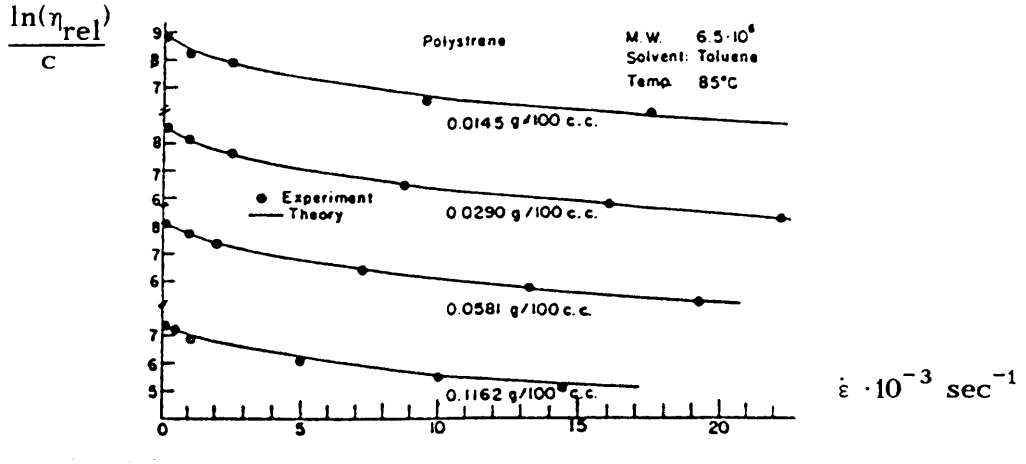

Fig. 3.6.2. Effects of concentration on η_{inh} of polystyrene solved in benzene, molecular weight: $6.5.10^6$; temperature 85 ^{0} C; $\eta_0 = 2.99.10^{-3}$ poise [17] The theoretical curves are according to eq.(43).

and it appears that $N_i = N_0$ and $\lambda_0 = \lambda'_0 T$ and $H'_0 = H'_1$. Thus, flow of the solvent is determining and the internal stress on the dilute is such that this flow-rate is followed with the same apparent parameters. In eq.(45) is N_0 independent of the concentration because the concentration of the solvent is ~ 1 and the number of activated sites N_0 is not influenced by the small dilute concentration.

The curve fitting further shows that $1/(c\phi_1 A_1 \eta_0)$ is independent of the concentration $c = c'N$. Because $A_1\eta_0$ is independent of the concentration according to eq.(45), $c\phi$ also has to be independent of the concentration and of N. Thus:

$$c\phi_1 = c'N\lambda_1 / (NkT) = c'\lambda_1 / kT = c'\lambda'_1 / k \qquad (46)$$

This needs not be the case in a poor solvent for the second and third process (i = 2,3) where N_i is a function $N_i(c)$ of the concentration c that is more than linearly increasing with c :

$$c\phi_i = c\lambda_i / kTN_i = c\lambda_i / (kTN_i(c)) \qquad (47)$$

showing that another process is acting causing the increase of flow units. This only is possible if a no bonded (folded) flow unit unfolds, and makes bonds with its neighbours. Because $1/\phi$ is larger in a good solvent than in a poor one, the polymer molecule extends more in a good solvent. Consequently, the polymer in a good solvent also has more probability of making strong bond types with the neighbours

It can be seen that the slope of the curves in fig. 3.6.2 is constant irrespective of the concentrations. It follows from eq.(41) of these curves, that the inherent viscosity, $\eta_{inh} = (\ln(\eta_{rel}))/c \approx (\eta_{rel} - 1)/c$ for dilute solutions, is:

$$\eta_{inh} \approx \frac{1}{c\phi_1 A_1 \eta_0} + \sum \frac{\operatorname{arcsinh}(\dot{\varepsilon} / A_i)}{c\dot{\varepsilon}\phi_i \eta_0}$$

Because $c\phi_1 A_1 \eta_0$ is constant, the difference of η_{inh} for 2 concentrations c_1 and c_2 is:

$$\eta_{inh,1} - \eta_{inh,2} = \sum \frac{\operatorname{arcsinh}(\dot{\varepsilon} / A_{i,1})}{c_1\dot{\varepsilon}\phi_{i,1}\eta_0} - \sum \frac{\operatorname{arcsinh}(\dot{\varepsilon} / A_{i,2})}{c_2\dot{\varepsilon}\phi_{i,2}\eta_0} =$$

$$= \frac{1}{n}\left(\sum \operatorname{arcsinh}(\dot{\varepsilon} / A_{i,1}) - \sum \operatorname{arcsinh}(\dot{\varepsilon} / A_{i,2})\right) \approx$$

$$\approx \frac{1}{n}\left(\sum \ln(2\dot{\varepsilon} / A_{i,1}) - \sum \ln(2\dot{\varepsilon} / A_{i,2})\right) =$$

$$= \frac{1}{n}\sum \ln(A_{i,1} / A_{i,2}),$$

independent of $\dot{\varepsilon}$, as necessary for a vertical shift of the curve, without a change of the form of the curve, at a change of concentration. Thus:
$A_{i,2} / A_{i,1} = \left(\exp(S'_{i,1} - S'_{i,2})/k\right)(N_{i,1} / N_{i,2})$, proportional to: $N_{i,1} / N_{i,2}$ and N_i is known from the shifts of the curves depending on the concentration c.
Further is n constant or:

$$n = c\dot{\varepsilon}\phi_i\eta_0 = c' N_i \dot{\varepsilon}\phi_i / A_0\phi_0 = c'\dot{\varepsilon}\lambda'_i h / k\lambda_0 \exp(-E'_0/kT) \qquad (48)$$

The influence of the temperature on η_{inh} and $[\eta]$ follows from reduced curves of η obtained by using reduced shear rates: $\eta_0\dot{\varepsilon}$. The η_0-reduced curve: η/η_0 versus $\eta_0\dot{\varepsilon}$ is:

$$\frac{\eta}{\eta_0} = 1 + \frac{1}{\phi_1 A_1 \eta_0} + \sum \frac{\operatorname{arcsinh}(\dot{\varepsilon}\eta_0 / A_i\eta_0)}{\phi_i \eta_0 \dot{\varepsilon}} \qquad (49)$$

This means that $1/A_1\phi_1\eta_0$; $1/\phi_i$ and $1/A_i\eta_0$ are independent of the temperature. From eq.(45) follows: $1/A_1\phi_1\eta_0 = (\lambda'_0 N_1 / \lambda'_1 N_0)\cdot\exp(-(E'_0 - E'_1)/kT)$. This is independent of the temperature when: $\exp(-(E'_0 - E'_1)/kT)$ is independent of the temperature. Thus when: $\exp(-(H'_0 - H'_1)/kT + (S'_0 - S'_1)/k) = \exp((S'_0 - S'_1)/k)$ or: $H'_0 = H'_1$.
Thus, this reducibility shows that the activation heat for the flow process of the polymeric flow units is the same as that for the solvent (in a good solvent). The processes are determined by activation of the solvent molecules. As mentioned before, from eq.(45) it also follows that $H'_0 = H'_1$ is necessary for the constancy of $1/A_i\eta_0$, independent of the temperature. Further, eq.(46) gives the constant ϕ_i independent of the temperature.
In fig. 3.6.5, experimental values of $[\eta]$ at 65 ^{0}, 50 ^{0}, and 35 ^{0} C are given. It is seen that, for a poor solvent, a reduced curve is not obtained. The higher the temperature, the larger is the limiting intrinsic viscosity $[\eta]$. In this case, $1/\phi_2$ increases with temperature,

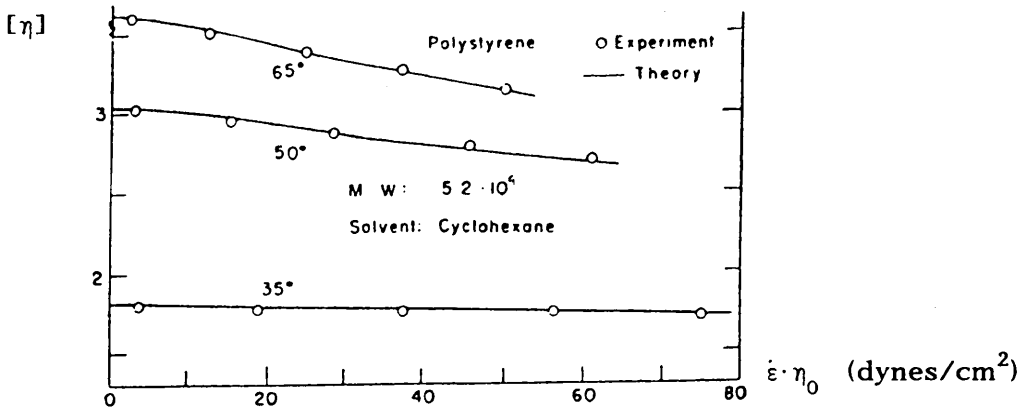

Fig. 3.6.5. Effects of temperature on η_{inh} for polystyrene solutions, in a "poor" solvent [17]; polystyrene m.w. = 5.2 10^6; solvent cyclohexane; concentration, infinite dilution. The theoretical curves are according to eq.(43).

although it should be independent of the temperature. This thus indicates the increase of "N" and thus that in a poor solvent the polymers unfold with increasing temperature while

they fold with decreasing temperature. The non-reducibility is due to the change of the structure by unfolding of the molecules with increasing temperature.
When η_0, of the solvent, becomes negligible, reducibility is obtained by multiplication of $\dot{\varepsilon}$ with: exp(H'$_i$/kT), as follows from reaction kinetics. This is the case for concentrated solutions and for solids. Both types of reductions are measured for instance at flow of a dilute solution, a concentrated solution and a pure solid of X-518 GR-S rubber (24 % styrene and 76 % butadiene copolymer).
The reduced shear rate for the concentrated solution and the solid is:
$\dot{\varepsilon}_r = \dot{\varepsilon} \exp(H_i / RT)$ and the activation heats are: 3.9 and 9.75 kcal/mol, respectively for the 10 % and 50 % polymer solutions. The activation heat (activation enthalpy) of the solid (100 % concentration) is 12.5 kcal/mol.
The activation heat 3.9 kcal-mol of the 10% (dilute) solution is about that of the solvent and for this case the curve thus shows the η_0 - reduction explained before.
The rate equation of flow of the 50 % solution follows exactly:

$$\sigma = \frac{\operatorname{arcsinh}(\dot{\varepsilon}/A_1)}{\phi_1} + \frac{\operatorname{arcsinh}(\dot{\varepsilon}/A_2)}{\phi_2} \qquad (50)$$

and thus acts as the pure (100 %) solid polymer, also showing the 2 non-linear groups according to eq.(50).
For dilute solutions H_i (equal to the solvent value) and ϕ_i (in the case of no unfolding) are independent of the concentration. For concentrated solutions $1/\phi_1$ and $1/\phi_2$, increase with concentration as do the activation heats H_i and the reduced values: $A_i \exp(H_i/RT)$. As mentioned before, because $1/\phi = NkT/\lambda$, the increase with concentration shows that there is an increase of the concentration of flow units N by unfolding and bond formation between a flow unit and its neighbours. The increase of the reduced A-value: $A_i \exp(H_i/RT) = (kT/h)N_i \exp(S_i/R)$ with increasing concentration, if more than linearly, indicates that also the activation entropy S_i increases with concentration as can be expected by the increase of bonds between a flow unit and its neighbour with increasing concentration. Because now the solvent is not determining any more (as is the case for the η_0 - reduction) the solvent molecules are able to flow only when the bonding between the solute molecules flow. In highly concentrated solutions, the solvent molecules move together with the polymer flow units. Thus, the 50 % solution behaves like the pure solid (see 3.7).
The before mentioned reducibility by division by η_0 or, what is the same, the equality of the activation heats of the polymer and solvent $H_1 = H_0$ and the temperature and concentration independent ϕ_1, shows that the solvent determines the process and the rate determining step for the solute unit involves the jump of the solvent molecule. The solvent molecule must move in the opposite direction, while the flow unit moves forward to fill out the space vacated by the solvent molecule. The same occurs in the diffusion of a large molecule in a solvent of small molecules. This has been tested. A foreign molecule similar in structure and length as the monomeric unit, dissolved in the monomer has a translator friction coefficient $\zeta_1 = kT/D_0$, where D_0 is the diffusion constant at vanishing concentration of this low-molecular weight component (D_0 is measured by transpiration, absorption-desorption or radio-activity of tagged molecules). Far above the glass temperature T_g (e.g. in rubber) ζ_1 is the same as ζ_0, the friction coefficient of the monomeric unit of the polymer backbone. Thus activated units move as if there is no chain and essential is the kinetics, where the entropy is determined by the entropy of random mixing and the enthalpy is calculated in terms of the nearest neighbour bonds and their bond strengths as in a regular

solution model (in stead of a flexible chain model). However, when T_g is approached, the kinetics of the determining process is quite different because then $\zeta_0 >> \zeta_1$ showing that now the scale of activation is reduced to that of the side bonds and now the attached chain units prevent free moving of activated monomeric parts of the backbone.

3.7. Undiluted solid polymers

Chain models are also applied for the description of the behavior of solids. This however is not possible, as shown before, and follows from the exact description and explanation of the behavior in the following.
As discussed before, linear visco-elastic behavior will show, on the plot of η versus $\dot{\varepsilon}$, a straight line parallel to the $\dot{\varepsilon}$- axis (line 1 of fig. 3.7.1). Because this never is the case for solids, an extrapolation of the η versus $1/\dot{\varepsilon}$ plot should be made to the zero value of $1/\dot{\varepsilon}$ giving the apparent Newtonian value η_∞ because the other terms in eq.(40') or, the here determining, eq.(51), are zero then.

$$\eta = \frac{1}{\phi_1 A_1} + \frac{\operatorname{arcsinh}(\dot{\varepsilon}/A_2)}{\dot{\varepsilon}\phi_2} = \eta_\infty + \frac{\operatorname{arcsinh}(\dot{\varepsilon}/A_2)}{\dot{\varepsilon}\phi_2} \qquad (51)$$

It is possible that this extrapolation gives a negligible value of η_∞ (indicating no Newtonian behavior) while at low rates a good fit of eq.(51) is possible. This indicates that non-Newtonian behavior may become Newtonian according to:
$\dot{\varepsilon} = A\sinh(\phi\sigma) \approx A\phi\sigma = \sigma/\eta$.
As mentioned before this only may apply for very short molecules and not for structural materials because $\sigma_0\phi$ then mostly is constant and a low initial stress σ_0 will cause a high value of ϕ and the rate $\dot{\varepsilon}$ still follows the non-linear sinh-dependence of σ.

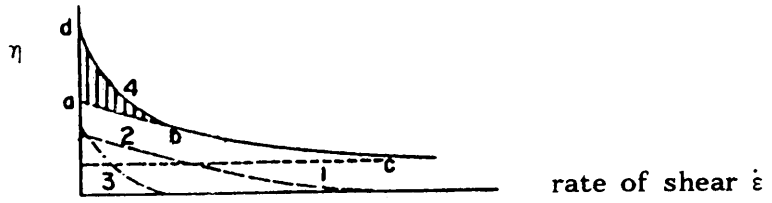

Fig. 3.7.1. Viscosity dependent of $\dot{\varepsilon}$. Curve 1: $\eta = 1/A_1\phi_1$.
Curve 2: $\eta = (\operatorname{arcsinh}(\dot{\varepsilon}/A_2))/(\dot{\varepsilon}\phi_2)$.
Curve 3: $\eta = (\operatorname{arcsinh}(\dot{\varepsilon}/A_3))/(\dot{\varepsilon}\phi_3)$.
Curve 4 is the sum of curve 1 to 3. Curve abc is the sum of 1 and 2.

Knowing η_∞, (if any), the fit of the second process should be done at higher rates (line bc in fig. 3.7.1) and extrapolation of this process to low values of $\dot{\varepsilon}$ (line abc in fig. 3.7.1) makes it possible to determine the third process (if any) by the difference of the measurements and line abc (see fig. 3.7.1).
In fig. 3.7.2, a flow curve is given of natural rubber (a masticated rubber of lightly milled crepe). In order to obtain a reduced curve, H' should be constant and

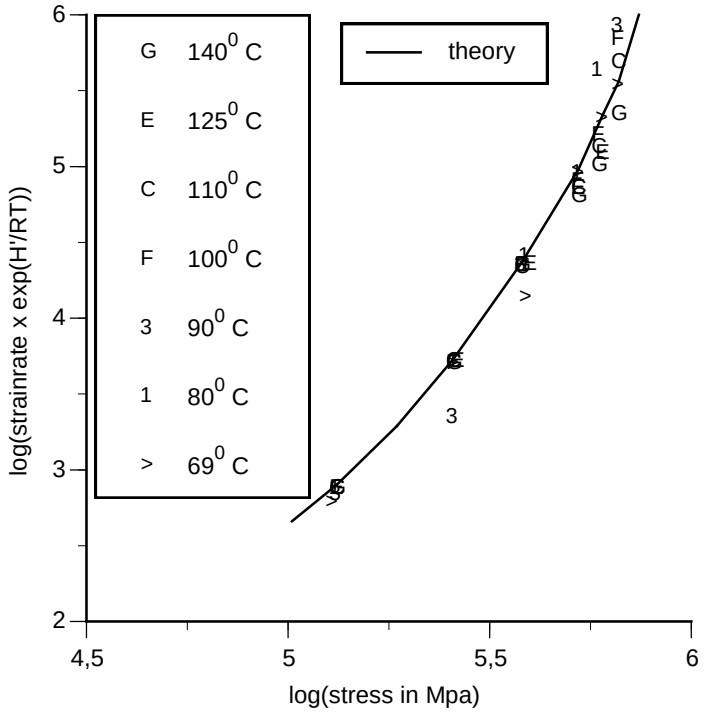

Fig. 3.7.2. Reduced shear rate, dependent on the stress, of rubbers [15]

$\phi = \lambda/(NkT) = \lambda'/(Nk)$ has to be independent of the temperature. As to be expected from the m.w., this material shows (quasi) Newtonian behavior (eq.(51)) at low stresses and shows two non-linear processes, given by eq.(50), at high stresses. Stronger crushed material, with a still lower m.w., did show a Newtonian process, in the whole tested rate range, and followed eq.(51), as to be expected. The higher m.w. causes a longer relaxation time 1/A, while the enthalpy H' (8 kcal/mol) and activation volume ϕ ($1/\phi \approx 1.4\ 104\ N/m^2$) are the same as for the material with low m.w. This shows the same segmental motions (the same volume ϕ and energy of a jump H'), that are more difficult to coordinate by the longer molecules. This causes a high negative activation entropy [2], (i.e. the coordinated segmental motions in long molecules are much less probable) (as applies for wood).
In fig. 3.7.3, flow behavior is given of polystyrene, measured by the capillary visco-meter at temperatures between 165^0 and 250^0 C.
The reduced curve of fig. 3.7.3 is obtained by using
$\dot{\varepsilon}\,\eta_S$, where η_S is the viscosity at small $\dot{\varepsilon}$, thus $\eta_S = 1/\phi_1 A_1 + 1/\phi_2 A_2$. Thus, eq.(50) becomes:

$$\sigma = \frac{\operatorname{arcsinh}(\dot{\varepsilon}\eta_s / A_1\eta_s)}{\phi_1} + \frac{\operatorname{arcsinh}(\dot{\varepsilon}\eta_s / A_2\eta_s)}{\phi_2} \qquad (50')$$

and represents a reduced curve when ϕ_1, ϕ_2, $\eta_s A_1$, $\eta_s A_2$ are independent of the temperature. Because $\eta_s A_1 = (1 + A_1\phi_1 / A_2\phi_2)/\phi_1$ and $\eta_s A_2 = (1 + A_2\phi_2 / A_1\phi_1)/\phi_2$ is also necessary that A_1/A_2 is independent of the temperature and thus the enthalpy is the same $H'_1 = H'_2$ what is typical for the possible liquid-like character of rubbery materials where different relaxation times (differing here 2 to 3 orders) are determined by differences in entropy. The behavior of the short bulky polymers may, by the small activation volume parameter, also be quasi-linear visco-elastic in the glass state. The storage and loss shear modules

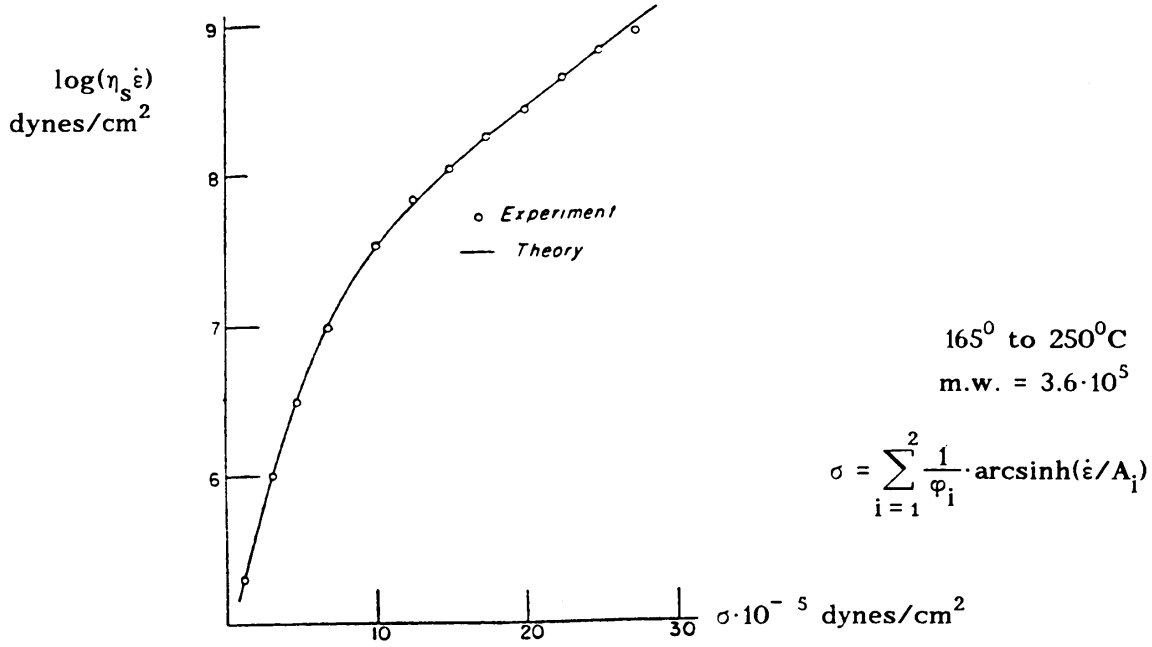

Fig. 3.7.3. Reduced shear rate dependent on the stress of polystyrene, [15].

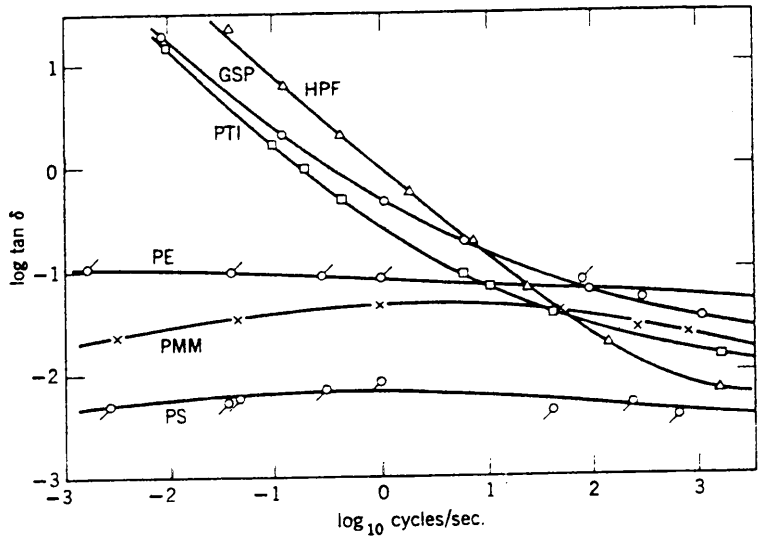

Fig. 3.7.4. Loss tangent - frequency - plot for three glasses of low molecular weight and other polymeric glasses and a crystalline polymer. HPF, hydroxypentamethylflavan; GSP, glycerol sextol phthalate; PTI, 2-phenyl-3-p-tolylindanone; (PS, polystyrene; PMM, polymethyl mehacrylate); see [8].

follows the frequency dependence of a single Maxwell element over the range of 4 logarithmic decades (10^{-3} to 1 cycle/sec., see fig. 3.7.4). For a Maxwell element, tan(δ) is inversely proportional to the frequency and thus the logarithmic plot of tan(δ) in fig. 3.7.4 shows a slope of - 1. At high frequencies, the figure shows that the behavior is non-linear just like the long chain polymers where tan(δ) becomes nearly constant, independent of the frequency.

3.8. Crystalline materials

Flow of crystalline polymers at high temperatures, that is possible for short molecules, the best can be studied in pure crystalline materials as single and poly-crystalline metals. At flow, secondary (or steady) creep occurs according to the simple equation (50). At this stage, the tertiary creep (e.g. by fracture) is not noticed because of the long delay time of such a structural change process. The steady creep of metals at high temperatures (T > 0.45 Tm, where Tm is the melting temperature) is due to self-diffusion. Dislocations are held up by "bad sites" (such as: impurities, alloying elements, crystal imperfections, etc.), causing stress concentration in the neighbourhood. This stress is relieved by diffusion of the neighbours of the bad site, because the activation heat for creep equals that for self-diffusion. Operations as cold working, heat treatment, annealing, etc., introduce certain types of bad sites into the metals. This appears to be the main reason for the occurring of more processes. An example of only one process is given in fig. 3.8.1, of steady creep of pure aluminum and Al-Mg alloys. The equation of the creep curves thus is:

$$\dot{\varepsilon} = A\sinh(\phi\sigma) \qquad (52)$$

Beside creep tests, also tensile test were conducted for verification of the real molecular parameters, making prediction of behavior possible. Temperature reduction is obtained

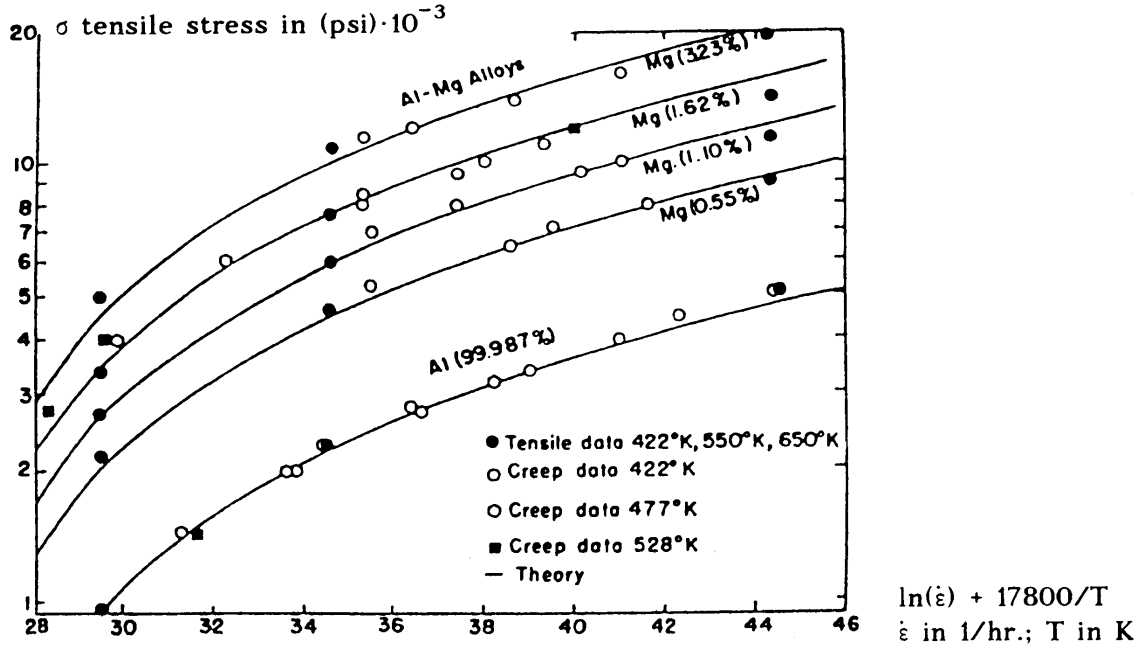

fig. 3.8.1. Steady creep of aluminum and aluminum-magnesium alloys [1]

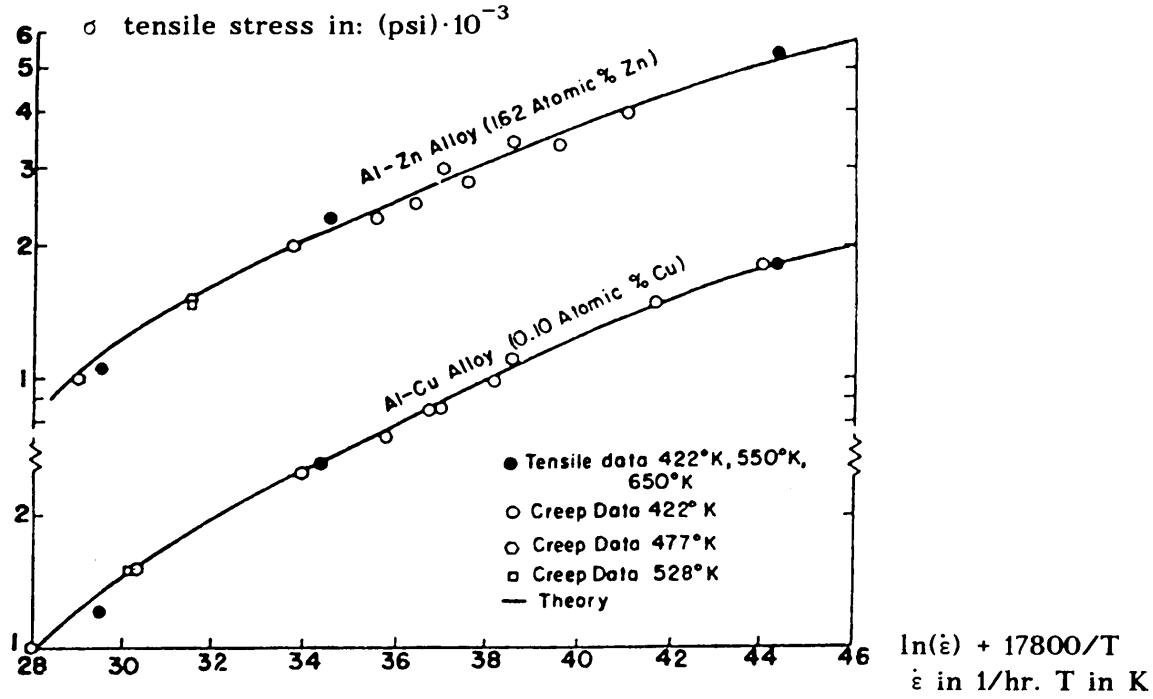

Fig. 3.8.2. Creep curves of Al-Cu and Al-Zn alloys [1].

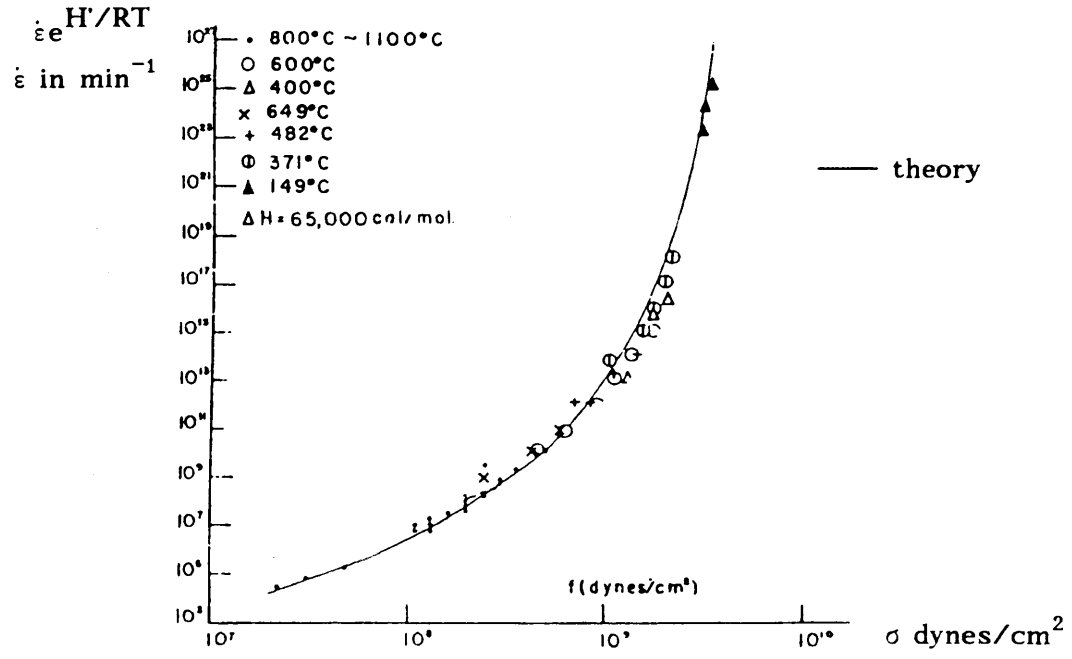

Fig. 3.8.3. Creep curve for polycrystalline nickel.

by multiplication of the rate by exp(H'/RT) with H' = 35.6 kcal/mol for aluminum and its alloys. For all curves, φ is independent of the temperature. In fig. 3.8.2, creep curves of the alloys Al-Cu and Al-Zn are given that cannot be expressed by one kind of flow unit, but require two kinds according to eq.(50). The same applies for polycrystalline material as e.g. nickel in fig. 3.8.3.
Data of creep of pre-crept Al-Mg alloys did show 3 processes according to eq.(40). Also annealed Al-Mg alloys showed 3 processes with quite different parameters.

It thus appears that structural changes due to previous treatments have a strong influence and separate structural change processes did cause the special additional bad sites. The relaxation times of the 2 processes determining the curves of fig. 3.8.2 to 3.8.3 differ about 5 to 6 orders with respect to each others, showing that a real spectrum does not exist.
The behavior thus is similar to that of all solids and high polymers and because (quasi) linear visco-elasticity only is possible for very short molecules, the general conclusion is that linear visco-elasticity cannot exist in structural materials like wood. The conclusions of RILEM T.C. 112, based on linear behavior, thus are invalid because long-term predictions of behavior then are totally wrong.

4. Conclusions

- As shown in [2] and here, the exact equilibrium theory of molecular deformation kinetics, explains precisely (correlation ~ 1) all aspects of time dependent behavior like creep, damage, transformations, etc. New is here, that the same constitutive equation with the same molecular parameters as e.g. N, λ and λ_1 as for creep and damage, is shown here to explain all aspects of flow behavior (as given in the figures of 3.6, 3.7 and 3.8) as well. The influence on dilute solutions of: the molecular weight; the concentration, or the shift of the η - lines dependent of the concentration and temperature; the effects of good and of poor solvents (that respectively do and don't follow the time-temperature equivalence); etc.; and the influence of the same factors on concentrated solutions, undiluted polymers and solids etc., are all determined and explained by the same parameters and equation. Any other model (as the free chain model or rubber theory or the descriptive linear visco-elastic spectrum, etc.) is far away from only the possibility of representing very roughly one of the mentioned aspects.
- The rubber theory or theory of isolated flexible molecules was meant to apply for polymers that may show a steady-state flow viscosity and thus are not cross- linked. The theory thus was not supposed to apply for viscoelastic behavior in the glassy, or in the plateau zones, nor for cross-linked networks and is not able to describe this behavior. This of course is evident because short chain units can not be randomly coiled and have the Gaussian distribution of configurations and thus also cannot behave like entropy springs. Chain models thus don't apply for, and have nothing to do with (always at least cross-linked) structural materials, even not above glass transition.
- Further, long "isolated" chains of uncross-linked polymers also don't behave according to the free chain theory. At long times or low frequencies G or G' should vanish (because of the resumption of random average configurations by the macro-molecular coils in the deformed state). This is not the case and also G" shows still finite values and thus no equilibrium. At high frequencies, the perfect elastic behavior is predicted and G" also should be zero. This is also not the case and on the contrary G" increases and becomes many orders higher at high frequencies, showing the same values as for crystalline and glassy materials and thus showing the same type of process of time dependent behavior.
- The behavior according to the rubber theory only approximately applies for very dilute Newtonian solutions, where isolated chains of not too short molecules (to make chain statistics and coiling possible), and of not too long molecules, (thus of low molecular weight), to prevent entanglement coupling.
This is the case because rubber theory, is based on the Brownian motion of isolated flexible chains at higher temperatures above glass transition, thus deals with a very dilute solution where a separated long molecule is surrounded by solvent.
- As model, the motions of segment junctions of the chain are expanded into modes (like a vibrating string) and each mode corresponds to a discrete contribution to the spectrum H.

To keep the series of the contributions to the response convergent, for finite results, an early, arbitrary, cut-off of the series is used.
-Because therefore the influence of short relaxation times is not regarded in the model, the theory is not general and only is an analog for behavior after long times (or lower frequencies). The theory thus does not deal with higher frequencies and short-range relationships and the prediction of infinite rigidity and infinite loss at infinite high frequencies is invalid.
- Because of the cut-off of the series, to obtain a convergent series for finite responses, the Rouse model predicts, for all materials, a slope of the logarithmic plot of G' of 2 and a slope of 1 for the loss modulus G". As can be seen from the given pictures at 2.6 of all types of polymeric materials, this never applies. Thus, the best linear visco-elastic spectrum is not able to explain time dependent behavior. Only at a steep descent, thus in the terminal zone of uncross-linked polymers, series expansion of the non-linear process shows roughly a similar behavior as a spectrum given by such a converging series.
- Zimm introduced hydrodynamic interaction between the moving sub-molecules based on the calculation of steady-flow viscosity of dilute solutions. However visco-elastic data of e.g. dilute solutions of polystyrene etc., in the range and conditions where the theory should apply (e.g. in the terminal zone), don't show behavior according to the Zimm theory but do show behavior close to the Rouse equation, despite the neglect of hydrodynamic interaction and internal viscosity (= intramolecular steric effects) according to the Rouse equation. This shows that the Zimm model also is not right as also is explained by the exact kinetic theory.
- It is shown in this Section that the determining deformation kinetics equation of the visco-elastic behavior at longer times can be expanded into a row that is identical to the row of the Rouse equation. A still later cut-off, near equilibrium at nearly zero stress, at the end of the relaxation process, gives the Zimm value with the slope of 2/3. The Rouse line spectrum thus is a row-expansion of one special non-linear process. There thus is no restriction of an application to only dilute solutions, as is the basis of the chain models. This further explains why at zero relaxation, (when there is no relaxation although the specimen is still loaded after a relaxation test), the spectrum is not present. Because the "spectrum" only exists as expanded terms of one process, it does not exist when this single process is not acting by the zero internal stress on the sites at zero relaxation.
Because the row according to the Rouse model needs an early cut-off of the expanded row, it therefore gives no explanation of the applied row.
- The explanation of the Rouse equation as an expansion of one non-linear deformation kinetics process also explains why this line spectrum (that seems physical improbable, but exists as terms of the row expansion of the exact equation) gives better results than a continuous spectrum (that does not exist).
- Further, it explains why the theory also can be applied to undiluted polymers, using only one friction coefficient for all types of coordinated motions. These motions, represented by the separate terms, are in fact the expanded terms of one process with one relaxation time, thus one friction coefficient.
- The steeper Zimm slope, occurring at shorter times than theoretical possible, in undiluted polymers in stead of in the postulated dilute solutions, certainly can not be explained by the Zimm theory because the internal friction is of higher order with respect to a solvent friction. As shown here, this slope is characteristic for the midpoint of glass-transition.
- The ladder networks of Blizard and Marvin are identical with the Rouse theory with the dense line spectrum approximated by a continuous spectrum. A thorough study in the past of ladder networks with both lumped and distributed parameters, has shown that a continuous dynamic modulus function as eq.(21) corresponds to a discontinuous relaxation spec-

trum with discrete lines. This confirms again the explanation of the behavior according to the Rouse model being a row expansion of the deformation kinetics equation.
- Several modifications of the series of the spectrum H (to apply it for cross-linked networks) by arbitrary characteristic modes of linked strands and networks (or series of networks) only give qualitative descriptions of the behavior at transition, e.g. with square root (Rouse; Bueche), linear, and square dependence of J" on τ, all roughly in accordance with the range of the measurements of the different types of polymers. None of these models however is able to explain, or to describe, the flat plateau at small times. This only is possible by reaction kinetics [2].
- Real quantitative reasonable fits of the whole behavior are not possible by the chain and power "models". This is evident because the very long relaxation times can not be explained by extrapolation of the model to motions of large groups of strands of large dimensions, while physics (reaction kinetics) shows that the behavior is explained by the very local movement of small flow units (as side bond breaking and reformation or dislocations movements in crystals, etc.).
- After a sufficient long relaxation test, a lower load level can be found of zero relaxation, showing no relaxation although the specimen still is loaded. This shows that a single non-linear process is acting because the internal stress on the sites can be zero at a lower load level. A spectrum of relaxation times thus cannot exist. This non-linear process is acting in a wide time interval of many decades (e.g. 5 to 6 decades in "crystalline" materials like metals). None of the other methods (chain models, power laws, general functions, etc.), that are based, or implicitly based, on the existence of spectra, is able to explain zero relaxation.
- As shown, Newtonian behavior only is possible in dilute solutions of low molecular weight solutes in Newtonian solvents at the given, not too high strain rates. At increasing molecular weight the probability of formation of stronger types of bonds increases. This also is the case for higher concentrations and when molecules unfold in poor solutions at higher temperatures. These stronger bond types are not acting through the Newtonian solvent and thus are non-Newtonian.
- There appear to be 3 types of bonding for solutions. The first type (of rolling shear) acts through the solvent, in dilute solutions, on short molecules (= low molecular weight) and, (depending on the strain rate), may show linear behavior when the solvent is Newtonian. The second type may become determining for longer molecules (because there is a noticeable local side bonding connecting chains) and shows non-linear behavior but may become quasi Newtonian at low stresses and strain rates in a dilute solution (also because the activation volume parameter of a single, local bond has a small value). The third type shows non-linear behavior and is a more firmly side bonding along some length and may show segmental jumps as flow movement. Thus, the probability of having all 3 types of flow units is larger for the molecules with high molecular weights.
- The reducibility by division by η_0 or, what is the same, $H_1 = H_0$, or the activation heat of the polymer is equal to that of the solvent and the temperature and concentration independent ϕ_i, or $N_i = N_0$, shows that the solvent determines the process and the rate determining step for the solute unit involves the jump of the solvent molecule. The independency of ϕ of the temperature is found to apply generally, for most materials, also below glass transition.
- Thus for dilute solutions H_i (equal to the solvent value) and ϕ_i (in the case of no unfolding) are independent of the temperature and concentration.
- For a poor solvent $1/\phi_2$ is not constant (as applies for a good solvent) but in-creases with temperature (by unfolding) and the time temperature equivalence thus does not exist. This

shows the increase of "N" and thus that in a poor solvent the polymers unfold with increasing temperature while they fold with decreasing temperature. The non-reducibility is due to the change of the structure by unfolding of the molecules with increasing temperature. This has to be described by a separate bond formation process (as is applied for transformations in the main section) to determine the driving force and molecular parameters of the transition.

- The properties of short molecules, as linear behavior, and of solutions, showing η_0-reducibility etc., should not be applied to solids with long molecules as is done.
- Mostly one or two processes act in concentrated solutions and solids and the rate equation of flow is:

$$\sigma = \frac{\text{arcsinh}(\dot{\varepsilon} / A_1)}{\phi_1} + \frac{\text{arcsinh}(\dot{\varepsilon} / A_2)}{\phi_2}$$

- For concentrated solutions and for solids, η_0 becomes negligible and reducibility is obtained by multiplication of $\dot{\varepsilon}$ with: $\exp(H'_i/kT)$.
- Because now the solvent is not determining any more (as is the case for the η_0-reduction) the solvent molecules are able to flow only when the bonding between the solute molecules flow. In highly concentrated solutions, the solvent molecules move together with the polymer flow units. Thus, the 50 % solution behaves like the pure solid.
- For crystalline materials, like metals, steady flow is also due to self-diffusion. Dislocations are held up by bad sites (impurities, alloying elements, crystal imperfections, etc), causing stress concentration in the neighbourhood. This stress is relieved by diffusion of the neighbours of the bad site, because the activation heat for creep equals that for self-diffusion.
- Only when no phase- or other transitions are involved, the time-temperature and time-stress equivalence may apply, as in the glass-state. The reverse statement that this only applies for transitions [16], is shown here to be not true.
- It now clearly is shown that linear viscoelastic behavior does not exist for structural materials like wood, even not above glass transition.

References

The references [2], [3], [6], [8], [15] and [16] are the same as given in the main part

Appendix II: Explanation of annealing by molecular kinetics and derivation or the WLF-equation

This Appendix is expired here and the theory, **B(2010),** is, in final form, given in a next Section: B.3, and is first published as “Theoretical derivation of the WLF- and annealing equations” in: Journal of Non-Crystalline Solids 356 (2010) p 394–399.

B.3. Theoretical derivation of the WLF- and annealing equations

T.A.C.M. van der Put,
TU-Delft, Civil Engineering and Geosciences, Timber Structures and wood technology,
PO Box 5048, NL-2600 GA Delft, Netherlands Tel: +31 152851980, E-mail: vanderp@xs4all.nl:

Discussion and extension of B(2010): "Theoretical derivation of the WLF-and annealing equations", **Journal of Non-Crystalline Solids 356 (2010) p 394–399**

Abstract: Based on the deformation kinetics approach, the theoretical derivation is given of the empirical WLF-equation of the time-temperature equivalence. The same is done for annealing at glass transition. The derivation provides a general theory for any loading history and replaces the inconsistent free volume model.

PACS 64.70.Q-

1. Introduction

Time dependent behaviour is explained by the equilibrium theory of deformation kinetics (see [1]) and it never is necessary to apply the phenomenological relaxation time spectra. It is, on the contrary, easy to show (see [2]) that the row expansion of the kinetic equation gives the Rouse spectrum and e.g. the Zimm spectrum, explaining the success of the use of line spectra. The apparent need of linear viscoelastic spectra thus indicates non-linear behaviour according to deformation kinetics. This exact approach also applies for glass transition and annealing and there is no need of the phenomenological free volume model and Doolittle viscosity equation giving no explanation of the WLF-equation. This follows from the theoretical derivation based on the, in Appendix A discussed, deformation kinetics of structural changes and the constitutive equations of Appendix B. Annealing has to be discussed because the determination of the constants of the WLF-equation and of the glass transition temperature T_g is based on annealing experiments.

Two connected cases are regarded, one with the Arrhenius shift and the other with a dominating WLF-shift. The results are given in the conclusions.

2. Derivation of the WLF-equation of time-temperature equivalence

As known, viscosity curves, compliance curves, etc. measured at different temperatures may show the same shape independent of the temperature and can be shifted along a logarithmic time or frequency axis to form one curve, predicting the behaviour after long times at the lower temperature. Near glass transition temperature, the horizontal shift factor $\ln(a_T)$ of the displacement of the curves, by temperature difference, along the log-time axis follows WLF-equation, Eq.(4), applying for amorphous uncross-linked polymers and

other super-cooled non-crystallizing liquids. According to the classical model, e.g. in [3] pg.225, this shift factor is equal to the differences in relaxation times on logarithmic scale:

$$\ln(a_T) = \ln(t_{r1}) - \ln(t_{r2}) \tag{1}$$

where t_{r1} and t_{r2} are the relaxation times at temperatures T_1 and T_2 (see Fig. 1).

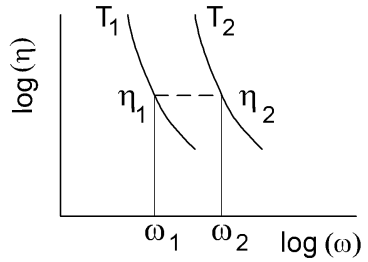

Fig. 1 – Temperature shift of the viscosity plot along the frequency axis

It is assumed for the viscosity η that:

$$\ln(\eta_1) - \ln(\eta_2) = \ln(t_{r1}) - \ln(t_{r2}) \tag{2}$$

With the Doolittle viscosity equation:

$$\ln(\eta) = \ln(A) + B(v - v_f)/v_f = A' + Bv/v_f = A' + B/f \tag{3}$$

in which $f = v_f/v$ is the free volume fraction of volume v, the shift factor a_T becomes:

$$\begin{aligned} \ln(a_T) &= \ln(t_{r1}) - \ln(t_{r2}) = \ln(\eta_1) - \ln(\eta_2) = B/f_1 - B/f_2 = \\ &= B\frac{f_2 - f_1}{f_1 f_2} = \frac{(B/f_1)\cdot(T_2 - T_1)}{(f_1/\alpha) + (T_2 - T_1)} = \frac{c_1(T_2 - T_1)}{c_2 + T_2 - T_1} \end{aligned} \tag{4}$$

where: $f_2 = f_1 + \alpha(T_2 - T_1)$ and α is the difference of the thermal expansion coefficients below and above the glass-transition temperature T_g, determining the increase in free volume.

Because this free volume model is a phenomenological model, there are many inconsistencies. For instance:

- The necessity of volume changes without shear, (because of the independency of the molecular weight), while the WLF-equation also applies for shear.
- The value of α, being an order too low for e.g. inorganic glasses, or still more for e.g. Cellulose derivatives and orders to low for wood material, shows the amount of free volume increase not to be a parameter but an accompanying phenomenon.
- Eq.(2): $\ln(t_{r1}/t_{r2}) = \ln(\eta_1/\eta_2)$ can not be true for a horizontal shift of the $\ln(\eta)$-plot along the frequency axis as shown in Fig.(1). Because when $\ln(\eta_1)$ at T_1 is equal to $\ln(\eta_2)$ at T_2, then also $t_{r1} = t_{r2}$ which can not be right for shifted positions.
- Also the Doolittle equation, Eq.(3), can not be applied for a horizontal shift.

If $\ln(\eta_1) = \ln(\eta_2)$, then $f_1 = f_2$ (constant independent of temperature).

The Doolittle equation thus should be replaced by the empirical relation:

$$\eta = A'' \cdot \exp(B/f) \cdot \omega t_r \tag{5}$$

in order to show the shift and to be proportional to t_r according to the classical Eq.(2). Then, when $\ln(\eta_1) = \ln(\eta_2)$, Eq.(5) becomes:

$$\ln(a_T) = \ln(\omega_2) - \ln(\omega_1) = \ln(t_{r1}/t_{r2}) + B(1/f_1 - 1/f_2) \tag{6}$$

equal to Eq.(15) and Eq.(6) thus is explained by deformation kinetics providing the theoretical derivation of the WLF-equation as follows.
According to Eq.(a6) of Appendix A, the rate equation for structural change is:

$$\frac{dN}{dt} = B \cdot N \cdot 2\sinh\left(\frac{\sigma_v \lambda'}{Nk}\right) \approx B \cdot N \exp\left(\frac{\sigma_v \lambda'}{Nk}\right) \tag{7}$$

This equation is extensively verified e.g. as damage equation for the change of bonds N, also within transition zones with changing N and λ. For instance in [1], pg. 51) $\lambda = \lambda_0\left(1 + C_0(T - T_0) \cdot \rho/\rho_0\right)$ applies exactly at temperature T within the temperature range of the transition for the compression strength of wood at moisture content ρ. Because the WLF-equation shows about the same activation volume parameter value: $\sigma_v \lambda / Nk = 2.3 \cdot c_1 = 2.3 \cdot 17.44 = 40$, characteristic for self-diffusion, creep and creep to failure, the same mechanism and parameter form can be expected to apply at this "melting" of the secondary bonds, which can be given as:

$$\lambda' = \lambda_g + \beta\left(T - T_g\right). \tag{8}$$

The same applies for the concentration N, as also applied in the empirical Eq.(4):

$$N = N_g + \alpha(T - T_g) \tag{9}$$

These linear changes with temperature T are shown in [1] to be in accordance with the thermodynamics of molecular activation. The activation volume term of Eq.(7) then is

$$\frac{\sigma\lambda'}{kN} \cdot = \frac{\sigma}{k} \cdot \frac{\lambda_g + \beta\left(T - T_g\right)}{N_g + \alpha(T - T_g)} \tag{10}$$

In this equation is N_g the site concentration at T_g, the glass transition temperature.

Because of the stress dependency of "N", comparison of viscosities at different temperatures is difficult. Therefore, the shift of the curve of the apparent creep modulus (the inverse of the creep compliance) along the time axis is chosen as simple illustration of the behaviour. The rate of bond breaking and bond reformation in shifted position dN/dt is proportional to the viscous strain rate and neglecting the minor important temperature dependent pre-exponential terms, the steady creep strain rate $\dot{\varepsilon}$ is according to Eq.(7) in the form of Eq.(a5) of Appendix A:

$$\dot{\varepsilon} = A\exp(\varphi\sigma) = (\exp(\varphi\sigma))/t_r \tag{11}$$

where t_r is the relaxation time. Integration of Eq.(11) gives: $\varepsilon = (\exp(\varphi\sigma)) \cdot t/t_r$ and the

apparent creep modulus is: $E = \sigma / \varepsilon = \sigma \cdot t_r / (t \exp(\varphi\sigma))$

Thus, at the same loading σ (which should be kept the same because of the stress dependency of N), the shift of the E - plot follows from:

$$\ln(E_1) - \ln(E_2) = \ln(t_2 / t_1) + \ln(t_{r1} / t_{r2}) + \phi_2\sigma - \phi_1\sigma \tag{12}$$

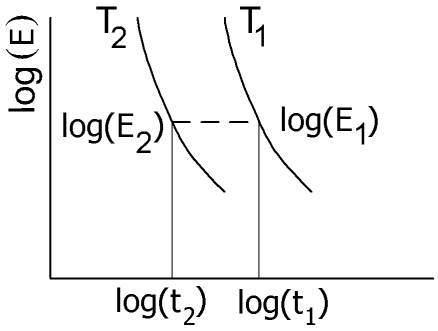

Fig. 2 – Temperature shift of the apparent creep modulus E, ($T_2 > T_1$).

For a shift of the plot along the time axis, a value $\ln(E_1)$ at temperature T_1 must be equal to $\ln(E_2)$ at temperature T_2. Thus: $\ln(E_1) - \ln(E_2) = 0$, (see Fig. 2) or according to Eq.(12):

$$\ln(t_1 / t_2) = \ln(t_{r1} / t_{r2}) + \phi_2\sigma - \phi_1\sigma \tag{13}$$

In this equation is:

$$\phi_2\sigma - \phi_1\sigma = \frac{\sigma\lambda_2'}{N_2 k} - \frac{\sigma\lambda_1'}{N_1 k} = \frac{\sigma}{k} \cdot \left(\frac{\lambda_g + \beta(T_2 - T_g)}{N_2} - \frac{\lambda_g + \beta(T_1 - T_g)}{N_1} \right) =$$

$$= \frac{\sigma \cdot (\beta N_g - \alpha\lambda_g) \cdot (T_2 - T_1)}{k \cdot N_1 N_2} = \frac{\sigma\lambda_g}{k N_1} \cdot \frac{((\beta N_g / \alpha\lambda_g) - 1) \cdot (T_2 - T_1)}{(N_1 / \alpha) + T_2 - T_1} \tag{14}$$

because: $N_2 = N_g + \alpha(T_2 - T_g) = N_g + \alpha(T_2 - T_1) + \alpha(T_1 - T_g) = N_1 + \alpha(T_2 - T_1)$.

With $n_1 = \sigma\lambda_g / k N_1$ and $m = \beta N_g / \alpha\lambda_g - 1$, Eq.(13) becomes according to Eq.(14):

$$\ln(a_T) = \ln\left(\frac{t_1}{t_2}\right) = \ln\left(\frac{t_{r1}}{t_{r2}}\right) + \frac{n_1 m \cdot (T_2 - T_1)}{(N_1 / \alpha) + (T_2 - T_1)} = \ln\left(\frac{t_{r1}}{t_{r2}}\right) + \frac{c_1 (T_2 - T_1)}{c_2 + T_2 - T_1} \tag{15}$$

giving the corrected, general form of the WLF-equation. In Eq.(15) is mainly:

$$\ln\left(\frac{t_{r1}}{t_{r2}}\right) \approx \frac{H}{k T_1} - \frac{H}{k T_2} \tag{16}$$

giving the Arrhenius shift and thus a combined Arrhenius–WLF shift always applies:

$$\ln(a_T) \approx \frac{H}{k T_1} - \frac{H}{k T_2} + \frac{c_1 (T_2 - T_1)}{c_2 + T_2 - T_1} \tag{17}$$

being noticeable when both amounts are comparable near transition (e.g. for methacrylate polymers, see [3]). The WLF shift thus only approximately applies when the enthalpy H is small. The Arrhenius shift in the transition zone applies separately when $c_1 = 0$, thus when m = 0 and thus when: $\beta N_g = \alpha\lambda_g$, giving:

$$\frac{d\lambda \cdot N_g}{dT} = \frac{dN \cdot \lambda_g}{dT}, \tag{18}$$

Because N is proportional to the free volume Eq.(18) states that the relative increase of the activation volume with temperature is proportional to the relative increase of the free volume. This is e.g. the case for glass. When the WLF-shift applies, thus when there is a relative higher increase of specific activation volume λ / λ_g with respect to the increase of specific free volume N / N_g, this will be due to an increase of the density of active sites. If at a certain temperature step, the effective distance between the sites is halved, the number of sites is doubled and "m" can be expected to be:
$m = \beta N_g / \alpha\lambda_g - 1 = \partial(\lambda / \lambda_g) / \partial(N / N_g) - 1 = 2 - 1 = 1$.
Eq.(15) then, due to this site multiplication, also can be written as:

$$\ln(a_T) = \ln\left(\frac{t_1}{t_2}\right) = \ln\left(\frac{t_{r1}}{t_{r2}}\right) + n_1 N_1 \left(\frac{1}{N_1} - \frac{1}{N_2}\right) \tag{19}$$

explaining the extended empirical Eq.(6) when f is replaced by N.

By Eq.(14), it is shown that in the WLF-equation any reference temperature T_1 can be chosen in stead of T_g, when also N_g is replaced by N_1. Further it follows from this derivation, that, although c_1 and c_2 of Eq.(15) are temperature dependent, depending on the choice of T_1, the product $c_1 c_2$ is constant, temperature independent, because:

$$c_1 \cdot c_2 = m \cdot n \frac{N_1}{\alpha} = m \frac{\sigma\lambda_g}{kN_1} \cdot \frac{N_1}{\alpha} = m \frac{\sigma\lambda_g}{k\alpha} = m \frac{\sigma\lambda_g}{kN_g} \frac{N_g}{\alpha} = m \cdot n_g \frac{N_g}{\alpha} \tag{20}$$

In the equations above is: H the enthalpy and k, Boltzmann's constant. The temperature T is in K and "N" is the concentration of mobile segments and not the free volume concentration and thus α is not necessarily the difference of the thermal expansion coefficients below and above the transition temperature.

3. Annealing of amorphous solids

Arrhenius temperature dependence

When an amorphous material, (equilibrated far above T_g), is suddenly cooled near T_g, the liquid-like molecular adjustment to a new equilibrium becomes slow. The system is under internal stress and annealing is a process relieving the stress when the system passes to equilibrium. Accompanying this relaxation, some properties of the system (as: birefringence, specific volume, viscosity, concentration, etc.) change with time. This is discussed in Appendix B, where it shown that one and the same equation describes all these types of

changes.

According to Appendix B, the rate equation of viscous flow at annealing is:

$$\dot{\varepsilon}_v = -2B\varepsilon_v \sinh(\phi K\varepsilon_v) \quad (21)$$

Performing the division 1/sinh(x), or:

$\frac{1}{e^x - e^{-x}} = e^{-x} + e^{-3x} + e^{-5x} + \ldots$, Eq.(21) becomes:

$d\ln(\varepsilon_v)\cdot\left(e^{-\phi K\varepsilon_v} + e^{-3\phi K\varepsilon_v} + e^{-5\phi K\varepsilon_v} + \cdots\right) = -B dt$, giving as solution ($\varepsilon_{v0} > \varepsilon_v$):

$$B\cdot t = \sum_{n=0}^{\infty}\left(E_1(\phi K\varepsilon_v(1+2n)) - E_1(\phi K\varepsilon_{v0}(1+2n))\right) \quad (22)$$

being a row solution of one process. Fitting this equation shows that there always is a high internal stress on the sites. For these high values of $\phi K\varepsilon_v$ a more simple solution is possible because Eq.(21) then becomes:

$$\frac{d\ln(\varepsilon_v)}{dt} = -Be^{\phi K\varepsilon_v} \quad (23)$$

or: $d\ln(\varepsilon_v)\cdot e^{-\phi K\varepsilon_v} = B\cdot dt$, or integrated:

$$E_1(\phi K\varepsilon_v) - E_1(\phi K\varepsilon_{v0}) = Bt \quad (24)$$

where $E_1(x)$ is the exponential integral: $E_1(x) = \int_x^{\infty}\frac{e^{-s}}{s}ds$. Thus:

$$\phi K\varepsilon_v = E_1^{-1}\left(E_1(\phi K\varepsilon_{v0}) + Bt\right) \quad (25)$$

In [4], measurements are given of the birefringence and density of a crown glass and Eq.(23) or Eq.(b5) apples exactly with a correlation close to 1 in the given temperature range between 490 to 540 ^0C (see Fig. 3).

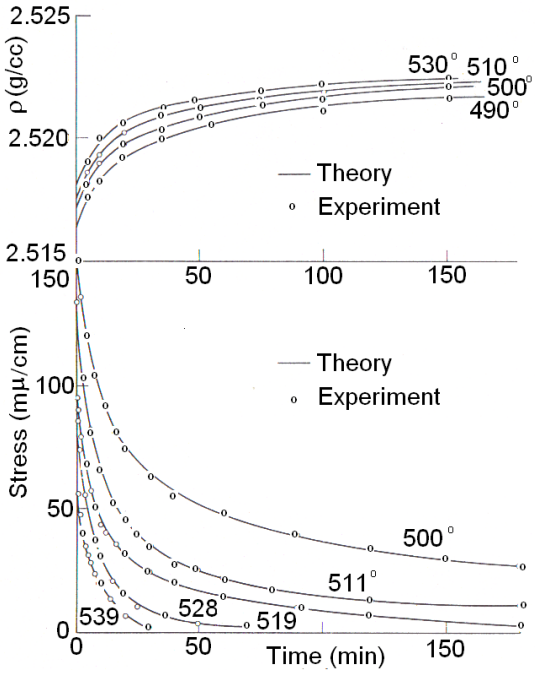

Fig.3 – Density increase and stress decrease during annealing of crown glass.
The theoretical curves follow from Eq.(24).

The test-specimens showed mutually variability of the parameters. Every specimen is an unique giant molecule. The average value of $\phi K\varepsilon_{v0} = \phi\sigma_0$, from the fit of stress relaxation and of the volume contraction data, was 4.7. However, there might be a sudden change of $\phi K\varepsilon_{v0}$, between 520 and 530 ^{0}C, from about 5 to nearly halve this value, indicating two processes acting. More data are necessary to confirm this. The variability of $\phi K\varepsilon_{v0}$ among the test-specimens is a property of glasses having a structure depending on the thermal history. This also applies for the viscosity, specific heat, specific volume, index of refraction, etc. Eq.(24) can be written for higher values of $\phi K\varepsilon_v$ as:

$$E_1(\phi K\varepsilon_v) - E_1(\phi K\varepsilon_{v0}) \approx \frac{\exp(-\phi K\varepsilon_v)}{\phi K\varepsilon_v} - \frac{\exp(-\phi K\varepsilon_{v0})}{\phi K\varepsilon_{v0}} = Bt \quad \text{or:}$$

$$\frac{\varepsilon_v}{\varepsilon_{v0}} \approx 1 - \frac{1}{\phi K\varepsilon_{v0}} \ln\left(1 + B\phi K\varepsilon_v t \exp(\phi K\varepsilon_{v0})\right), \quad (26)$$

After the delay time, the value $1/\phi K\varepsilon_{v0}$ is the slope of the approximate straight line on ln(t) scale. This slope has to be constant independent of temperature and stress to have shifted lines along the time axis at different temperatures. The independency of stress means that in $\phi K\varepsilon_{c0} = \phi\sigma_0 = \sigma_0\lambda / NkT$, the number of sites N is proportional to the maximal initial stress σ_0. This time-stress equivalence combined with the time temperature equivalence is mentioned in [5], pg. 94, where it is found that high strain has the same effect on aging as an increase in temperature. The time-stress equivalence is an important property of e.g. building materials, making it possible to determine the long term strength by constructing the master creep curve at constant temperature (see e.g. [1] pg.70).
From Eq.(26) follows for the shift along the time axis at different temperatures:
$\varepsilon_{v1}/\varepsilon_{v01} - \varepsilon_{v2}/\varepsilon_{v02} = 0$, that $B_1\phi K\varepsilon_{v1}t_1 = B_2\phi K\varepsilon_{v2}t_2$ or:
$B_1\phi K\varepsilon_{v10}(\varepsilon_{v1}/\varepsilon_{v10})t_1 = B_2\phi K\varepsilon_{v20}(\varepsilon_{v2}/\varepsilon_{v20})t_2$ or: $B_1t_1 = B_2t_2$,
giving the Arrhenius shift:

$$\ln(t_1) - \ln(t_2) = \ln(B_2) - \ln(B_1) = H'/kT_1 - H'/kT_2 \quad (27)$$

WLF temperature dependence

With reference to the equilibrium values N_e and using Eq.(19), Eq.(7) becomes:

$$\frac{dN}{dt} = -B(N - N_e)\cdot\exp\left(n_eN_e\left(\frac{1}{N_e} - \frac{1}{N}\right)\right) \quad (28)$$

with: $n_e = \sigma\lambda_g / kN_e$ and N - N_e as active amount of sites.

Eq.(28) can not be solved in terms of familiar functions and solutions in the form of infinite series can be obtained that can be tabulated, just like is done with sin(x), that represents an infinite series as solution of its appropriate differential equation. However, also a precise approximation is possible as follows:
Eq.(28) can be written:

$$\frac{d}{dt}\left(\frac{1}{N}\right) = B\left(\frac{1}{N_e} - \frac{1}{N}\right)\frac{N_e}{N}\exp\left(n_eN_e\left(\frac{1}{N_e} - \frac{1}{N}\right)\right) \quad (29)$$

or: $\frac{ds}{dt} = -Bs\frac{N_e}{N}\exp(s)$, where: $s = n_e N_e\left(\frac{1}{N_e} - \frac{1}{N}\right)$ or:

$$d\ln(s)\cdot\exp(-s) = -B\cdot\frac{N_e}{N}\cdot dt \qquad (30)$$

At the end stage of the process $N_e / N \approx 1$ and integration of Eq.(30) then gives:

$$E_1(s) - E_1(s_0) = Bt \qquad (31)$$

where $E_1(x)$ is the exponential integral.

More general the solution is: $E_1(s) - E_1(s_0) = BtN_e / \bar{N}$, with a weighted mean value $\bar{N}$.

For high values of "s" $E_1(s) = \exp(s)/s$ and the solution then becomes:

$e^{-s}/s - e^{-s_0}/s_0 = BtN_e/\bar{N}$, being approximately:

$$Ne^{-s} - N_0 e^{-s_0} = BnN_e t = B't \qquad (32)$$

because for high values of s_0 and s is: $s = n_e(1 - N_e/N) = n_e(1 - N_e/\bar{N}) \approx n$, about constant and the best estimate of $\bar{N}$ is N in the first term and N_0 in the second term.

Because Eq.(31) is the solution at the safe side and Eq.(32) the solution at the unsafe side, the mean of both equations can be taken as total solution of Eq.(29):

$$Ne^{-s} - N_0 e^{-s_0} + E_1(s) - E_1(s_0) = B''t = t/t_r \qquad (33)$$

The proof that this is right, follows from differentiation of Eq.(33). This gives Eq.(30) with a small negligence of $(N - N_e)/nN_e$ ($\approx (N - N_e)/40N_e$) with respect to 1. Examples of curve fitting to Eq.(33) of materials showing the WLF-shift at annealing, as glucose, Polystyrene, Polyvinyl acetate, are given in [3]. There also Fig. 4, of A Kovacs is given, showing a perfect fit by the theoretical Eq.(33).

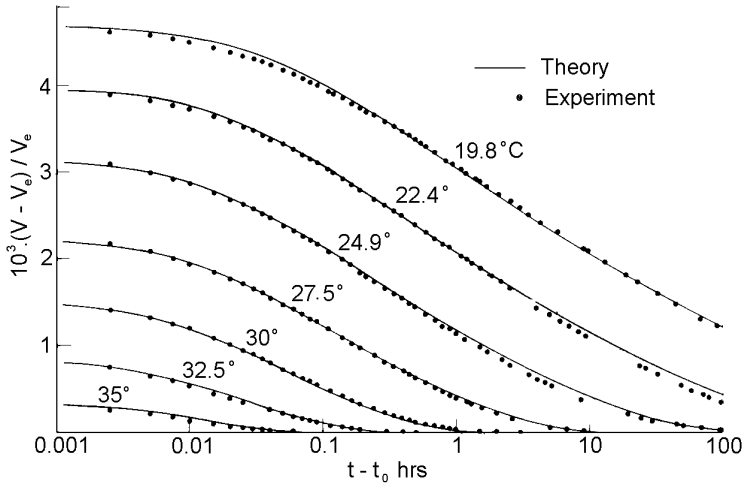

Fig. 4. Isothermal volume contraction of glucose measured after sudden cooling to the temperatures indicated from [3] (test-points and theory: Eq.(33))

4. Conclusion

- Not the volume effect, but the structural change equation (Eq.(7), Eq. (21), Eq.(28) or

Eq.(b5)) of the equilibrium theory of molecular deformation kinetics, as treated in [1], which is shown to explain all aspects of time dependent behaviour of wood, is shown here to also give the theoretical explanation of the empirical WLF-equation and of the volume change and stress relaxation at annealing.

- The form of the WLF-equation is explained by the properties of the activation volume parameters near transition, as given by Eq.(10).
- It is shown by Eq.(17) that the WLF- shift is accompanied by the Arrhenius shift. The right WLF-shift has to be done on an by a factor exp(H/kT) reduced curve.
- The constant value of $\sigma\lambda_g / kN_g$, or the proportionality of N_g (the concentration of sites) with the initial applied stress σ, is a similar property of the activation volume as applies for glasses, wood, concrete and some metals (see [1]) which explains the time-stress-equivalence.
- The equations show that always high internal stresses are acting even at the end of stress relaxation, probably by the high molecular attraction forces in the voids. The decrease of stress then is due to a decrease of restrained voids.
- The WLF-shift is due to site multiplication with temperature increase near T_g.
- The WLF temperature shift applies, when the increase of specific activation volume λ / λ_g is twice the increase of specific free volume N / N_g with temperature.
- The Arrhenius temperature shift in the transition zone applies when the increase of the specific activation volume with temperature is proportional to the increase of the specific free volume.

Appendix A - Basic equation of structural change

As discussed in [1], the reaction rate equation for structural change:

$$d\rho / dt = B \cdot \rho \cdot 2\sinh(f_a A_a \lambda / (kT)) \qquad (a1)$$

can be expressed in the concentration term:

$$\rho = N_a \lambda A_a / \lambda_1 \quad (a2)$$

where λ is the jump distance of the activated unit; A_a, the cross-section of that unit; λ_1 the distance between the activated sites, and N_a, the number of these sites per unit area. Then $N_a / \lambda_1 = N_t$ is the number of activated elements per unit volume. The work of the stress f_a on the activation unit is: $f_a A_a \lambda$.

The equivalent work by the part of the mean macro stress σ that acts at the site is σ times the unit area thus is:

$$\sigma_v \cdot 1 \cdot 1 \cdot \lambda = N_a f_a A_a \lambda \quad \text{or:} \quad f_a A_a \lambda = \sigma_v \lambda / N_a \,. \quad (a3)$$

Also the chemical work, expressed as an equivalent chemical driving stress, can be added as stress to the external stress. Eq.(a1) thus becomes:

$$d(N_a \lambda A_a / \lambda_1) / dt = B \cdot (N_a \lambda A_a / \lambda_1) \cdot 2\sinh(\sigma\lambda / (N_a kT)) \quad (a4)$$

$d(N_a \lambda A_a / \lambda_1) / dt$ can be the rate of increase of activation volume. If this is proportional to the free volume, this term also gives the rate of free volume increase. $N_a \lambda A_a / \lambda_1$

also may be the mean viscous strain per unit area and Eq.(a4) then becomes:
$\dot{\varepsilon}_v = 2B\,\varepsilon_v \sinh(\phi K\varepsilon_v)$. For pure creep, at bond breaking and bond reformation in a shifted position, the number of bonds or sites remains constant and Eq.(a4) becomes: $\dot{\varepsilon}_v$ = -

$$2B\,\varepsilon_{v0} \sinh(\phi K\varepsilon_v) \approx -B\varepsilon_{v0} \exp(\phi K\varepsilon_v) \qquad \text{(a5)}$$

For a process of changing site density at annealing Eq.(a4) becomes with $\lambda = \lambda' T$ because of the entropic driving force:

$$dN/dt = B \cdot N \cdot 2\sinh(\sigma_v \lambda'/(Nk)) \approx B \cdot N \exp(\sigma_v \lambda'/(Nk)) \quad \text{(a6)}$$

This last approximation of $2\sinh(x) \approx \exp(x)$ follows from the derivation of the WLF-equation showing always a high internal stress on the sites.

Appendix B - Basic equation of annealing relaxation

The following mechanism scheme is able to explain the measurements. At suddenly cooling, the shrinkage and configurationally change is confined by strong side bonds in the same way as crossing molecules bridging voids. It follows from the theory that the internal stress on these sites is always high and thus the crossing molecules are always under high pressure by the molecular attraction forces of the void boundaries trying to close the void. A segmental jump of the highest loaded crossing unit will unload this unit but increases the load on the adjacent crossing units causing the next one to be high loaded. The segmental jumps cause a decrease of the void volume (free volume) as well as a decrease of the number of jumping elements. This causes a process of decreasing sites according to Eq.(a6) also by the decreasing void volume, a mean stress decrease in the visco-elastic material surrounding the voids. The rate of decrease of the void volume determines the rate of viscous displacement and thus the rate of density increase and a relief of the elastic stress in the surrounding material and a description is possible in terms of elastic and viscous strains, ε and ε_v of that material. The stress on the elastic material of the unit cross section is $\sigma - \sigma_v$ and the strain: $\varepsilon = (\sigma - \sigma_v)/E_2$, where E_2 is the modulus of elasticity of the elastic material. This strain causes a stress on the viscous sites of $\sigma_v = (\varepsilon - \varepsilon_v)E_1$ where E_1 is the equivalent modulus of elasticity of the elastic material at the site.

These constitutive equations are the same as given by the non-linear three-element analogy of Fig. 5, applied to annealing.

At a sudden cooling and no external loading, the free spring can be assumed to shorten directly what is not followed by the dashpot, and there is an internal stress

$$\sigma_v = E_1(\varepsilon_v - \varepsilon) \qquad \text{(b1)}$$

This is in equilibrium with the force on the parallel spring. Thus:

$$\sigma_v = E_2\varepsilon \quad \text{(b2)}$$

and from Eq.(b1) and (b2) follows that:

$$(E_1 + E_2)\varepsilon = E_1\varepsilon_v \qquad \text{or:} \quad \sigma_v = E_2\varepsilon = \frac{E_1E_2}{E_1 + E_2}\varepsilon_v = K\varepsilon_v \quad \text{(b3)}$$

The strain rate of the non-linear Maxwell element, for a structural change process, is:

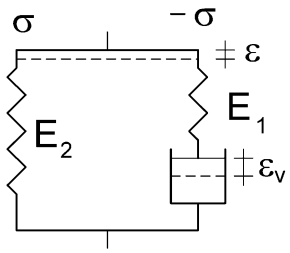

Fig. 5. Three-element model

$$\dot{\varepsilon}_v = -2B\varepsilon_v \sinh(\phi K\varepsilon_v) \approx -B\varepsilon_v \exp(\phi K\varepsilon_v) \qquad \text{(b4)}$$

According to Eq.(b3), this equation also can be written in $\sigma = \sigma_v$:

$$\dot{\sigma} = -B\sigma \exp(\phi\sigma) \qquad \text{(b5)}$$

giving the stress relaxation of annealing.

Eq.(b5) is the stress relaxation equation for high stresses, that does not only apply at the start, but also at the end of the relaxation process when σ approaches zero. As discussed before, this is due to the remaining high loaded units crossing the voids.

As discussed in Appendix A, a segmental jump of λ, of the bridging segments, decreases the void volume with λA_v when A_v is the surface of the bridged void. The relative decrease of the free volume then is $N_v A_v \lambda / \lambda_1$, when N_v is the number of adjacent voids per unit cross section and λ_1 the distance perpendicular. This decrease of the free volume is $N_v A_v$ times the viscous strain λ / λ_1 thus is proportional to viscous strain ε_v. In Eq.(b4), ε_v can be replaced by the free volume change being the same as the total volume change (as contraction or density increase). The same equation gives in the form of Eq.(b5) the stress relaxation.

Because the birefringence (mm/mm) is proportional to the stress (for most real glasses 0.1 N/mm^2 produces a birefringence of 3.10^{-7}), Eq.(b5) also gives the decrease of the birefringence. Further, when the equation is written in σ/σ_0, it also gives the change of the relaxation modulus: $(\sigma/\varepsilon_0)/(\sigma_0/\varepsilon_0)$, or the change of the viscosity: $(\sigma/\dot{\varepsilon}_0)/(\sigma_0/\dot{\varepsilon}_0) = \eta/\eta_0$ with time, when the relaxation modulus is measured at the different temperatures with the same ε_0, and the viscosity with the same $\dot{\varepsilon}_0$.

References

[1]- van der Put, TACM (1989) Deformation and damage processes in wood, Delft University Press NL.

[2]- van der Put TACM (2003) Transformations in wood, Tech. Rep. CiTG TU-Delft

[3]- Ferry JD, (1961) Viscoelastic properties of polymers, London, John Wiley & Sons.

[4]- Eyring H, Hahn SJ, Ree T, (1960) Non-Newtonian Relaxation in Amorphous Solids, in: Non-Crystalline Solids, chapt. 12: ed. V.D. Frechette, Wiley, New York,

[5]- Struik LCE (1978) Physical aging in amorphous polymers and other materials, Elsevier Scientific Publishing Company, Amsterdam.

B.4. A new theory of nucleation

T.A.C.M. van der Put,
TU-Delft, Civil Engineering and Geosciences, Timber Structures and Wood Technology, PO Box 5048, NL-2600 GA Delft, Netherlands Tel: +31 152851980, E-mail: vanderp@xs4all.nl

Discussion and extension of B(2011): "A new theory of nucleation" Phase Transitions Vol. 84, Nos. 11–12, November–December 2011, 999–1014

Abstract: The classical nucleation and growth model is modified and it is shown that the concept of fluctuations, instability and surface energy is not needed and that, (as applies for glass transition), nucleation is a common example of the kinetic theory of structural change processes, with a special driving force and a special property of the activation volume parameter. This last follows from explanation of diffusion tests. This new nucleation equation leads to a new vision on heterogeneous nucleation, applicable to solids. The equation also provides, as necessary, the theoretical equation of the thus far empirical C-curves of the TTT-diagrams (time-temperature-transformation diagrams).

PACS-codes: 02 – 64 – 81.
Keywords: Characterization – Nucleation – Solidification – Stresses - Reaction kinetics.

1. Introduction

Based on the kinetics equation for structural change of Appendix A, which by its form is e.g. able to explain transient nucleation and structural relaxation of glasses, a new theory of nucleation is derived starting by extension and correction of the classical model. Therefore the essence of the classical model is first discussed in Section 2.

In Section 3, based on general conditions, the derivation of the equilibrium concentration of the embryos depending on size is given. Herewith information is obtained on the nucleation mechanism and on the driving force for embryo formation. The classical distinction between volume free energy and temperature independent surface free energy of the embryo is shown to be superfluous and questionable.

In Section 4, heterogeneous nucleation is derived which generally applies, also for solids. The derivation is based on continuity condition of the growth rate, replacing the classical model of surface energy, in the form of non existent surface stresses in solids.

In Appendix C, based on diffusion tests, the theoretical explanation is given of the different empirical equations by their different activation volume parameters, based on the derivation of the empirical power law equation in Appendix B. Herewith the special form of the activation volume term of the driving force of nucleation is found as applied in Section 5.

It is shown in Section 5, that the special expression of the activation volume of the basic rate equation explains the data and nucleation behaviour (as well for homogeneous as for heterogeneous nucleation by one equation). As discussed in Section 6, this rate equation shows the well known increase of the rate at the increase of undercooling up to a maximum value and then a decrease of the rate at larger undercooling steps giving thus a theoretical equation and explanation of the C-curves of the time-temperature-transformation diagrams (TTT-diagrams).

2. Discussion of the classical nucleation model

For homogeneous nucleation is, according to the classical nucleation theory, the change in free energy of the system ΔE_e due to the formation of a spherical phase cluster of radius *R*:

$$\Delta E_e = (4/3)\pi R^3 \Delta g + 4\pi R^2 \gamma \quad (1)$$

where Δg is the change of the free energy per unit volume and γ is the free energy of the interface between parent phase and fluctuation, which is assumed to be constant, independent of the temperature. When $\Delta g < 0$, ΔE_e of eq.(1) has a maximum at the critical size of R_c and fluctuations with $R < R_c$ are more probable to shrink and dissolve than to grow because of the decrease of the free energy, while the fluctuations of $R > R_c$ grow spontaneously, also because of the decrease of the free energy. The critical value $R = R_c$, follows from:

d(ΔE)/dR = 0, or according to eq.(1):

$$4\pi R^2 \Delta g + 8\pi R\gamma = 0 \quad \text{or: } R_c = -2\gamma/\Delta g \quad (2)$$

Substitution of R_c of eq.(2) into eq.(1) gives the critical value for nucleation:

$$\Delta E_c = (16\pi\gamma^3)/(3\Delta g^2) \quad (3)$$

Because Δg has the form $\Delta g = \Delta h - T\Delta s = \Delta s(T_e - T)$ and γ is assumed to be constant, with respect to temperature, eq.(3) gets the empirical form of $\Delta E_c = C_2/(T_e - T)^2$. In literature, e.g. [1], [2], [3], [4], also other expressions for ΔE_c are chosen to adapt better to data.

The general thermodynamic reasoning on shrinking or grow gives no explanation of behaviour because it may happen in infinite ways and only knowledge of the mechanism provides predictable behaviour. For instance, it should be explained how a single fluctuation in solids transformation may exist involving so many molecules that a distinction is possible

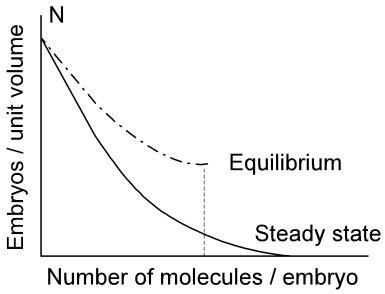

Figure 1. Concentration of embryos depending on size

between a separate constant surface energy and a volume energy, up to the size of the critical embryo. As an answer the modification was proposed to regard embryo formation as result of successive reactions. In [5], e.g., embryo formation is regarded to occur by a large number of successive bimolecular reactions (explaining also why specific activation energies have to be applied) as follows:

$O_1 + O_1 \rightleftarrows O_2$ and: $O_2 + O_1 \rightleftarrows O_3$ etc. summed up to: $nO_1 \rightleftarrows O_n$.

For equilibrium of these reactions is for n_i, the number of embryos per unit volume containing *i* molecules each:

$$\exp(-\Delta E_i / kT) = \frac{n_i / (n_1 + \Sigma n_i)}{n_1 / (n_1 + \Sigma n_i)^i} \approx n_i / n_1 \approx n_i / n \quad (4)$$

because $\Sigma n_i << n_1 \approx n$, where n is the total number per unit volume. ΔE_i follows from eq.(1) and eq.(4) similar as the dash-dot line in fig.1. Thus, the number of embryos per unit volume, which get converted from size i to size $(i + 1)$, is the same for all values of i at the same conversion rate equal to the nucleation rate. The amount of embryos n_i is constant within each size but decreases by the increase of R.

At nucleation the stationary case is regarded, determined by the rate at nucleation of the critical embryo, the nucleus. To explain eq.(5), which has the empirically found form of a forward reaction only at nucleation, it was assumed that for small embryos, the concentration is about the equilibrium concentration $n_{i,e}$. For large sizes the concentration was assumed to be far below the equilibrium value and to be zero for $i \to \infty$ (see fig. 1), loosing therefore its backwards reaction term. This apparent forward nucleation rate thus is assumed to be:

$$\dot{n} = \nu n \exp((-\Delta E_t + \Delta E_c) / kT) \quad (5)$$

in agreement with measurements. In eq.(5), ΔE_t is the energy barrier for transfer of atoms across the interface for nucleation at frequency ν and ΔE_c, the driving force required for nucleus formation.

Substitution of eq.(3), with $\Delta g = \Delta s(T_e - T) = \Delta s \Delta T$, shows that eq.(5) has the form of:

$$\dot{n} = A_1 \exp(-A_2 / (T_e - T)^2 = A_1 \exp(-A_2 / \Delta T^2) \quad (6)$$

for homogeneous nucleation.

Analogous is for the step growth mechanism of fig. 2:

$$\Delta E_e = \pi R^2 h \Delta g + 2\pi R h \gamma, \quad (7)$$

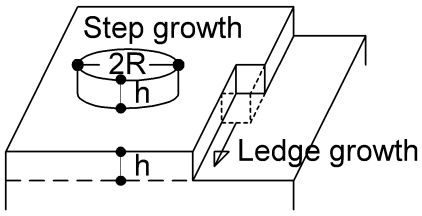

Figuur 2. Step-growth after finished ledge growth

leading by d(ΔE)/dR = $2\pi R h \Delta g + 2\pi h \gamma = 0$ to the critical size for nucleation of:

$$R_c = -\gamma / \Delta g \quad (8)$$

and to the general form of eq.(5) of:

$$\dot{n} = A_1 \exp(-A_2 / (T_e - T)) \quad (9)$$

This is regarded to be confirmed in fig.3, by the empirical straight line of ln($\dot{n}$) against $1/(T_e - T)$ with the negative slope of $-A_2$. Equation (9) is given in fig.3 by the drawn line.

Regarding the above given classical model the following remarks can be made:

- The free energy ΔE of eq.(1) is based on a constant γ independent of temperature. This is improbable because no real equilibrium, $\dot{n} = 0$, is possible at $T = T_e$ because eq.(2) and

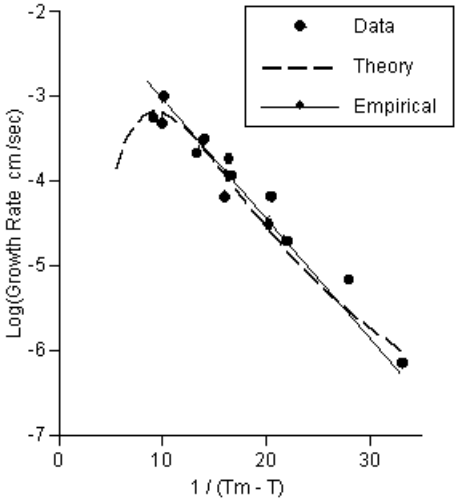

Fig. 3 Nucleation and growth rate of ice crystal

eq.(3) show impossible infinite values of the nucleus dimensions (R_c) and of reaction heat to obtain equilibrium. Because $A_2 / (T_e - T)$ has the form of $\Delta E / kT$ according to eq.(5), ΔE becomes infinite when $T = T_e$. This will be corrected to the right values in Section 5, by applying the right driving force and regarding the backwards reaction for small driving forces.

- Because the volume increase of the growing embryo, up to $(4/3)\pi R^3$ and the surface increase up to $4\pi R^2$ are coupled being one and the same process, γ and Δg should show one and the same temperature dependence. In fact thus one temperature dependent embryo growth process has to be regarded as is shown to apply in the following sections.
- The free energy representation by e.g. eq.(5): $\Delta E_c = (16\pi\gamma^3) / (3\Delta g^2)$, is confusing because it contains both specific heat and driving force values for volume and surface Δg and γ. Because of the identical growth of volume and of surface, the defined apparent surface energy γ should be proportional to Δg and ΔE_c. This follows directly from the elimination of γ, in stead of R_c, from eq.(1) and eq.(2), giving:

$$\Delta E_c = -(2/3)\pi R_c^3 \Delta g \ , \quad (10)$$

the right form of the activation energy. Mathematically eq.(10) is identical to eq.(3).
As shown in Section 3, γ is a superfluous parameter.

3. Derivation of the embryo equilibrium concentration

Because ΔE_c is the highest for nucleation, the nucleation reaction is the slowest and is determining for the conversion rate of all embryos of the sequence of bimolecular reactions. The real rate and equilibrium equations of the classical model can be derived as follows. Because in fig.1 the amount of embryos per unit volume *n* is a function of the radius *R* and growth is per step, the rate of sequential cylindrical embryo formation of fig.2 is:

$$dV / dt = \dot{V} = d(nh\pi R^2) / dt = ((\partial n / \partial R) h\pi R^2 + 2nh\pi R) \cdot \dot{R} \quad (11)$$

where the dot means derivative to the time t: $\dot{R} = dR / dt$. In this equation $\dot{R}$ or $\dot{V}$ follows from the kinetic diffusion equation in the form of eq.(A5) of Appendix A.
Eq.(11) can be given per embryo to get the growth rate in number of molecules per em-

bryo:

$$\dot{v} = (((\partial n / \partial R) / n) h\pi R^2 + 2h\pi R) \cdot \dot{R} = ((\partial \ln n / \partial R) + 2\pi Rh / \pi R^2 h) h\pi R^2 \dot{R} \qquad (12)$$

because *n* is constant, independent of time *t* at steady state. This can be written:

$$\dot{v} = ((\partial \ln n / \partial R) + A_e / V_e) h\pi R^2 \dot{R}, \qquad (13)$$

The determining reaction is the slowest reaction thus $\dot{v}$ is minimal at the nucleation step. This is the case when in eq.(13) A_e / V_e, the interface surface/embryo volume ratio, is minimal, as is satisfied by the spherical and by the cylindrical form of the step in fig.2 and this minimum also applies when *n* is minimal, thus when $\partial \ln n / \partial R = 0$ at $R = R_c$. Then, $\partial \ln n / \partial R = -a + aR / R_c$ is required to have a real minimum at $R = R_c$, necessary for having an end-product of the successive reactions (being for other cases) the start of grain growth and necessary to have a negative slope for decreasing *n* at increase of *R* (for $R < R_c$) and finally to have an exponential quadratic function in *R*, necessary for the possibility of an expression in specific free energy values. Thus integrated:

$$n = n_0 \exp(-aR + aR^2 / (2R_c) - \Delta E_{t,d} / kT) = n_0 \exp((-\Delta E - \Delta E_{t,d}) / kT) = \\ = n_a \exp(-\Delta E / kT) \qquad (14)$$

where n_a is the active reactant concentration and $\Delta E_{t,d}$ (independent of *R*) acts as resultant energy barrier for every migrating molecule between every embryo. Because R^2 is proportional to the total number of molecules per embryo, eq.(14) represents the equilibrium curve of the classical steady-state model, given in fig.1. The positive term $aR^2 / 2R_c$ acts as driving force for embryo formation and by the term R^2 it is related to the specific volume free energy term Δg, (with $\Delta \bar{g}$ as absolute value of Δg) by:

$aR^2 / 2R_c = \Delta E_d / kT = (\pi R^2 h \Delta \bar{g}) / kT$. The negative term in *R*, related to the surface of the embryo as derivative of the volume term, gives: $-aR = -2\pi Rh\Delta \bar{g} R_c / kT$, where $R_c \Delta \bar{g}$ is the specific energy barrier for embryo formation, replacing constant γ of the classical model.

The same result is found by applying the classical volume- and surface energy terms: $(\pi R^2 h \Delta \bar{g} - 2\pi Rh\gamma) / kT = aR^2 / 2R_c - aR$, giving $a = 2\pi R_c h \Delta \bar{g} / kT$ and $\gamma = R_c \Delta \bar{g}$.

Thus ΔE of eq.(14) is: $\Delta E = -\pi R^2 h \Delta \bar{g} + 2\pi R R_c h \Delta \bar{g}$

For $R = R_c$, the critical embryo for nucleation, the value of ΔE_c is:

$$\Delta E_c = -\pi R_c^2 h \Delta \bar{g} + 2\pi R_c h\gamma = -\Delta \bar{g} V_c + R_c \gamma A_c = (aR_c / 2) kT = \pi h R_c^2 \Delta \bar{g} = V_c \Delta \bar{g} \qquad (15)$$

According to eq.(11), the nucleation and sequential growth rate is:

$$\dot{V} = 2\pi h R_c n_c \cdot \dot{R} \qquad (= 2\pi h R_c n_0 \exp(-(V_c \Delta \bar{g} + \Delta E_{t,d}) / kT) \cdot \dot{R}) \qquad (16)$$

This equation will be discussed in Section 5.

4. Equilibrium condition of homogeneous and heterogeneous embryos

4.1. Homogeneous nucleation

The derivation of Section 3 can be repeated for homogeneous nucleation. Analogous to eq.(11) and (12) of Section 3 is for spherical embryos:

$$dV / dt = \dot{V} = d(n(4/3)\pi R^3) / dt = ((\partial n / \partial R)(4/3)\pi R^3 + n4\pi R^2) \cdot \dot{R} \qquad (17)$$

$$\dot{v} = ((\partial \ln n / \partial R)(4/3)\pi R^3 + 4\pi R^2) \cdot \dot{R} = ((\partial \ln n / \partial R) + A_e / V_e)(4/3)\pi R^3 \cdot \dot{R} \qquad (18)$$

For $\partial \ln n / \partial R = 0$ at $R = R_c$ is now required: $\partial \ln n / \partial R = (-a + aR / R_c)R$, to have a negative slope for decreasing *n* at increasing *R* (for $R \le R_c$) and to have an exponential third degree term in *R*, necessary for the possibility of the expression in a specific free energy value. Integrated is:

$$n = n_c \exp(-aR^2 / 2 + aR^3 / (3R_c) - \Delta E_{t,d} / kT) = n_c \exp((-\Delta E - \Delta E_{t,d}) / kT) \qquad (19)$$

and: $aR^3 / 3R_c = ((4/3)\pi R^3 \Delta \bar{g}) / kT$, or: $a = 4\pi R_c \Delta \bar{g} / kT$ and $-aR^2 / 2 = -4\pi R^2 (R_c \Delta \bar{g} / 2)$. The classical value γ now is: $\gamma = R_c \Delta \bar{g} / 2$ as also found in Section 2. The critical value for $R = R_c$ is $\Delta E_c / kT = aR_c^2 / 6 = (2/3)\pi R_c^3 \Delta \bar{g} / kT$ (or: $= 16\pi\gamma^3 / (3(\Delta g)^2 kT)$) (20)

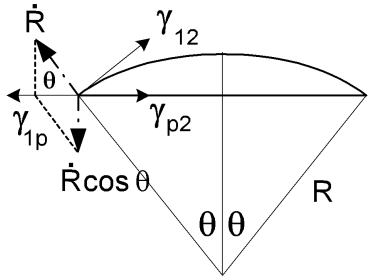

Fig. 4. Spherical cap

4.2. ***Heterogeneous nucleation***

The formation of a critical embryo on a foreign surface will show the minimum A_e / V_e shape by its form of a spherical cap (see fig. 4). According to the classical model, the free energy of formation of this heterogeneous embryo is:

$$\Delta E = \Delta g(\pi/3)(2 - 3\cos\theta + \cos^3\theta)R^3 + 2\pi(1 - \cos\theta)R^2\gamma_{1,2} + \pi(R\sin\theta)^2(\gamma_{2p} - \gamma_{1p}) \qquad (21)$$

where surface energies are regarded to be identical to surface stresses, (see fig.4). Resolving these surface stresses into horizontal components: $\gamma_{1p} = \gamma_{2p} + \gamma_{12}\cos\theta$, the critical value: $\Delta E_c = 4\pi\gamma_{1,2}^3(2 - 3\cos\theta + \cos^3\theta) / (3\Delta g^2)$ is found when also $R_c = 2\gamma / \Delta\bar{g}$ is applied. This is a factor $((2 - 3\cos\theta + \cos^3\theta) / 4)$ times the homogeneous value of eq.(3). However the model of surface stresses, equal to the surface free energies, being in equilibrium at the intersects, does not apply for solids and should be replaced by continuity conditions of the growth rate. Because the rates $\dot{R}$ are perpendicular to the surfaces (see fig. 4), because of the radial growth, they are also perpendicular to the assumed fictive surface stresses in these planes and the same expressions occur by the condition of continuity of the rates, (the equilibrium of rates) as would occur by the equilibrium condition of the fictive surface stresses. The rate of growth of the spherical cap volume is:

$$d((\pi/3)(2 - 3\cos\theta + \cos^3\theta)R^3) / dR = \pi(2 - 3\cos\theta + \cos^3\theta)R^2\dot{R} \qquad (22)$$

This should be equal to the growth rates at the two surfaces.

The growth rate at the spherical surface is: $2\pi(1 - \cos\theta)R^2\dot{R}$.

The growth rate at the flat circular plane is: $-\pi(R\sin\theta)^2\dot{R}\cos\theta$ (where: $\dot{R}_{circle} = \dot{R}\cos\theta$)

Summing up, in total at the planes: $\pi R^2 \dot{R}(2-3\cos\theta+\cos^3\theta)$ due to the continuity condition of the rates in accordance with eq.(22). There thus is no need to introduce surface energies and γ - stresses and the continuity conditions are automatically fulfilled, as shown by the derivation according to Section 3.
According to Section 3 is analogous to eq.(11):

$$\dot{V} = d(n(4\pi R^3/3)((2-3\cos\theta+\cos^3\theta)/4))/dR \tag{23}$$

leading to the same equations as in Section 4.1 above for homogeneous nucleation when everywhere "π" is replaced by "$\pi(2-3\cos\theta+\cos^3\theta)/4$".
The critical value of ΔE then is:

$$\Delta E_c = ((\pi/6)(2-3\cos\theta+\cos^3\theta)R_c^3)\Delta\bar{g} \tag{24}$$

which is identical to the classical value when: $R_c = 2\gamma/\Delta\bar{g}$ is substituted.

5. Estimation of the nucleation equation

The step-growth mechanism, regarded in Section 3, of the liquid-solid transformation is discussed as example. The growth rate of the step is normally sufficiently high so that each step nucleated on a surface spreads to form one molecular plane of height *h* in fig.2, before the formation of a second nucleus on the surface. The growth rate then is equal to the nucleation rate times *h*.
According to eq.(16) this growth rate is: $\dot{V} = 2\pi h R_c n_c \dot{R}$, thus the number of reacting molecules *N* follows from: $\dot{N} = 2\pi h R_c n_c n \cdot \dot{R}$, where *n* is the molecule density of the n_c critical embryos. According to Appendix A this equation is:

$$\dot{N} = 2\pi h R_c n_c n\dot{R} = BN_t 2\sinh(\sigma_v\lambda/(NkT)) \approx C\exp(\sigma_v\lambda/(NkT)) \tag{25}$$

for high driving forces. Because of the first order transformation there is a discontinuity of the enthalpy, entropy and volume at the transformation temperature and the initial driving force thus has the form of:

$$\sigma_v\lambda/N_0 = \Delta H - T\Delta S = \Delta S(T_m - T) = \Delta S\Delta T, \tag{26}$$

while due to the volume change according to Appendix C:

$$N = N_m + b_1(\sigma_{v0}\lambda/N_m)^2 \tag{27}$$

The derivation in Appendix C is based on high stresses and according to eq.(C5), *N* is proportional to the square of the initial applied stress σ_{v0} at the sites. For small driving forces when $\sigma_{v0} \to 0$, *N* should approach the constant equilibrium value e.g. at "melting" N_m and thus the small term N_m has to be added to the expression of *N* accounting for lower stresses, which is negligible in the high stress segments nucleation of fig.5, given by eq.(C2). Eq.(25) then becomes for phase change at appropriate high driving forces:

$$\frac{dN}{dt} = C\exp\left(\frac{\sigma_v\lambda}{NkT}\right) = C\exp\left(\frac{\Delta S\cdot\Delta T\cdot N_0}{kT(N_m + b_1(\Delta S)^2(\Delta T)^2)}\right) = C\exp\left(\frac{D'}{\frac{a_1}{\Delta T}+\Delta T}\right), \tag{28}$$

where $D' = \Delta S N_0/(kTb_1\Delta S^2)$ and $a_1 = N_m/(b_1\Delta S^2)$.
Eq.(28) is given for ice in fig.3 by the dashed line together with eq.(9) of the classical nucleation model, given by the straight solid line.

By much higher stress due to much higher undercooling for homogeneous nucleation, σ_v of eq.(28) may become the maximal "flow" stress at that temperature and eq.(28) turns approximately to eq.(6):

$\dot{N} = C_1 \exp\left(\sigma_f \lambda / NkT\right) = C_1 \exp\left(C_2 / (N_m + b_1(\Delta S)^2(\Delta T)^2)\right)$,

but $\dot{N}$ is finite, = $C_1 \exp\left(C_2 / N_m\right)$, when $\Delta T = 0$. This high internal stress also may apply for heterogeneous nucleation and is e.g. found for crystallization of a metallic glass [5]

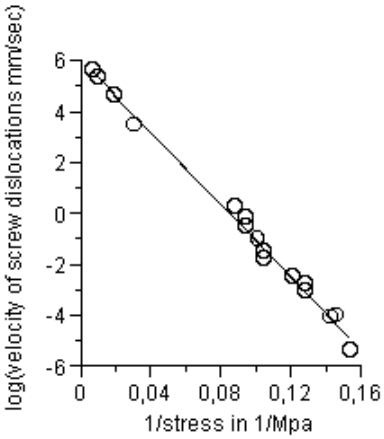

Fig. 5 | Dislocation velocity in LiF – Equation (C2)

showing the activation energy for viscous flow, in stead of the much lower activation energy for diffusion.

For low driving forces of liquids near melting, the sinh-equation of eq.(25) applies. Thus:

$\dot{N} = C'\sinh\left(\frac{\sigma_c \lambda}{NkT}\right) \approx C'\frac{\sigma_c \lambda}{NkT} \approx \frac{D''\Delta T}{a_1 + (\Delta T)^2} \approx D'''\Delta T$ and $\dot{N} = 0$ when $\Delta T = 0$.

This result is generally accepted in literature and applies e.g. at diffused interphase interfaces. The high driving stress "curve-fitting" of eq.(28) in fig. 3 follows from the mean value of the points at the ends at $1/\Delta T$ = 10 and 30, and one point of the classical straight line fit, eq.(9) at $1/\Delta T$ = 20. Then is: D = 1.27 and a_1 = 0,0116 or:

$\log(\dot{N}) = \log(C) + (D'\Delta T)/(a_1' + \Delta T^2) = -9.07 + (1.27\Delta T)/(0.0116 + \Delta T^2)$. (29)

It can be seen in fig. 3 that, in this case, the classical straight line fit in $1/\Delta T$, eq. (9): $\ln(\dot{N}) = \ln(A_1) - A_2/\Delta T$, only is straight in the given range of $1/\Delta T$ between 10 and 30. Eq.(9) thus is an approximation in a small range and is wrongly applied outside the range of allowable application e.g. for $\Delta T \to 0$.

The real curve, eq.(29) falls down to $1/\Delta T \approx 4$ and the curve thus explains the empirical maximum nucleation rate at some undercooling. Differentiating eq.(29) gives

$d\dot{N}/d\Delta T = \dot{N} \cdot d\left(D'\Delta T/(a_1' + \Delta T^2)\right)/d\Delta T = 0$, or $\Delta T_u^2 = a_1'$ (30)

In this case this maximal rate is at an undercooling of $\Delta T_u = \sqrt{a'} = \sqrt{0.0116} = 0.108$

Eq.(30) explains the measured C-curves of the time-temperature-transformation (TTT) diagrams as is shown in Section 6. The fact that the data of fig. 3 follow the forward reaction eq.(30) only, shows an always high driving stress of quenching experiments. As dis-

cussed in [6] for glass transition, the always high driving force can be explained as follows. At suddenly cooling, the shrinkage and configurationally change is confined by strong side bonds. This behaves in the same way as when crossing molecules are bridging voids. The internal stress on these sites is always high and thus the crossing molecules are always under high pressure by the molecular attraction forces of the void boundaries trying to close the void. A segmental jump of the highest loaded crossing unit will unload this unit but increases the load on the adjacent crossing units causing the next one to be high loaded. The segmental jumps cause a decrease of the void volume and length and thus also a decrease of the number of jumping elements. This causes a process of decreasing sites by the decreasing void volume and stress decrease in the visco-elastic material surrounding the voids while the driving force remains high until the end, explaining that there only is a forward (and thus no backwards) reaction at nucleation.

6. Derivation of the TTT-diagram

It is standard practice to plot the rates of diffusive transformation in the form of time-temperature-transformation (TTT) diagrams, often called “C-curves”

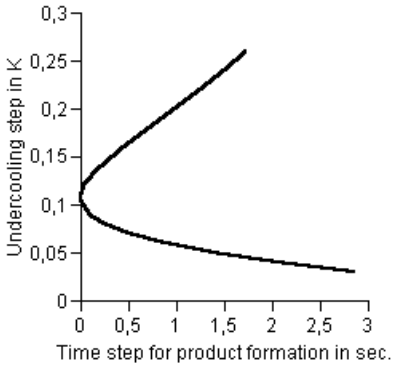

Figure 6. Reduced TTT-diagram based on data of Fig.3

According to eq.(30) is the product N after time t_1:

$$\log(N) = \log(\dot{N} \cdot t_1) = \log(\dot{N}) + \log(t_1) =$$

$$= -9.07 + (1.27\Delta T) / (0.0116 + \Delta T^2) + \log(t_1) \qquad (31)$$

At the maximal rate, the nose of the C-curve, $\Delta T = 0.108$, giving:

$$\log(N) = -3.17 + \log(t_1) \qquad (32)$$

t_1 is the time to produce the relative amount $N / N_{\max}$ at the maximal rate: $t_1 = N_1 / \dot{N}$, providing lines of e.g. 1%, 5%, 50 % etc. of transformed material.

In the same way is for time t_2 at an other temperature shift ΔT to get the same amount N:

$$\log(N) = -9.07 + (1.27\Delta T) / (0.0116 + \Delta T^2) + \log(t_2) \qquad (33)$$

Subtraction of eq.(33) from eq.(32) gives:

$$\log(t_2) - \log(t_1) = \Delta \log(t) = 5.9 - (1.27\Delta T) / (0.0116 + \Delta T^2) \qquad (34)$$

This represents the reduced curve of the TTT-diagram given in fig.6. The curve is upside down with respect to the usually given diagrams because the temperature T is on the vertical axis and not as here the undercooling step $\Delta T = T_m - T$.

7. Some remarks regarding the practical meaning of nucleation.

The formation of new phases is the result of a process of nucleation and therefore is a widely spread phenomenon in both nature and technology. Condensation and evaporation, crystal growth, electro deposition, melt crystallization, growth of thin films for microelectronics, volcano eruption, rain making and formation of e.g. glassy regions, vacancy clusters and particulate matter in space are only a few examples of nucleation processes. In practice, heterogeneous nucleation is normally involved, providing oriented and easily crystal growth at solidification or at phase change at surfaces as grain boundaries in solids.

Although a distinction is made between diffusive and displacive transformations as possible mechanisms of phase change, the nucleation equation also can be applied for the displacive mode being the reaction at the highest speed and driving force.

For practical steering of wanted results of these processes, explanation by theory is necessary. An example of application of the theory is the in section 6 given construction of the TTT-diagram, giving the necessary information on e.g. the speed of quenching or the way of ageing to obtain a wanted result. It is not necessary to measure all points of that diagram to obtain the parameters of the equation and the equation can be applied in different circumstances to predict and explain behaviour. The in Section 5 derived equation determines a single elementary process. For more complicated behaviour is, according to the equilibrium method of [7], description of real behaviour possible by parallel acting elementary processes. This provides consistent information, better than a kinetic equation with changing parameters.

8. Conclusions

The classical nucleation theory is shown to be questionable e.g. by the apparent infinite energy and infinite fluctuation dimensions as equilibrium requirement.

Because embryo volume- and surface formation is identically coupled, the defined classical surface free energy and volume free energy must have the same temperature dependence and the assumed temperature independent surface energy can not exist.

It is shown by the general derivation of sequential growth increase that this free energy distinction is superfluous and the surface energy term thus should be omitted. This is confirmed in Section 4.2 by the proof that the separate influence of surface energy in the form of surface stresses to explain heterogeneous nucleation is not needed because the assumed equilibrium of surface stresses has to be replaced by equilibrium of rates, thus by continuity conditions, to explain heterogeneous nucleation. These continuity conditions are automatically fulfilled by the derivative of the volume in the sequential growth rate equation.

Based on sequential growth conditions, the theoretical derivation of the equilibrium concentration of the embryos depending on size is given.

It is shown in Appendix B that every function can be represented by the power law equation. The power is identical to the slope of the double log-plot of the power equation and is identical to the activation volume parameter of the exact kinetics equation. It therefore is possible to compare the different empirical rate equations to get information on the form of the activation volume parameter.

In Appendix C, based on diffusion tests, the theoretical explanation is given of the different empirical equations by their different activation volume parameters, based on the

derivation of the empirical power law equation in Appendix B. Herewith the special form of the activation volume term of the driving force of nucleation is found as applied in Section 5.

It is shown in Section 5, that the special expression of the activation volume of the basic rate equation explains the data and nucleation behaviour as well for homogeneous as for heterogeneous nucleation. As discussed in Section 6, this rate equation shows the well known increase of the rate at the increase of undercooling up to a maximum value and then a decrease of the rate at larger undercooling steps giving thus a theoretical equation and explanation of the C-shape of the time-temperature-transformation diagrams (TTT-diagrams).

It thus is shown that nucleation follows the reaction rate equation of structural change. For the common case of high internal stresses, e.g. due to quenching, the equation can be given in stresses, determinable from measurements of the rate behaviour. It is important to know that the same applies for glass transition as shown in [6]

Appendix A

Basic equation of structural change

In general the reaction rate equation for structural change can be [7]:

$$d\rho / dt = B \cdot \rho \cdot 2\sinh(f_a A_a \lambda / (kT)) \tag{A1}$$

Where $B = \nu \exp(\Delta E_t / kT)$. This can be expressed in the concentration term:

$$\rho = N_a \lambda A_a / \lambda_1 \tag{A2}$$

where λ is the jump distance of the activated unit; A_a, the cross-section of that unit; λ_1 the distance between the activated sites and N_a, the number of these sites per unit area. Then $N_a / \lambda_1 = N_t$ is the number of activated elements per unit volume. The work of the stress f_a on the activation unit is: $f_a A_a \lambda$.

The equivalent work by the part σ_v of the mean macro stress σ that acts at the site is σ_v times the unit area thus is:

$$\sigma_v \cdot 1 \cdot 1 \cdot \lambda = N_a f_a A_a \lambda \quad \text{or:} \quad f_a A_a \lambda = \sigma_v \lambda / N_a . \tag{A3}$$

Also the chemical work, expressed as an equivalent driving stress, can be added as stress to the real external stress. Eq.(A1) thus becomes:

$$d(N_a \lambda A_a / \lambda_1) / dt = B \cdot (N_a \lambda A_a / \lambda_1) \cdot 2\sinh(\sigma_v \lambda / (N_a kT)) \tag{A4}$$

For constant λA_a at nucleation, eq.(A4) is, when $\lambda = \lambda' T$:

$$dN / dt = B \cdot N_t \cdot 2\sinh(\sigma_v \lambda' / (Nk)) \approx B \cdot N_t \exp(\sigma_v \lambda' / (Nk)) \tag{A5}$$

for high stresses. This structural change equation may show a long delay time and thus is able to explain transient nucleation. It also is able to explain the delay time and logarithmic time behaviour [7] of glass relaxation. Because of limited number of free spaces in solids, where molecules may jump in at diffusion, the zero order reaction occurs. The same situation follows from a high "reactant" concentration, causing the pre-exponential value of N_t to be constant in eq.(A5).

Appendix B

Derivation of the power law.

Any function $f(x)$ always can be written in a reduced variable x / x_0

$$f(x) = f_1(x / x_0)$$

and can be given in the power of a function:

$$f(x) = f_1(x / x_0) \; = \; \left[\left(f_1(x / x_0) \right)^{1/n} \right]^n$$

and expanded into the row:

$$f(x) = f(x_0) + \frac{x - x_0}{1!} \cdot f'(x_0) + \frac{(x - x_0)^2}{2!} \cdot f''(x_0) + ...$$

giving:

$$f(x) = \left[\left\{ f_1(1) \right\}^{1/n} + \frac{x - x_0}{x_0} \frac{1}{n} \left\{ f_1(1) \right\}^{1/n-1} \cdot f'(1) + ... \right]^n = f_1(1) \cdot \left(\frac{x}{x_0} \right)^n$$

when: $\left(f_1(1) \right)^{1/n} = \left(f_1(1) \right)^{1/n-1} f_1'(1) / n$ or: $n = f_1'(1) / f_1(1)$,

where: $f_1'(1) = \partial f_1(x / x_0) / \partial (x / x_0)$ for $x = x_0$ and $f_1(1) = f(x_0)$.

Thus: $f(x) = f(x_0) \cdot \left(\frac{x}{x_0} \right)^n$ with $n = \frac{f_1'(1)}{f_1(1)} = \frac{f'(x_0)}{f(x_0)}$

It is seen from this derivation of the power law, using only the first 2 expanded terms, that the equation only can be applied in a limited range of *x* around x_0.

Appendix C

Estimation of the activation volume parameter

Because diffusion is involved, the activation energy of processes as creep, damage, self-diffusion and growth are related and correlate e.g. with the melting temperature and measurements of the dislocation mobility, by stress σ pulses, may provide information on the kinetic parameters of transformations. The possible empirical equations of [8] are:
The power law equation:

$$\dot{v} = \dot{v}_0 (\sigma / \sigma_0)^m \qquad \text{(C1)}$$

where $\dot{v}$ is the dislocation velocity and σ the applied stress.
The nucleation equation, based on the classical nucleation model:

$$\dot{v} = C_1 \exp(-D / \sigma) \qquad (\approx \dot{v}_0 (\sigma / \sigma_0)^{D/\sigma_0}) \qquad \text{(C2)}$$

This eq.(C2) of point defect drag mechanism in LiF is given in Fig.6 applying here for high stress nucleation of mobile segments by overcoming peaks of the potential energy field.

The exact theoretical equation can be given in the form:

$$\dot{v} = 2C_2 \sinh(\varphi\sigma) \approx C_2 \exp(\varphi\sigma) \qquad (\approx \dot{v}_0(\sigma/\sigma_0)^{\varphi\sigma_0}) \qquad \text{(C3)}$$

for the applied higher stresses. eq.(C3) is given in fig.8 for Ni.
The parts between the parentheses are the power law approximations of the given equations, following from Appendix B. In a limited high stress range, fitting is possible according to all 3 equations (C1) to (C3) at the same time, as is done for Ge in [8]. An extended measured stress range is necessary to see which formula applies.
The power *m* of eq.(C1) can be found from the slope of the double log-plot, fig.7 (of Fe-Si), and for the other two equations in fig.6 and fig.8, *D* and φ follow from a semi-log-plot.

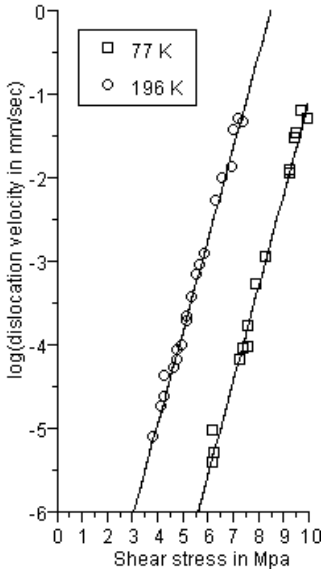

Fig. 7. Dislocation velocity in Ni, eq.(C3)

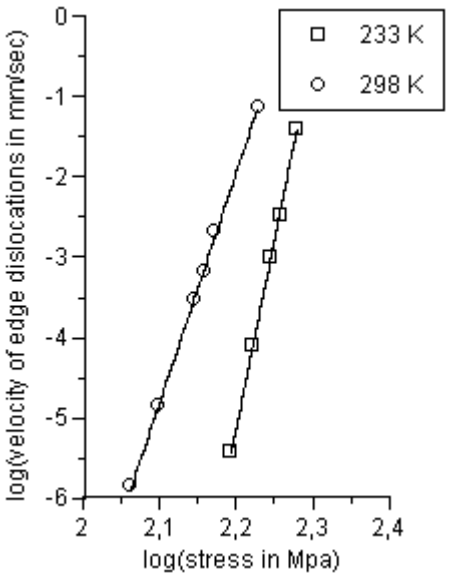

Fig. 8. Dislocation velocity in Fe-Si, eq.(C1)

According to the double log-plot of the power law approximations of these equations is:

$$m = D/\sigma_0 = \varphi \cdot \sigma_0 \qquad \text{(C4)}$$

giving information on the form of the parameter φ of the applying exact equation, Eq.(C3). When over a long range of stresses, eq.(C2) applies and the semi log-plot of $\log(\dot{v})$ against $1/\sigma$ shows a constant slope: - *D*, then the parameter φ of the exact equation is according to: $\varphi\sigma_0 = D/\sigma_0$, equal to $\varphi = D/\sigma_0^2$. This parameter will be shown below to be right for the nucleation mechanism. The semi log-plot of the exact equation, eq.(C3) now is for nucleation:

$$\ln(\dot{v}) = \ln(C_2) + \varphi\sigma = \ln(C_2) + D\sigma/\sigma_0^2 \qquad \text{(C5)}$$

for high stresses. Because the dislocation mobility tests are done with stress pulses, long enough to get steady state velocities the applied stress σ is equal to the initial applied stress σ_0 and eq.(C5) becomes equal to eq.(C2) which thus is the equation of the collection of all different pulse tests with different values of σ_0. The value $D\sigma/\sigma_0^2$ becomes $D\sigma_0/\sigma_0^2 = D/\sigma_0$ in the positive σ-direction. Because $\partial\sigma/(\sigma_0)^2 = -\partial(1/\sigma_0)$, this is an negative slope in the $(1/\sigma)$-direction. Eq.(C5) shows that for stress relaxation (one σ_0 in one test) there will be a straight-line on the $\ln(\dot{v})$ - σ plot but not on the $\ln(\dot{v})$ - $1/\sigma$ - plot, as is verified by experimental data of [8].

The power law behaviour, eq.(C1), when applying over a long range of stresses, also represents a mechanism with a special property of the activation volume parameter φ. The constant slope *n* of the double log-plot of eq.(C1) is equal to $\varphi\sigma_0$ The mechanism with this property of φ is found in many materials as in BCC, FCC and HPC metals and non-metallic crystals and also in e.g. concrete and wood. This property of φ causes the time-stress equivalence and because normally φ also is independent of the temperature, the time-temperature equivalence also applies. With the special value of $\varphi = m/\sigma_0$, eq.(C3) becomes:

$$\ln(\dot{v}) = \ln(C_2) + \varphi\sigma = \ln(C_2) + m\sigma/\sigma_0 \qquad \text{(C6)}$$

and the semi-log-plot of $\ln(\dot{v})$ against $\sigma\,(=\sigma_0)$ now shows a slope of m/σ_0 which is different for every pulse test value of $\sigma\,(=\sigma_0)$ in the plot, thus is a curved line, as e.g. given in [8]. It follows also from eq.(C6) for the double log-plot:

$$d\ln(\dot{v})/d\ln(\sigma) = \sigma \cdot d\ln(\dot{v})/d\sigma = \sigma \cdot m/\sigma_0 . \qquad \text{(C7)}$$

This is equal to: $\sigma_0 \cdot m/\sigma_0 = m$ for the σ_0-pulse tests collection of the dislocation mobility tests, where each applied stress σ is equal to the initial applied stress σ_0. Only in this case the constant value *n* of the slope of the double log-plot may exist in a wide stress range, as given in [8]. At the same time, for the stress-relaxation tests, (which is one test with one σ_0 over many decades of time) at high stress, the straight semi log-plot: $\ln(\dot{v})$ - σ - plot applies according to the exact eq.(C6), thus is fully explained here by the type of loading.

There also exists a mechanism with a constant value of φ in eq.(C3). This does not only apply for polycrystalline material like Ni, but also occurs in other materials and in wood, for instance in a species with a wavy grain.

The explanation of the form of the activation volume parameter φ follows from Appendix C: $\sigma\varphi = \sigma\lambda/NkT = \sigma\lambda'/Nk$. Thus the power law here applies when the concentration of sites *N* is proportional to the initial stress σ_0: $\sigma\varphi = \sigma\lambda'/Nk = \sigma\lambda'/c\sigma_0 k = c'\sigma/\sigma_0$. For nucleation *N* is proportional to σ_0^2 (for high stresses), as applied in eq.(30).

References

[1] Anisimov MP (2003) Nucleation theory and experiment, Russian Chem. Rev. pp.591-600.

[2] Girshick SI and CP Chiu (1990) The J of chem. Phys. 93 pp 1273-1277

[3] Dobberstein H and Schwartz RW (2002) Modeling the Nucleation and Growth Behavior of Solution Derived Thin Films, Proc. 1st Symposium on Advanced Materials for Next Generation – Prelude to Functional-Integrated Materials AIST Chubu, Nagoya, Japan.

[4] Nitsche H (2005) Kinetics of Crystallization in Amorphous Alloys; Dissertation Stuttgart University, Bericht Nr. 168

[5] Jena AK and Chaturvedi MC (1992) Phase Transformations in Materials, Prentice Hall.

[6] van der Put TACM (2010) Theoretical derivation of the WLF- and annealing equations, J. Non Crys. Solids 356, p. 394-399.

[7] van der Put TACM (1989) Deformation and damage processes in wood, Delft University Press, NL.

[8] Krausz AS and H Eyring (1975) Deformation Kinetics, John Wiley & sns New York.